

Politecnico di Torino

INGEGNERIA ENERGETICA E NUCLEARE
Sustainable Nuclear Energy
A.a. 2024/2025
Sessione di Laurea Ottobre 2025

Investigation and Validation of Spectral History Model in SCIENCEV2

Relatori Aziendali:

Laurent Graziano Marc-Antoine Dor

Relatori Accademico:
Prof. Sandra Dulla

Candidati:

Stefania Centeno Rospigliosi S318387

Contents

Li	st of	Figures	3
1	Intr	roduction	1
	1.1	Thesis Objective and Structure	2
2		eoretical background	3
		Neutrons and interaction with the matter	3
	2.2	Integro-differential Boltzmann equation: neutron transport	5
		2.2.1 Phase space	5
		2.2.2 Total neutron balance	6
		2.2.3 Critical equation - Introduction of the effective multiplication factor .	8
	2.3	Multigroup Theory	8
		2.3.1 Expansion of the Scattering Function using spherical harmonics	9
		2.3.2 Energy groups	11
3	Ind	ustrial Reactor Simulation	13
	3.1	Two-step calculation	13
	3.2	Lattice Calculation	14
		3.2.1 Neutron slowing-down and resonance self shielding	15
		3.2.2 The neutron leakage model	16
		3.2.3 Isotopic depletion	17
	3.3	Core Calculation	19
		3.3.1 The steady state diffusion equation	19
		3.3.2 Continuity and Boundary Conditions	22
	3.4	Multiparametrized Homogenized Cross Section tables	24
	3.5	Limits of Two-step calculation and 3D direct calculation	25
4	Цic	tory effect in PWR modeling	27
4	4.1	Sensitivity Analysis	27
	4.1	Spectral History Modeling	38
	4.2	4.2.1 Interpolation parameters	38
		4.2.2 Performance of the methods	41
	4.3	Multi-Parametrized Libraries and History Model of SCIENCE V2	44
	4.5	Multi-1 arametrized Libraries and History Model of SCIENCE V2	44
5		a Analysis	48
		Taishan Reactor	48
	5.2	Historical Analysis from SCIENCE V2 data	49
		5.2.1 Data distribution within the Core	49
	5.3	Deviations of the state parameters	53

	5.4	Correlations	55
		5.4.1 Correlations in each case study	58
6	Val	idation 6	32
U		Selection of the nodes	
	0.1		
		6.1.1 First case	
		6.1.2 Second case	
	6.2	Methodology for comparison	j 4
		6.2.1 Detailed procedure	35
		6.2.2 Fuel depletions	35
		6.2.3 Restart calculations	36
		6.2.4 Third step: Bilinear interpolation	36
	6.3	Case study: Assembly 1	73
		6.3.1 J0909: middle of cycle	76
		6.3.2 J0909: end of cycle	31
		6.3.3 J0913: middle of cycle	37
		6.3.4 J0913: end of cycle	
	6.4		
	0.1	6.4.1 G1105: middle of cycle	
		6.4.2 G1105: end of cycle	
		6.4.3 G1109 + environment: middle of cycle	
		6.4.4 G1109 + environment: end of cycle	r G
=		nclusion 19	
'7	COL	ncuisioni	, h

List of Figures

2.1	Cartesian reference system 4	6
2.2	Neutron balance	6
2.3	Thermal and fast neutron spectrum 5	9
2.4	Division of neutron energy range into G groups 7	11
3.1	Global calculation scheme 3	14
3.2	Depression of the neutron flux in resonance region	16
3.3	Case of study: 17x17 UOX 3.7%	18
3.4	Principle scheme of equivalence for the example of a 3-D core calculation 1.	20
3.5	Two-group approximation 6	21
3.6	Two group full core calculations 6	22
3.7	Spatial distribution of the flux 6	23
3.8	Spatial domain with symmetries	24
3.9	Symmetry boundary condition	24
4.1	Evolution of the moderator density of a node during the cycle. It can be	
	observed how it differs from nominal value used in the depletion	28
4.2	Representation of local data on an industrial fuel cycle depletion of density	
	of the moderator, fuel temperature, boron concentration and xenon concen-	
	trations. Those realistic data are of one assembly type, as it is possible to see	
	trations. Those realistic data are of one assembly type, as it is possible to see the distribution of each of them is not concentrated in a restricted range of	
	the distribution of each of them is not concentrated in a restricted range of values.	29
4.3	the distribution of each of them is not concentrated in a restricted range of values	
4.3	the distribution of each of them is not concentrated in a restricted range of values.	29
4.3	the distribution of each of them is not concentrated in a restricted range of values	
	the distribution of each of them is not concentrated in a restricted range of values. Effect on neutron spectrum changing water density. The higher value of water density is approximately 7% more than the reference value.	30
4.4	the distribution of each of them is not concentrated in a restricted range of values. Effect on neutron spectrum changing water density. The higher value of water density is approximately 7% more than the reference value. Moderator density effect on nuclide contents for some isotopes	30 32
4.4	the distribution of each of them is not concentrated in a restricted range of values. Effect on neutron spectrum changing water density. The higher value of water density is approximately 7% more than the reference value. Moderator density effect on nuclide contents for some isotopes Doppler Effect Broadening 111	30 32
4.4	the distribution of each of them is not concentrated in a restricted range of values. Effect on neutron spectrum changing water density. The higher value of water density is approximately 7% more than the reference value. Moderator density effect on nuclide contents for some isotopes Doppler Effect Broadening 111	30 32 33
4.4 4.5 4.6	the distribution of each of them is not concentrated in a restricted range of values. Effect on neutron spectrum changing water density. The higher value of water density is approximately 7% more than the reference value. Moderator density effect on nuclide contents for some isotopes. Doppler Effect Broadening [11]	30 32 33 33
4.4 4.5 4.6	the distribution of each of them is not concentrated in a restricted range of values. Effect on neutron spectrum changing water density. The higher value of water density is approximately 7% more than the reference value. Moderator density effect on nuclide contents for some isotopes Doppler Effect Broadening [11] Effect on neutron spectrum changing fuel temperature. The higher value is 44% more than the nominal value. Fuel temperature effect on nuclide contents for some isotopes	30 32 33 33
4.4 4.5 4.6	the distribution of each of them is not concentrated in a restricted range of values. Effect on neutron spectrum changing water density. The higher value of water density is approximately 7% more than the reference value. Moderator density effect on nuclide contents for some isotopes. Doppler Effect Broadening 11	30 32 33 33 34
4.4 4.5 4.6 4.7 4.8	the distribution of each of them is not concentrated in a restricted range of values. Effect on neutron spectrum changing water density. The higher value of water density is approximately 7% more than the reference value. Moderator density effect on nuclide contents for some isotopes. Doppler Effect Broadening [11] Effect on neutron spectrum changing fuel temperature. The higher value is 44% more than the nominal value. Fuel temperature effect on nuclide contents for some isotopes. Effect on neutron spectrum changing boron concentration. The higher value is 27% more than the nominal value. Boron effect on nuclide contents for some isotopes.	30 32 33 33 34
4.4 4.5 4.6 4.7 4.8	the distribution of each of them is not concentrated in a restricted range of values. Effect on neutron spectrum changing water density. The higher value of water density is approximately 7% more than the reference value. Moderator density effect on nuclide contents for some isotopes Doppler Effect Broadening [11] Effect on neutron spectrum changing fuel temperature. The higher value is 44% more than the nominal value. Fuel temperature effect on nuclide contents for some isotopes Effect on neutron spectrum changing boron concentration. The higher value is 27% more than the nominal value. Boron effect on nuclide contents for some isotopes	30 32 33 33 34
4.4 4.5 4.6 4.7 4.8 4.9 4.10	the distribution of each of them is not concentrated in a restricted range of values. Effect on neutron spectrum changing water density. The higher value of water density is approximately 7% more than the reference value. Moderator density effect on nuclide contents for some isotopes. Doppler Effect Broadening [11]	30 32 33 33 34 35 36
4.4 4.5 4.6 4.7 4.8 4.9 4.10	the distribution of each of them is not concentrated in a restricted range of values. Effect on neutron spectrum changing water density. The higher value of water density is approximately 7% more than the reference value. Moderator density effect on nuclide contents for some isotopes. Doppler Effect Broadening [11]	30 32 33 33 34 35 36
4.4 4.5 4.6 4.7 4.8 4.9 4.10 4.11 4.12	the distribution of each of them is not concentrated in a restricted range of values. Effect on neutron spectrum changing water density. The higher value of water density is approximately 7% more than the reference value. Moderator density effect on nuclide contents for some isotopes. Doppler Effect Broadening [11]	30 32 33 33 34 35 36 37

4.14 Correlation between relative change of macroscopic cross sections and ^{239}Pu	
concentrations in different depletions. $8 \ldots \ldots \ldots \ldots \ldots$	40
4.15 Homogenized macroscopic cross sections for the depletion with deviation in	
moderator temperature. DYN3D-Pu is regarding the core code with correc-	
tion and DYN3D without correction. 8	41
4.16 Burnup-averaged error with all the history parameters and for the given use	
cases 13	43
4.17 Homogenization of all the elements inside an assembly	44
4.18 Graphical visualization of depletion and restart calculations. The parameters	
inside the boxes are the ones that change during the restart calculations	45
4.19 Representation of the base evolution	46
4.20 Heavy product depletion chain in SCIENCE V2 in SMART	47
5.1 Fuel assembly loading of the EPR1750 core	49
5.2 Histogram of the distribution for the assembly UOX 2.1 (Assembly 1)	50
5.3 Histogram of the distribution for the assembly UOX 2.1 + 8 Gd pins (As-	
sembly 2) $\dots \dots \dots \dots \dots$	51
5.4 Histogram of the distribution for the assembly UOX $3.2 + 16$ Gadolinium	
pins (Assembly 3) \dots	51
5.5 Histogram of the distribution for the assembly UOX 3.2 + 20 Gadolinium	
pins (Assembly 4) \dots	52
5.6 Histogram of the distribution for the assembly UOX $4.2 + 16$ Gd pins (As-	
sembly 5)	53
5.7 Histogram of the cumulative deviation for all nodes for each state parameter.	54
5.8 Graphical representation of the deviations.	57
5.9 Zoomed-in view of the first row.	58
5.10 Zoomed-in view of the first row without top and bottom core nodes	58
5.11 Correlation representation considering different assembly types	59
5.12 Representation of the correlations the assembly 1	59
5.13 Representation of the correlations for assembly type 2	60
5.14 Representation of the correlations for assembly type 3	61
5.15 Representation of the correlations for assembly type 4	61
5.16 Representation of the correlations for assembly type 5	61
6.1 First case: Deviation in plutonium correlated to different density and the	
environment	63
6.2 Second case: Deviation in plutonium correlated to different density and the	
environment	64
6.3 Representation of the base and perturbed depletion	67
6.4 Representation of the branches for base and perturbated depletions	68
6.5 Representation of the branches for base and perturbated depletions. σ at S_0	
conditions is necessary for the validation.	69
6.6 Representation of the branches for base and perturbated depletions. PU at	
S_0 conditions is necessary for the validation.	70
6.7 Graphical representation of the real core depletion	71
6.8 Burnup interval considered for the interpolation	71
6.9 Real evolution of water density and fuel temperature along the cycle on a	
node ones of the 3D core coarse mesh	72
6.10 Graphical representation of the geometry implemented in APOLLO3 [®]	74
6.11 Real depletion for node J0909.	74

6.12	Real depletion for node J0913.	74
6.13	Fast group absorption cross sections - relative for assembly J0909 middle of	
	the cycle.	76
6.14	Fast group absorption cross sections - absolute for assembly J0909 middle of	
	the cycle.	76
6.15	Thermal group absorption cross sections - relative for assembly J0909 middle	
	of the cycle.	77
6.16	Thermal group absorption cross sections - absolute for assembly J0909 middle	_
	of the cycle.	77
6.17	Fast group fission cross sections - relative for assembly J0909 middle of the	_
	cycle	78
6.18	Fast group fission cross sections - absolute for assembly J0909 middle of the	_
	cycle.	78
6.19	Thermal group fission cross sections - relative for assembly J0909 middle of	
	the cycle.	79
6.20	Thermal group fission cross sections - absolute for assembly J0909 middle of	_
	the cycle.	79
6.21	Absolute Macroscopic Cross Section correction for assembly J0909 middle of	_
	the cycle.	80
6.22	Relative Macroscopic Cross Section correction for assembly J0909 middle of	
	the cycle.	80
6.23	Fast group absorption cross sections - relative for assembly J0909 end of the	_
	cycle.	82
6.24	Fast group absortion cross sections - absolute for assembly J0909 end of the	_
	cycle.	82
6.25	Thermal group absorption cross sections - relative for assembly J0909 end of	
	the cycle.	83
6.26	Thermal group absorption cross sections - absolute for assembly J0909 end	
	of the cycle.	83
6.27	Fast group fission cross sections - relative for assembly J0909 end of the cycle.	84
6.28	Fast group fission cross sections - absolute for assembly J0909 end of the cycle.	84
6.29	Thermal group fission cross sections - relative for assembly J0909 end of the	
	cycle	85
6.30	Thermal group fission cross sections - absolute for assembly J0909 end of the	
	cycle.	85
6.31	Absolute Macroscopic Cross Section for assembly J0909 end of the cycle	86
6.32	Relative Macroscopic Cross Section for assembly J0909 end of the cycle	86
6.33	Fast group absorption cross sections - relative for assembly J0913 middle of	
	the cycle.	88
6.34	Fast group absorption cross sections - absolute for assembly J0913 middle of	
	the cycle.	88
6.35	Thermal group absorption cross sections - relative for assembly J0913 middle	
	of the cycle.	89
6.36	Thermal group absorption cross sections - absolute for assembly J0913 middle	
		89
6.37	Fast group fission cross sections - relative for assembly J0913 middle of the	
	cycle.	90
6.38	Fast group fission cross sections - absolute for assembly J0913 middle of the	
	cycle.	90

the cycle.	91
6.40 Thermal group fission cross sections - absolute for assembly J0913 middle of	
the cycle.	91
6.41 Absolute Macroscopic Cross Section for assembly J0913 middle of the cycle	92
6.42 Relative Macroscopic Cross Section for assembly J0913 middle of the cycle	92
6.43 Fast group absorption cross sections - relative for assembly J0913 end of the	
cycle	94
6.44 Fast group absorption cross sections - absolute for assembly J0913 end of the	94
	94
cycle.	94
6.45 Thermal group absorption cross sections - relative for assembly J0913 end of	05
the cycle.	95
6.46 Thermal group absorption cross sections - absolute for assembly J0913 end	
of the cycle.	95
6.47 Fast group fission cross sections - relative for assembly J0913 end of the cycle.	•
6.48 Fast group fission cross sections - absolute for assembly J0913 end of the cycle	. 96
6.49 Thermal group fission cross sections - relative for assembly J0913 end of the	
cycle	97
6.50 Thermal group fission cross sections - absolute for assembly J0913 end of the	
cycle	97
6.51 Absolute Macroscopic Cross Section for assembly J0913 end of the cycle	98
6.52 Relative Macroscopic Cross Section for assembly J0913 end of the cycle	98
6.53 Graphical representation of the geometry implemented in APOLLO3® (infi-	
nite medium).	100
6.54 Graphical representation of the geometry including the surrounding environ-	
ment implemented in APOLLO3	100
6.55 Real depletion for node G1105 (infinite medium)	100
6.56 Real depletion for node G1109 (with environment).	100
0.00 Tecar depiction for node GITO (with chynolinent).	
6.57 Fast group absorption cross sections - relative for assembly G1105 middle of	
6.57 Fast group absoprtion cross sections - relative for assembly G1105 middle of	
the cycle. Gd treated as macro.	102
the cycle. Gd treated as macro	102
the cycle. Gd treated as macro. 6.58 Fast group absoprtion cross sections - absolute for assembly G1105 middle of the cycle. Gd treated as macro.	
the cycle. Gd treated as macro	102 102
the cycle. Gd treated as macro. 6.58 Fast group absoprtion cross sections - absolute for assembly G1105 middle of the cycle. Gd treated as macro. 6.59 Thermal group absoprtion cross sections - relative for assembly G1105 middle of the cycle. Gd treated as macro.	102 102
the cycle. Gd treated as macro. 6.58 Fast group absoprtion cross sections - absolute for assembly G1105 middle of the cycle. Gd treated as macro. 6.59 Thermal group absoprtion cross sections - relative for assembly G1105 middle of the cycle. Gd treated as macro. 6.60 Thermal group absoprtion cross sections - absolute for assembly G1105 middle	102 102 103
the cycle. Gd treated as macro. 6.58 Fast group absoprtion cross sections - absolute for assembly G1105 middle of the cycle. Gd treated as macro. 6.59 Thermal group absoprtion cross sections - relative for assembly G1105 middle of the cycle. Gd treated as macro. 6.60 Thermal group absoprtion cross sections - absolute for assembly G1105 middle of the cycle. Gd treated as macro.	102 102 103
the cycle. Gd treated as macro. 6.58 Fast group absoprtion cross sections - absolute for assembly G1105 middle of the cycle. Gd treated as macro. 6.59 Thermal group absoprtion cross sections - relative for assembly G1105 middle of the cycle. Gd treated as macro. 6.60 Thermal group absoprtion cross sections - absolute for assembly G1105 middle of the cycle. Gd treated as macro. 6.61 Fast group fission cross sections - relative for assembly G1105 middle of the	102 102 103 103
the cycle. Gd treated as macro. 6.58 Fast group absoprtion cross sections - absolute for assembly G1105 middle of the cycle. Gd treated as macro. 6.59 Thermal group absoprtion cross sections - relative for assembly G1105 middle of the cycle. Gd treated as macro. 6.60 Thermal group absoprtion cross sections - absolute for assembly G1105 middle of the cycle. Gd treated as macro. 6.61 Fast group fission cross sections - relative for assembly G1105 middle of the cycle. Gd treated as macro.	102 102 103 103
the cycle. Gd treated as macro. 6.58 Fast group absoprtion cross sections - absolute for assembly G1105 middle of the cycle. Gd treated as macro. 6.59 Thermal group absoprtion cross sections - relative for assembly G1105 middle of the cycle. Gd treated as macro. 6.60 Thermal group absoprtion cross sections - absolute for assembly G1105 middle of the cycle. Gd treated as macro. 6.61 Fast group fission cross sections - relative for assembly G1105 middle of the cycle. Gd treated as macro. 6.62 Fast group fission cross sections - absolute for assembly G1105 middle of the	102 103 103 104
the cycle. Gd treated as macro. 6.58 Fast group absoprtion cross sections - absolute for assembly G1105 middle of the cycle. Gd treated as macro. 6.59 Thermal group absoprtion cross sections - relative for assembly G1105 middle of the cycle. Gd treated as macro. 6.60 Thermal group absoprtion cross sections - absolute for assembly G1105 middle of the cycle. Gd treated as macro. 6.61 Fast group fission cross sections - relative for assembly G1105 middle of the cycle. Gd treated as macro. 6.62 Fast group fission cross sections - absolute for assembly G1105 middle of the cycle. Gd treated as macro.	102 103 103 104
the cycle. Gd treated as macro. 6.58 Fast group absoprtion cross sections - absolute for assembly G1105 middle of the cycle. Gd treated as macro. 6.59 Thermal group absoprtion cross sections - relative for assembly G1105 middle of the cycle. Gd treated as macro. 6.60 Thermal group absoprtion cross sections - absolute for assembly G1105 middle of the cycle. Gd treated as macro. 6.61 Fast group fission cross sections - relative for assembly G1105 middle of the cycle. Gd treated as macro. 6.62 Fast group fission cross sections - absolute for assembly G1105 middle of the cycle. Gd treated as macro. 6.63 Thermal group fission cross sections - relative for assembly G1105 middle of	102 103 103 104 104
the cycle. Gd treated as macro. 6.58 Fast group absoprtion cross sections - absolute for assembly G1105 middle of the cycle. Gd treated as macro. 6.59 Thermal group absoprtion cross sections - relative for assembly G1105 middle of the cycle. Gd treated as macro. 6.60 Thermal group absoprtion cross sections - absolute for assembly G1105 middle of the cycle. Gd treated as macro. 6.61 Fast group fission cross sections - relative for assembly G1105 middle of the cycle. Gd treated as macro. 6.62 Fast group fission cross sections - absolute for assembly G1105 middle of the cycle. Gd treated as macro. 6.63 Thermal group fission cross sections - relative for assembly G1105 middle of the cycle. Gd treated as macro.	102 103 103 104 104
the cycle. Gd treated as macro. 6.58 Fast group absoprtion cross sections - absolute for assembly G1105 middle of the cycle. Gd treated as macro. 6.59 Thermal group absoprtion cross sections - relative for assembly G1105 middle of the cycle. Gd treated as macro. 6.60 Thermal group absoprtion cross sections - absolute for assembly G1105 middle of the cycle. Gd treated as macro. 6.61 Fast group fission cross sections - relative for assembly G1105 middle of the cycle. Gd treated as macro. 6.62 Fast group fission cross sections - absolute for assembly G1105 middle of the cycle. Gd treated as macro. 6.63 Thermal group fission cross sections - relative for assembly G1105 middle of the cycle. Gd treated as macro. 6.64 Thermal group fission cross sections - absolute for assembly G1105 middle of	102 103 103 104 104
the cycle. Gd treated as macro. 6.58 Fast group absoprtion cross sections - absolute for assembly G1105 middle of the cycle. Gd treated as macro. 6.59 Thermal group absoprtion cross sections - relative for assembly G1105 middle of the cycle. Gd treated as macro. 6.60 Thermal group absoprtion cross sections - absolute for assembly G1105 middle of the cycle. Gd treated as macro. 6.61 Fast group fission cross sections - relative for assembly G1105 middle of the cycle. Gd treated as macro. 6.62 Fast group fission cross sections - absolute for assembly G1105 middle of the cycle. Gd treated as macro. 6.63 Thermal group fission cross sections - relative for assembly G1105 middle of the cycle. Gd treated as macro.	102 103 103 104 104
the cycle. Gd treated as macro. 6.58 Fast group absoprtion cross sections - absolute for assembly G1105 middle of the cycle. Gd treated as macro. 6.59 Thermal group absoprtion cross sections - relative for assembly G1105 middle of the cycle. Gd treated as macro. 6.60 Thermal group absoprtion cross sections - absolute for assembly G1105 middle of the cycle. Gd treated as macro. 6.61 Fast group fission cross sections - relative for assembly G1105 middle of the cycle. Gd treated as macro. 6.62 Fast group fission cross sections - absolute for assembly G1105 middle of the cycle. Gd treated as macro. 6.63 Thermal group fission cross sections - relative for assembly G1105 middle of the cycle. Gd treated as macro. 6.64 Thermal group fission cross sections - absolute for assembly G1105 middle of	102 103 103 104 104
the cycle. Gd treated as macro. 6.58 Fast group absoprtion cross sections - absolute for assembly G1105 middle of the cycle. Gd treated as macro. 6.59 Thermal group absoprtion cross sections - relative for assembly G1105 middle of the cycle. Gd treated as macro. 6.60 Thermal group absoprtion cross sections - absolute for assembly G1105 middle of the cycle. Gd treated as macro. 6.61 Fast group fission cross sections - relative for assembly G1105 middle of the cycle. Gd treated as macro. 6.62 Fast group fission cross sections - absolute for assembly G1105 middle of the cycle. Gd treated as macro. 6.63 Thermal group fission cross sections - relative for assembly G1105 middle of the cycle. Gd treated as macro. 6.64 Thermal group fission cross sections - absolute for assembly G1105 middle of the cycle. Gd treated as macro.	102 103 103 104 104 105
the cycle. Gd treated as macro. 6.58 Fast group absoprtion cross sections - absolute for assembly G1105 middle of the cycle. Gd treated as macro. 6.59 Thermal group absoprtion cross sections - relative for assembly G1105 middle of the cycle. Gd treated as macro. 6.60 Thermal group absoprtion cross sections - absolute for assembly G1105 middle of the cycle. Gd treated as macro. 6.61 Fast group fission cross sections - relative for assembly G1105 middle of the cycle. Gd treated as macro. 6.62 Fast group fission cross sections - absolute for assembly G1105 middle of the cycle. Gd treated as macro. 6.63 Thermal group fission cross sections - relative for assembly G1105 middle of the cycle. Gd treated as macro. 6.64 Thermal group fission cross sections - absolute for assembly G1105 middle of the cycle. Gd treated as macro. 6.65 Absolute Macroscopic Cross Section for assembly G1105 middle of the cycle.	102 103 103 104 104 105

6.67 Fast group absorption cross sections - relative for assembly G1105 end of the	
cycle. Gd treated as macro.	. 108
6.68 Fast group absorption cross sections - absolute for assembly G1105 end of the	
cycle. Gd treated as macro.	. 108
6.69 Thermal group absorption cross sections - relative for assembly G1105 end of	
the cycle. Gd treated as macro.	. 109
6.70 Thermal group absorption cross sections - absolute for assembly G1105 end	
of the cycle. Gd treated as macro.	. 109
6.71 Fast group fission cross sections - relative for assembly G1105 end of the cycle.	
Gd treated as macro.	. 110
6.72 Fast group fission cross sections - absolute for assembly G1105 end of the	
cycle. Gd treated as macro.	. 110
6.73 Thermal group fission cross sections - relative for assembly G1105 end of the	
cycle. Gd treated as macro.	. 111
6.74 Thermal group fission cross sections - absolute for assembly G1105 end of the	
cycle. Gd treated as macro.	. 111
6.75 Absolute Macroscopic Cross Section for assembly G1105 end of the cycle with	
Gd treated as macro.	. 112
6.76 Relative Macroscopic Cross Section for assembly G1105 end of the cycle with	
Gd treated as macro.	. 112
6.77 Fast group absorption cross sections - relative for assembly G1109 with envi-	
ronment middle of the cycle. Gd treated as macro.	. 114
6.78 Fast group absorption cross sections - absolute for assembly G1109 with en-	
	. 114
6.79 Thermal group absorption cross sections - relative for assembly G1109 with	
environment middle of the cycle. Gd treated as macro	. 115
6.80 Thermal group absorption cross sections - absolute for assembly G1109 with	
environment middle of the cycle. Gd treated as macro	. 115
6.81 Fast group fission cross sections - relative for assembly G1109 with environ-	
ment middle of the cycle. Gd treated as macro	. 116
6.82 Fast group fission cross sections - absolute for assembly G1109 with environ-	
ment middle of the cycle. Gd treated as macro.	. 116
6.83 Thermal group fission cross sections - relative for assembly G1109 with envi-	
ronment middle of the cycle. Gd treated as macro.	. 117
6.84 Thermal group fission cross sections - absolute for assembly G1109 with en-	
vironment middle of the cycle. Gd treated as macro.	. 117
6.85 Absolute Macroscopic Cross Section for assembly G1109 with environment	
middle of the cycle with Gd treated as macro	. 118
6.86 Relative Macroscopic Cross Section for assembly G1109 with environment	
middle of the cycle with Gd treated as macro	. 118
6.87 Fast group absorption cross sections - relative for assembly G1109 with envi-	
ronment end of the cycle. Gd treated as macro.	. 120
6.88 Fast group absorption cross sections - absolute for assembly G1109 with en-	
vironment end of the cycle. Gd treated as macro.	. 120
6.89 Thermal group absorption cross sections - relative for assembly G1109 with	
environment end of the cycle. Gd treated as macro.	. 121
6.90 Thermal group absorption cross sections - absolute for assembly G1109 with	
environment end of the cycle. Gd treated as macro.	. 121

6.91	Fast group fission cross sections - relative for assembly G1109 with environ-
	ment end of the cycle. Gd treated as macro
6.92	Fast group fission cross sections - absolute for assembly G1109 with environ-
	ment end of the cycle. Gd treated as macro
6.93	Thermal group fission cross sections - relative for assembly G1109 with envi-
	ronment end of the cycle. Gd treated as macro
6.94	Thermal group fission cross sections - absolute for assembly G1109 with en-
	vironment end of the cycle. Gd treated as macro
6.95	Absolute Macroscopic Cross Section for assembly G1109 with environment
	end of the cycle with Gd treated as macro
6.96	Relative Macroscopic Cross Section for assembly G1109 with environment
	end of the cycle with Gd treated as macro

Abstract

Accurate modeling of spectral history effects in Pressurized Water Reactors (PWRs) is crucial to improve fuel cycle predictions and optimize core performance. This study investigates the impact of spectral history on neutron transport calculations using SCIENCE V2, a state-of-the-art computational tool for nuclear reactor analysis. The methodology includes the reconstruction of multi-parametrized libraries through a stepwise approach: fuel depletion simulations, restart calculations (branching), and bilinear interpolation techniques. A detailed sensitivity analysis is performed to assess the influence of state parameters, such as moderator density, fuel temperature, boron concentration, and spectral index, on plutonium production and cross-section variations. The study demonstrates that environmental factors, including the presence of neighbouring assemblies and control rods, significantly alter local neutron spectra, thus affecting fuel depletion and isotopic composition. The validation phase employs APOLLO3[®] calculations to benchmark SCIENCE V2 results, confirming the model's capability to capture spectral history effects with high fidelity. This research provides a refined methodology for improving nuclear data processing, enhancing reactor safety, and operational efficiency.

Chapter 1

Introduction

A nuclear reactor is a complex system in which several phenomena take place and interact with each other. From an engineering perspective, it is necessary to take these interactions into account and identify the best way to address such interdisciplinarity. Neutronics represents the central aspect in the study and design of a reactor, as it describes power generation.

The reaction rate that drives power generation depends on several factors, such as the material and the neutron population. The latter is governed by the Boltzmann equation, also known as the transport equation, while the evolution of isotope concentrations is described by the Bateman equations. Reactors operate through self-sustained chain reactions, in which fissions trigger further fissions.

To solve the Boltzmann equation and the Bateman equation, it is necessary to choose the most suitable approach for the reactor under study. Two approaches are possible: deterministic and statistical, the latter based on the Monte Carlo Method. Furthermore, one must consider the simplifications introduced in the resolution of the equations. Indeed, a detailed 3D simulation of a reactor is computationally expensive and incompatible with working times. It is therefore essential to ensure that each model is both robust and faithful to the actual neutronics of the reactor.

Reactor multiphysics is a key aspect, since the reactor is heterogeneous and exhibits different thermal-hydraulic conditions. Even at the assembly level, differences arise due, for example, to the choice of uranium enrichment or their positioning within the core. To address such complexities, a computational system capable of handling both heterogeneities and time constraints is required.

In particular, with reference to the deterministic method, this goal can be achieved through the so-called two-step approach. It involves:

- First step: resolution of the transport equation on a basic pattern of the core. This is a 2D simulation, specifically on an infinite medium, which allows the extraction of neutronic characteristics (for example, macroscopic cross sections) that are homogenized and condensed. Homogenization refers to space, while condensation refers to energy, depending on the number of groups chosen. This significantly reduces the amount of data.
- Second step: 3D simulation of the core by solving the diffusion equation. In this case, the homogenized and condensed cross sections obtained in the first step are used.

Nevertheless, this approach also presents limitations.

1.1 Thesis Objective and Structure

This thesis is the subject of my six-month internship at FRAMATOME, mainly focused on the SCIENCE V2 package. In particular it is based on the two step method, a 2D assembly calculation is performed by APOLLO2-F code and the core calculation is performed by SMART code. The objective is to investigate and validate the generation of homogenized cross sections obtained in the first step. The project stems from the need to verify that, although the conditions of the assemblies and the reactor are not known a priori, the model that generates the homogenized cross sections is reliable. Since the core conditions are not known a priori, the cross sections are prepared by exploring the phase space. In the case of burnup, however, this approach is too complex to be applied. To overcome this difficulty, the assembly is evolved under fixed conditions, chosen to be as close as possible to the average conditions of the core, with the expectation that the reactor behavior will follow the predicted trend. This model is called the Spectral History Model. The case study considered is the Taishan reactor. Only the first cycle will be studied. Moreover, with the use of the new APOLLO3® code, it will be possible to complete the final validation phase. The structure of the thesis will be as follows:

- Chapter "Theoretical Background": This chapter describes the fundamental principles of neutron physics, their interactions with matter, and the Boltzmann transport equation for neutrons. It also introduces the multigroup theory, which is useful for energy discretization in numerical modeling.
- Chapter "Industrial Reactor Simulation": This chapter presents the two-step method
 for core calculation, including the lattice calculation and the full-core calculation.
 Topics such as neutron slowing-down, resonance self-shielding, isotopic depletion,
 and steady-state neutron diffusion are addressed, with particular attention to multiparametrized homogenized cross-section tables and the limitations of the method.
- Chapter "History Effects in PWR Modelling": This chapter presents a sensitivity analysis of the neutron spectrum under different conditions, with a particular focus on its impact on isotopic concentrations. Special attention is given to the literature, the development of the history model, and the interpolation parameters with their performance. An introduction to multiparametrized libraries and the history model in SCIENCE V2 is also provided.
- Chapter "Data Analysis": The main objective of this chapter is to study the Taishan reactor and the evolution of its assemblies during the first cycle.
- Chapter "Validation": A set of nodes in the reactor is selected, chosen according to specific characteristics of interest. For these nodes, the spectral history model is applied as implemented in SCIENCE V2 and compared with the depletion of the nodes under real conditions using APOLLO3[®].

Chapter 2

Theoretical background

Neutronics, also known as neutron physics, is the study of how neutrons interact with matter, the conditions necessary to maintain a chain reaction, and the alterations in matter's composition induced by nuclear reactions [1]. It plays a crucial role in the design and operation of nuclear reactors and fuel cycle facilities. Using data from the atomic world (i.e., interactions between neutrons and atomic nuclei) to compute quantities such as reactor's power, neutronics fills a gap between the microscopic and the macroscopic worlds. Neutronics span on time, space, and energy scales that are very different from each other and extending over more than a dozen orders of magnitude.

The rapid growth of computing resources is reshaping traditional experimental paradigms, significantly enhancing the potential of numerical simulations for reactor design and operation. Different challenges have to be addressed as the coupling between neutronics and the thermohydraulic behavior of the reactor. In this chapter, some fundamental concepts for the description of physics inside a nuclear fission reactor will be presented. To predict the distribution of neutrons within the space, the Boltzmann equation adapted to neutron transport and interaction with the matter is employed. Subsequent sections will explore various simplifications of this equation to facilitate practical calculations and simulations within reactor systems.

2.1 Neutrons and interaction with the matter

The neutron, which was hypothesized to be one of the constituents of the atomic nucleus, was discovered by James Chadwick in 1932 during an experiment involving the bombardment of a beryllium target with an alpha particle emitted by a radioactive material. Neutrons are electrically neutral, and they travel in straight lines until they collide with atomic nuclei. The physics of neutrons led to the development of the so-called neutronics, which aims to describe how neutrons interact with matter [1]. These interactions differ in nature and are associated with different probabilities of occurrence. Neutrons may interact with nuclei in one of the following ways: capture, fission, elastic scattering, and inelastic scattering. The stochastic behavior of these events is described using the concept of macroscopic cross section Σ , which represents the probability of a specific interaction occurring per unit length and its unit is $[cm^{-1}]$.

Conversely, the microscopic cross section, usually denoted by σ , represents the effective target area of a single nucleus for an incoming neutron, with units of [barn] or [cm²]. A barn is defined as 1 barn = 10^{-24} cm².

For example, if surface A [cm²] and s [cm] are the dimensions of a wall, N [nuclei/cm³] is

the number density of nuclei, and a flux of neutrons passes through it, then the probability of a collision occurring can be estimated as the ratio between the total effective volume of target particles and the total volume of the wall [2].

$$\frac{NA_s\sigma_x}{A_s} = N\sigma_x = \Sigma_x \tag{2.1}$$

These microscopic data arising are necessary to calculate macroscopic quantities. One of the difficulties in neutronics is to consider all the complex variations in microscopic cross section in relation with energy [1]. As previously mentioned, neutrons can undergo various types of interactions. The most significant among them are absorption and scattering. The total macroscopic cross section is defined as the sum of the probabilities per unit length for absorption and for scattering events.

$$\Sigma_t(r, E, \Omega) = \Sigma_a(r, E, \Omega) + \Sigma_s(r, E, \Omega)$$
(2.2)

From eq. [2.2] it's possible to notice that the macroscopic cross sections depend on the position, the direction and of the energy of the neutron that collides on the target. In the majority of the industrial cases the material is considered as isotropic so the dependency on Ω can be considered negligible.

In particular, it is possible to make an additional distinction:

$$\Sigma_a(\vec{r}, E) = \Sigma_c(\vec{r}, E) + \Sigma_f(\vec{r}, E) \tag{2.3}$$

A neutron that is absorbed can be simply captured or a fission event may occur. If the neutron is not absorbed by a nucleus of the background material, it is deflected and their energy and direction change, the scattering probability is possible to define as the sum of the elastic and inelastic scattering:

$$\Sigma_s(\vec{r}, E) = \Sigma_e(\vec{r}, E) + \Sigma_i(\vec{r}, E) \tag{2.4}$$

Since neutron interactions are governed by probabilistic laws, it is useful to introduce statistical tools to describe the behavior of a large number of particles. Let x denote as a generic variable of interest and its probability density function P(x), which provides a mathematical framework for quantifying the likelihood of different outcomes, it satisfies the normalization condition:

$$<1> = \int_{D} dx P(x) = 1$$
 (2.5)

where D in the domain of interest. Given any function f(x), its mean value E(x) with respect to the probability density function is defined as

$$E[x] = \int_{D} dx f(x) P(x) \tag{2.6}$$

For the scattering collision it is also important to define the probability of a neutron with an initial energy E' and direction Ω' to being re-emitted after a scattering event, in a certain cone $d\Omega$ with the energy in the range of (E, E+dE).

$$f_s(\vec{r}, E' \to E, \vec{\Omega}' \to \vec{\Omega})$$
 (2.7)

In particular, in an isotropic medium, probability does not depend on the incoming direction of the neutron but just on the angle between the directions. The most useful property of the probability density function is that if an integral over all the energies and

directions is performed, the result will be 1 (normalization condition).

$$\oint_{4\pi} \int_{E} f_s(\vec{r}, E' \to E, \vec{\Omega}' \to \vec{\Omega}) d\Omega dE = 1$$
(2.8)

2.2 Integro-differential Boltzmann equation: neutron transport

The Boltzmann equation describes the statistical behavior of a gas of particles and the time evolution of their probability distribution function in statistical mechanics. The neutron population in a nuclear reactor can be considered analogous to an ideal gas because neutron-neutron interactions are negligible. This is due to the relatively low neutron density, typically in the range of $\left[10^{12};10^{15}\right]$ neutrons/cm³, which is much lower than the atomic density of solid materials ($\approx 10^{24}$ particles/cm³, i.e., Avogadro's number). As a result, neutrons interact predominantly with the reactor materials rather than with each other. For this reason, the Boltzmann equation is well suited to simulate neutron transport physics in a reactor, complementing the Bateman equations that describe nuclide transmutation and decay.

2.2.1 Phase space

The solution of the neutron transport equation requires a formal description of the space in which neutrons are moving. The direction of a moving particle in three dimensional (3D) domain is represented by its solid angle, a unit vector pointing in the direction of the particle. The vector velocity $\vec{V_n}$ of the particle is written in terms of its solid angle as 3:

$$\vec{V_n} = V_n \vec{\Omega} \tag{2.9}$$

where

$$V_n = |\vec{V_n}| \ and \ |\vec{\Omega}| = 1$$
 (2.10)

In particular, the position of a neutron is denoted by the vector $\vec{r} = (x, y, z)$ and the direction of the flight is indicated by $\vec{\Omega}$. In Fig. 2.1 $\vec{\Omega}$ represents a point on the surface of a unit radius sphere surrounding the neutron, indicating the direction of motion, $d\Omega$ is noted as infinitesimal solid angle.

The $\vec{\Omega}$ can be decomposed by its components:

$$\begin{cases}
\vec{\Omega} = \Omega_x \vec{i} + \Omega_y \vec{j} + \Omega_z \vec{k} \\
\Omega_x^2 + \Omega_y^2 + \Omega_z^2 = 1
\end{cases}$$
(2.11)

One of the possible coordinates that can be used are the spherical, in which the polar angle is indicated by θ and the azimuthal by φ .

$$\begin{cases} \Omega_x = \sin(\theta)\cos(\varphi) = \sqrt{1 - \mu^2}\cos(\varphi) \\ \Omega_y = \sin(\theta)\sin(\varphi) = \sqrt{1 - \mu^2}\sin(\varphi) \\ \Omega_z = \cos(\theta) = \mu \end{cases}$$
 (2.12)

That is

$$\vec{\Omega} = \sqrt{1 - \mu^2} cos(\varphi) \vec{i} + \sqrt{1 - \mu^2} sin(\varphi) \vec{j} + \mu \vec{k}$$
 (2.13)

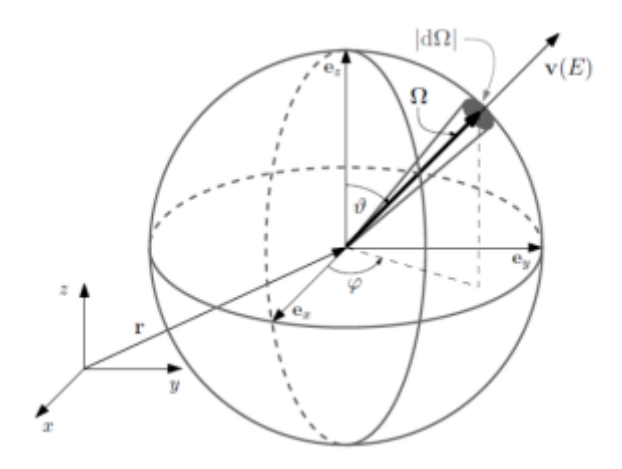


Figure 2.1: Cartesian reference system [4]

The neutron kinetic energy is therefore linked to the neutron speed by the classical formula:

$$E = \frac{1}{2}mV_n^2 \tag{2.14}$$

Finally it is possible to define the phase-space as $(\vec{r}, \vec{\Omega}, E)$, a system of six independent variables that describes the neutron motion at time t.

2.2.2 Total neutron balance

The transport equation considers the net number of neutrons within a infinitesimal phasespace during a Δt , therefore, it is a neutron balance in a selected volume:

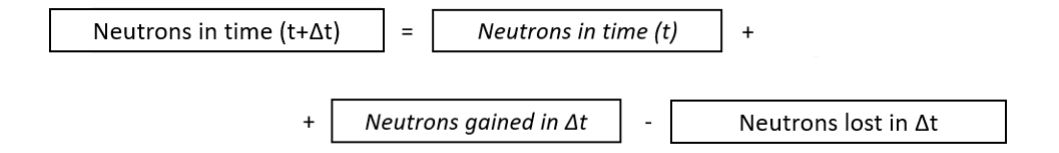


Figure 2.2: Neutron balance

In reactor physics, neutron populations undergo a statistical treatment. They are described using the notion of neutron density $n(\vec{r}, E, \vec{\Omega}, t)$, which stands for the average number of neutrons observed per unit volume, energy, radiant and time. However, this neutron density is a more general notion than the usual notion of density, for the elementary volume to be considered is not only a volume in physical space. The product by total distance traveled by neutrons and the macroscopic cross-section for a given interaction 'x' gives the number of the interactions in elementary volume during a time interval.

$$n(\vec{r}, E, \vec{\Omega}, t) dr dE d\Omega v dt \Sigma_x \tag{2.15}$$

The product of the neutron density function and the speed define the angular flux ϕ :

$$\phi(\vec{r}, E, \vec{\Omega}, t) = n(\vec{r}, E, \vec{\Omega}, t)v \tag{2.16}$$

By integrating over a defined volume in the phase space, it is possible to evaluate the total number of "x" interactions.

$$\oint_{V} \int_{E} \phi(\vec{r}, E, \vec{\Omega}, t) \Sigma_{x} \, d\vec{r} \, dE \, d\vec{\Omega} \, dt \tag{2.17}$$

Finally, the integro-differential form of the Boltzmann transport equation can be written in its mathematical form:

$$\frac{1}{v}\frac{\partial}{\partial t}\phi(\vec{r},E,\vec{\Omega},t) = -\nabla \cdot (\vec{\Omega}\phi(\vec{r},E,\vec{\Omega},t)) - \Sigma_{t}(\vec{r},E)\phi(\vec{r},E,\vec{\Omega},t)
+ \oint d\Omega' \int dE' \Sigma_{s}(\vec{r},E')\phi(\vec{r},E',\vec{\Omega'},t)f_{s}(\vec{r},E'\to E,\vec{\Omega'}\to\vec{\Omega})
+ \oint d\Omega' \int dE' (1-\beta)\nu(\vec{r},E')\Sigma_{f}(\vec{r},E')\phi(\vec{r},E',\vec{\Omega'},t)\frac{\chi_{p}(\vec{r},E)}{4\pi}
+ \frac{\chi_{d}(\vec{r},E)}{4\pi} \sum_{i=1}^{R} \lambda_{i}C_{i}S(\vec{r},E,\vec{\Omega},t)$$
(2.18)

Six terms are involved in this balance:

- (a) The first term is the variation of the neutron density between (t, t + dt).
- (b) The second is the streaming term, net balance of entering and exiting neutrons in the infinitesimal phase-space within the interval dt.
- (c) The third term is the removal term, which accounts for scattering and absorption. Scattering phenomena shift neutrons to different energies and directions, while absorption causes neutrons to disappear within the elementary time interval dt.
- (d) The fourth is the scattering term, it is a result of those neutrons that comes from other collisions. They had a previous energy and direction (E', Ω') and after the collision they arrive in the domain in which the balance is applied (E, Ω) . The probability of these neutrons to have scattering is given by the macroscopic cross sections Σ_s , the probability of those neutrons to have scattering and then enter into the phase space is represented by the probability density functions f_s .
- (e) The fifth and sixth term considers respectively the contribution of the prompt neutrons and the delayed neutrons therefore all the neutrons that comes from fission phenomena. In the delayed neutrons term R represents the families of precursors and C is the atomic density of the delayed neutron precursors. For each fissionable nuclide, the energy of emitted neutrons is distributed according to a probability density known as fission spectrum $\chi(E)$. The quantity $\chi(E)dE$ is the probability for an emitted neutron to have an energy equal to E (within the interval dE). The statistical information of a neutron to do fission is given by Σ_f . The fission spectrum is the probability of a neutron to be emitted in the phase space, ν is the average number of neutrons emitted by a spontaneous fission. The normalization condition is:

$$\int_0^{\inf} dE \chi(E) = 1 \tag{2.19}$$

(f) The last is the general source term.

For steady-state condition, the equation of the particle balance is written removing the dependence on time and the first term.

$$\nabla \cdot (\vec{\Omega}\phi(\vec{r}, E, \vec{\Omega})) = -\Sigma_{t}(\vec{r}, E)\phi(\vec{r}, E, \vec{\Omega})$$

$$\oint d\Omega' \int dE' \Sigma_{s}(\vec{r}, E')\phi(\vec{r}, E', \vec{\Omega}') f_{s}(\vec{r}, E' \to E, \vec{\Omega}' \to \vec{\Omega})$$

$$+ \oint d\Omega' \int dE' \nu(\vec{r}, E') \Sigma_{f}(\vec{r}, E')\phi(\vec{r}, E', \vec{\Omega}') \frac{\chi(\vec{r}, E)}{4\pi}$$

$$+ S(\vec{r}, E, \vec{\Omega})$$
(2.20)

2.2.3 Critical equation - Introduction of the effective multiplication factor

A system containing fissile material is critical if the chain reaction is self-sustaining in time in absence of an external source. Neutrons inserted in this system after sufficient time reach an asymptotic conditions in which losses are equal to neutrons producing by fission. If this condition is not reached then the distribution can increase (supercritical system) or decrease (subcritical system) exponentially in time. The presence of an external source will provoke an increasing of the neutron flux distribution in case of a critical or supercritical system. On the other hand if in a system subcritical it is introduce a source, it may reach the equilibrium state. From the mathematical point of view to get a physical solutions of the criticality problem, the eq. [2.20] is modified introducing a factor inside the fission term to be able to reach the equilibrium between production and losses. This factor is the eigenvalue of the equation and it is known as the effective multiplication factor.

$$\nabla \cdot (\vec{\Omega}\phi(\vec{r}, E, \vec{\Omega})) = -\Sigma_{t}(\vec{r}, E)\phi(\vec{r}, E, \vec{\Omega})$$

$$\oint d\Omega' \int dE' \Sigma_{s}(\vec{r}, E')\phi(\vec{r}, E', \vec{\Omega}') f_{s}(\vec{r}, E' \to E, \vec{\Omega}' \to \vec{\Omega})$$

$$+ \frac{1}{k_{eff}} \oint d\Omega' \int dE' \nu(\vec{r}, E') \Sigma_{f}(\vec{r}, E')\phi(\vec{r}, E', \vec{\Omega}') \frac{\chi(\vec{r}, E)}{4\pi}$$
(2.21)

where k_{eff} is defined as:

$$k_{eff} = \frac{\text{Numbers of neutrons in one generation}}{\text{Number of neutrons in the previous generation}}$$
 (2.22)

Three possible physical situation in a reactor:

$$\begin{cases} k_{eff} < 1 & \text{(Sub-critical reactor)} \\ k_{eff} = 1 & \text{(Critical reactor)} \\ k_{eff} > 1 & \text{(Super-critical reactor)} \end{cases}$$
 (2.23)

The equation 2.21 will be used in the following chapter to explain the multigroup formalism that is adopted in the majority of industrial applications.

2.3 Multigroup Theory

The multigroup theory is a very useful method based on the treatment of energy dependence. It is particularly effective when modeling systems such as a thermal reactor (e.g. PWR),

where thermal neutrons have a high probability of causing fission, and fast neutrons are generated. The energy range of fast neutrons is typically in the MeV range, and they slow down by scattering within the medium. As they lose energy, they eventually reach the thermal energy range, which spans from about eV to $10^{-2}eV$. On the other hand, neutrons spectrum of fast reactors behaves differently. Before going into the details of energy domain discretization, the scattering term must first be rearranged.

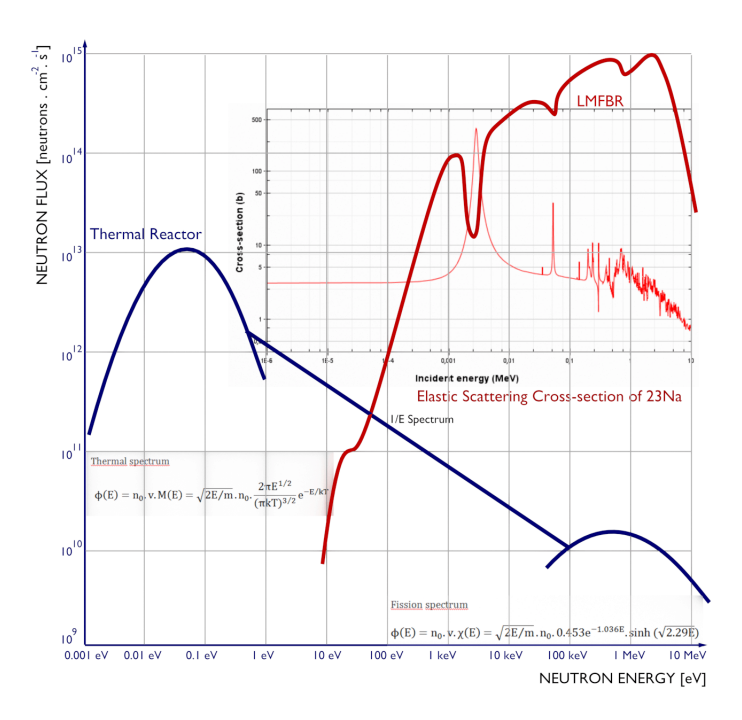


Figure 2.3: Thermal and fast neutron spectrum [5]

2.3.1 Expansion of the Scattering Function using spherical harmonics

Mostly of the discussion in this chapter is given concerning the plane geometry but all the treatment can be applied also to a generic geometry. From eq. 2.20 is considering the scattering term, in particular, on the angular behavior of the probability density function. In general the probability density function depends on the direction of the flight before the scattering phenomena and on the direction of the new flight but if the medium is isotropic the probability density function will depend on μ_0 , cosine of the deflection angle θ_0 between Ω ' and Ω .

$$f_s(\vec{r}, E' \to E, \vec{\Omega}' \to \vec{\Omega}) = f_s(\vec{r}, E' \to E, \vec{\Omega}' \cdot \vec{\Omega}) = f_s(\vec{r}, E' \to E, \mu_0)$$
 (2.24)

$$\mu_0 = \cos(\theta) \tag{2.25}$$

The output of the scalar product of Ω and Ω' belongs in the interval [-1, 1], the next step is to split the dependence of fs on the scalar product using the Legendre polynomials, the series representation, and the spherical harmonics. The Legendre polynomials, in mathematics, are a system of orthogonal and complete set of polynomials.

The spherical harmonics are eigenfunctions of Helmholz, a complete and orthogonal series of functions. Considering the direction Ω and Ω' they are defined as:

$$Y_n^{\beta} = \left(\frac{2n+1}{4\pi} \frac{(n-\beta)!}{(n+\beta)!}\right)^{\frac{1}{2}} P_n^{\beta} e^{i\beta\varphi}$$
 (2.26)

The adjoint spherical harmonics is the complex conjugate:

$$Y_n^{\beta*} = \left(\frac{2n+1}{4\pi} \frac{(n-\beta)!}{(n+\beta)!}\right)^{\frac{1}{2}} P_n^{\beta} e^{-i\beta\varphi}$$
 (2.27)

Since μ_0 belongs in [-1,1] the Legendre polynomials can be used.

$$\sum_{n=0}^{\inf} \frac{2n+1}{2} f_n(\vec{r}, E' \to E) P_n(\vec{\Omega'} \cdot \vec{\Omega})$$
 (2.28)

The dependency on the angle is now factorized, $f_n(\vec{r}, E' \to E)$ is obtain by the projection of $f_s(r, E' \to E, \Omega' \cdot \Omega)$. At this point, it is split in different parameters the dependency on Ω' and Ω , to obtain it the Legendre associated functions are used.

$$P_n(\vec{\Omega'} \cdot \vec{\Omega}) = P_n(\mu_0) = \sum_{\beta = -n}^n \frac{(n-\beta)!}{(n+\beta)!} P_n^{\beta}(\mu) P_n^{\beta}(\mu') e^{i\beta\varphi} e^{-i\beta\varphi'}$$
(2.29)

$$\sum_{n=0}^{\infty} \frac{2n+1}{2} f_n(\vec{r}, E' \to E) \sum_{\beta=-n}^{n} \frac{(n-\beta)!}{(n+\beta)!} P_n^{\beta}(\mu) P_n^{\beta}(\mu') e^{i\beta(\varphi-\varphi')} = \sum_{n=0}^{\infty} \sum_{\beta=-n}^{n} 2\pi f_n(\vec{r}, E' \to E) Y_n^{\beta}(\vec{\Omega}) Y_n^{\beta*}(\vec{\Omega}')$$
(2.30)

The scattering term becomes:

$$\int dE' \sum_{n} \sum_{\beta} 2\pi f_n(\vec{r}, E' \to E) Y_n^{\beta}(\vec{\Omega}) \Sigma_s(\vec{r}, E') \oint d\Omega' Y_n^{\beta*}(\vec{\Omega}') \phi(\vec{r}, E', \vec{\Omega}')$$
 (2.31)

In eq. 2.31 different quantities are defined:

1. Moments of the angular flux:

$$\phi_n^{\beta}(\vec{r}) = \oint d\Omega' \, Y_n^{\beta*}(\vec{\Omega'}) \phi(\vec{r}, E', \vec{\Omega'})$$

2. Moments of the scattering probability density function of a neutron to be deflected in a certain angle, integrating over the azimuthal angles around the direction of $\vec{\Omega}'$:

$$\eta_n(\vec{r}, E' \to E) = 2\pi f_n(\vec{r}, E' \to E)$$

3. Moments of the scattering transfer cross section:

$$\Sigma_n(\vec{r}, E' \to E) = \Sigma_s(\vec{r}, E') \eta_n(\vec{r}, E' \to E)$$

The transport equation without considering the fission term:

$$\nabla \cdot (\vec{\Omega}\phi(\vec{r}, E, \vec{\Omega})) + \Sigma_t(\vec{r}, E)\phi(\vec{r}, E, \vec{\Omega}) = \sum_{n=0}^{\infty} \sum_{\beta=-n}^{n} \int dE' \Sigma_n(\vec{r}, E' \to E) \phi_n^{\beta}(\vec{r}, E') Y_n^{\beta}(\vec{\Omega}) + S(\vec{r}, E, \vec{\Omega})$$

$$(2.32)$$

2.3.2 Energy groups

The domain of the energy variable is continuous and it is defined between few eV to some MeV. The first step in the multigroup formalism is to divide the neutron energy range in defined sub-intervals, G, separated by the energies E_g , where g=1,2,...,G, as reported in Fig. 2.4 Each sub-interval is called group and the conventional nomenclature is that for an increasing g, the value of the energy will decrease, e.g. $E_{(g)} > E_{(g+1)}$. Consequently, the usual strategy is to solve the transport equation for group 1, 2 and so on. For an accurate resolution of the equation several groups have to be chosen, but in the case of modeling PWR an energy mesh with 2 groups is a common approximation G. The passage from a group to another is given by the changing of cross section of several orders of magnitude, in this case the groups that are considered are thermal and fast neutrons G.

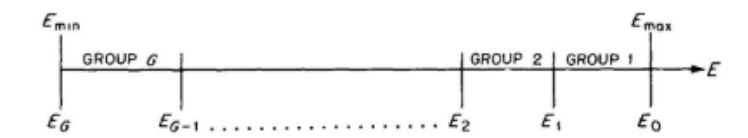


Figure 2.4: Division of neutron energy range into G groups 7

The next step is to integrate the transport equation over the energy groups, the integral over the energy is expressed as the sum of integrals over all the energy groups, i.e.,

$$\int dE' = \sum_{g} \int_{E_g}^{E_{g+1}} dE' \tag{2.33}$$

All the terms will be expressed integrating over the energy.

$$\int_{g} dE \phi(\vec{r}, E, \vec{\Omega}) = \phi_{g}(\vec{r}, \vec{\Omega})$$
(2.34)

$$\int_{q} dE \phi_{n}^{\beta}(\vec{r}, E) = \phi_{n,g}^{\beta}(\vec{r}) \qquad (2.35)$$

$$\int_{g} dE \vec{\Omega} \cdot \nabla \phi(\vec{r}, E, \vec{\Omega}) = \vec{\Omega} \cdot \nabla \phi_{g}(\vec{r}, \vec{\Omega})$$
(2.36)

$$\frac{1}{k} \int_{g} dE \frac{\chi(\vec{r}, E)}{4\pi} \sum_{g'} \oint d\Omega' \int_{g'} dE' \nu(\vec{r}, E') \Sigma_{f}(\vec{r}, E') \phi(\vec{r}, E, \vec{\Omega}') =
\frac{1}{k} \frac{\chi_{g}(\vec{r}, E)}{4\pi} \sum_{g'} \nu_{g'}(\vec{r}) \Sigma_{f,g'}(\vec{r}, \vec{\Omega}) \oint d\Omega' \phi_{g'}(\vec{r}, \vec{\Omega}')$$
(2.37)

$$\int_{g} dE \Sigma(\vec{r}, E) \phi(\vec{r}, E, \vec{\Omega}) = \Sigma_{g}(\vec{r}, \vec{\Omega}) \phi_{g}(\vec{r}, \vec{\Omega})$$
(2.38)

In this last integration the removal term is obtained where a macroscopic cross section collapsing in energy is introduce. The definition over Σ_g is averaging and collapsing, the main idea is to preserve the neutron reaction rate using a weighted spectrum inside its definition.

$$\Sigma_g(\vec{r}, \vec{\Omega}) = \frac{\int_g dE \Sigma(\vec{r}, E) \phi(\vec{r}, E, \vec{\Omega})}{\phi_g(\vec{r}, \vec{\Omega})}$$
(2.39)

The system is no longer isotropic, it becomes anisotropic, in fact, inside the definition there is the dependency on the direction. Average XS are not nuclear data and must be calculated and defined for each application, they depend on the flux approximation. The weighted function to generate averaging of the cross section is unknown but the flux distribution according to energy range is well known.

Also, the scattering term has to be integrated over dE and multiplied by $\frac{\phi_{n,g'}^{\beta}(\vec{r})}{\phi_{n,g'}^{\beta}(\vec{r})}$:

$$\int dE \sum_{n} \sum_{\beta} \underbrace{\sum_{g'} \int dE'}_{\int dE'} \oint d\Omega' \Sigma_{n}(\vec{r}, E' \to E) \phi_{n}^{\beta}(\vec{r}, E') Y_{n}^{\beta}(\vec{\Omega}) \frac{\phi_{n,g'}^{\beta}(\vec{r})}{\phi_{n,g'}^{\beta}(\vec{r})}$$
(2.40)

Here the definition of the energy transfer matrix is given:

$$\frac{\int_{g} dE \int_{g'} dE' \Sigma_{n}(\vec{r}, E' \to E) \phi_{n}^{\beta}(\vec{r}, E')}{\underbrace{\phi_{n,g'}^{\beta}(\vec{r})}_{f,g'}} = \Sigma_{n,g' \to g}(\vec{r}) \tag{2.41}$$

Hence, the complete multi-group steady-state transport equation is:

$$\vec{\Omega} \cdot \nabla \phi_g(\vec{r}, \vec{\Omega}) + \Sigma_g(\vec{r}) \phi_g(\vec{r}, \vec{\Omega}) =$$

$$\sum_n \sum_{\beta} \sum_{g'} \Sigma_{n,g' \to g}(\vec{r}) \phi_{n,g'}^{\beta}(\vec{r}) Y_n^{\beta}(\vec{\Omega}) +$$

$$\frac{1}{k} \frac{\chi_g(\vec{r}, E)}{4\pi} \sum_{g'} \nu_{g'}(\vec{r}) \Sigma_{f,g'}(\vec{r}, \vec{\Omega}) \oint d\Omega' \phi_{g'}(\vec{r}, \vec{\Omega}')$$
(2.42)

Chapter 3

Industrial Reactor Simulation

Simulating the reactor core means solving the transport equation for all the length scales present within it, from the fuel pellet to the diameter of the core. In an industrial application, the situation is more complex, as the core is heterogeneous, with varying thermodynamic conditions, different length scales, and several hundred fuel assemblies. All of these features must be simulated using computational tools designed to minimize computational effort. A direct calculation of the neutron flux distribution using an appropriate discretization in space and energy requires a huge computational effort and significant time. This is particularly challenging since the transport equation must be solved for orders of magnitude of millimeters and electron volts, while also accounting for the thermo-hydraulic behavior in both axial and radial directions. Furthermore, each assembly has a different configuration and undergoes different depletion processes, even under the same conditions. The main concepts presented in this chapter are taken from [3].

3.1 Two-step calculation

Considering that in industrial applications it is necessary to perform core simulations in different configurations, it is crucial to solve the transport equation for the full core in a reasonable amount of time. The resolution of the transport equation is generally very complex and involves two different approaches. The first method is the Monte Carlo approach, which is recognized as the most accurate technique for neutron transport simulations. However, full-core Monte Carlo simulations remain computationally prohibitive, especially when applied to feedback calculations and depletion analyses. In this method, a large number of particles are simulated using random variables. Usually, a continuous-energy or multigroup representation of the cross sections is considered. The second approach is the deterministic method, where the transport equation is solved without random variables, but instead involves numerical techniques with different spatial and energy approximations. The multigroup approach is typically used in this case, since millions of full core flux calculations must be performed during a standard neutronics design study.

The standard industrial approach, in this context, is the two-step calculation scheme, which is widely used for core modeling and design. It provides sufficient accuracy, and fast computation. This approach is based on homogenization theory to simplify and reduce the size of the full reactor problem. It consists of separating the micro-scale from the macro-scale by performing two distinct calculations: lattice using a fine mesh and core calculations using a coarse mesh. From the first step, multiparameterized libraries are generated, containing equivalence factors and homogenized macroscopic and microscopic cross sections (HXS),

which are then used in the second step. In addition, a library has to be generated in which different values of cross sections are collected. These values are retrieved through several calculations considering that actual reactor conditions are not known a priori. Once the conditions in the reactor are known the corresponding values of the cross sections are obtained, generally through some kind of interpolation. The libraries are constructed by changing the characterizing values, in order to cover all possible conditions that will be encountered in the reactor simulation. In this way In the following sections, these two steps will be discussed in more detail.

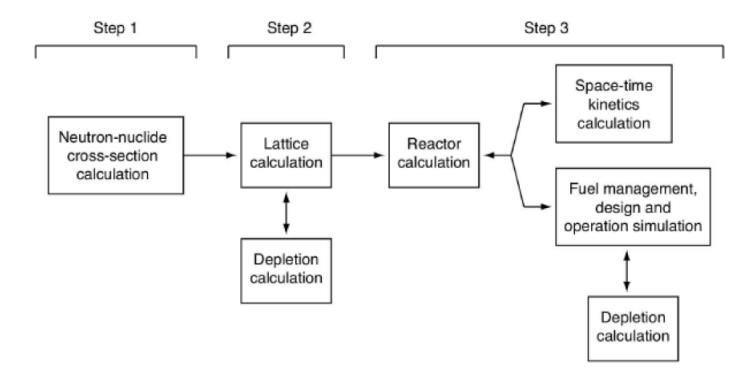


Figure 3.1: Global calculation scheme [3]

_

3.2 Lattice Calculation

The first step consists in a 2D resolution of the transport equation just for one geometry assembly considering the multigroup formalism. It is therefore usual to assume that the surrounding components are identical for the one being processed, the assembly is repeated to the infinity.

- Library access: The main goal of this step is to recover all the isotropic data from the cross sections libraries that will be used in the calculation. All this data vary as \sqrt{T} and they are interpolated in absolute temperature T. After that the data are ready to be use in the self-shielded and depleting mixture.
- Resonance self-shielding calculation: this step is needed in the context of the weighting flux depression considering cases where an energy group g contains many resonance in cross section.
- Neutron flux calculation: in this module the neutron flux over all the group structure of the library is provided, in particular the algorithm involved is the S_n method coupled with collision probability method (P_{ij}) although some recent lattice codes use the characteristic method. The neutron flux is computed using a leakage calculation.
- Collapse and homogenization of cross sections: Given the coarse mesh requirements
 of the core-level calculations, this module plays a crucial role in the context of this
 thesis. The collapsed and homogenized cross sections are computed to preserve the
 reaction rates. Furthermore, this process represents one of the key approximations in
 the two-step method.

• Isotopic depletion: in this module the isotopic depletion calculation is described, solving the Bateman equations taking into account the in-core and out-core depletion of every material selected from the isotopic cross-section library. This step permits to calculate the isotopic density in different conditions of different isotopes present in the reactor.

3.2.1 Neutron slowing-down and resonance self shielding

In the first chapter was explained how the particles can interact with the matter, different phenomena can occur and one of them is the slowing down of the particles due to these collisions. Let's consider scattering phenomena, which can be either elastic, when both momentum and energy are conserved, or inelastic, when a gamma ray is emitted and the secondary particle remains in an excited state. A neutron will lose a large fraction of its initial energy during an inelastic scattering reaction. It is state that this secondary type of collision only occur at high neutron energies and with relatively small probability. It is possible to conclude that the primary way to slowing the particle is the elastic scattering. It is important to remember that the parameter that measures the neutron slowing down is the lethargy and it is calculated as:

$$u = \ln(\frac{E_0}{E}) \tag{3.1}$$

where E_0 is the maximum energy of all neutrons in the reactor. Another important quantity to describe this phenomena is the maximum lethargy gain, defined as:

$$\epsilon = \frac{0}{\alpha} \tag{3.2}$$

where

$$\alpha = \left(\frac{A-1}{A+1}\right)^2 \tag{3.3}$$

where A is the atomic mass ratio, the ratio of the nucleus mass over the neutron mass. The slowing down is more important when are involved light nuclides as they have a smaller value of α . A neutron loses a fraction of its initial energy after each collision, if E in the initial energy and E' is the energy after the collision:

$$P_e(E \to E') = \frac{1}{(1 - \alpha)E} \tag{3.4}$$

Finally is possible to write the transport equation that is involved in this step considering the slowing down effect and the fission term.

$$\Omega \cdot \nabla \phi(\vec{r}, u, \Omega) + \Sigma(\vec{r}, u)\phi(\vec{r}, u, \Omega) = \frac{1}{4\pi} \left[S_f(\vec{r}, u) + \sum_{j=1}^J R_j \phi(\vec{r}, u) \right]$$
(3.5)

In the equation a new operator is introduce $R_j\phi(\vec{r},u)$ as the elastic slowing-down operator of the isotope j.

$$R_j \phi(\vec{r}, u) = \int_0 du' \Sigma_{s0,j}(\vec{r}, u' \to u) \phi(\vec{r}, u')$$
(3.6)

where $\Sigma_{s0,j}$ is the zeroth Legendre moment of the differential scattering cross section. In this step an isotropic approximation is considered since a more exact representation is considered in module of neutron flux calculation. Moreover, light isotopes are involved in

the slowing down phenomena but are not involved in the absorption phenomena. On the other hand heavy isotopes are the largest cause of absorption in resonant absorption. This is strictly correlated to the energy self-shielding phenomena where is observed a neutron flux depression due to the increasing of the absorption cross section so the rate of absorption decreases if compared with the other regions in energy domain. The correct solution of this problem is to use a fine mesh in energy of each resonance but in the case of heavy isotopes this will required thousand of regions, making the calculation too much expensive. This point is very delicate because is strictly correlated to the computing of homogenized cross section which depends indeed on the reaction rates.

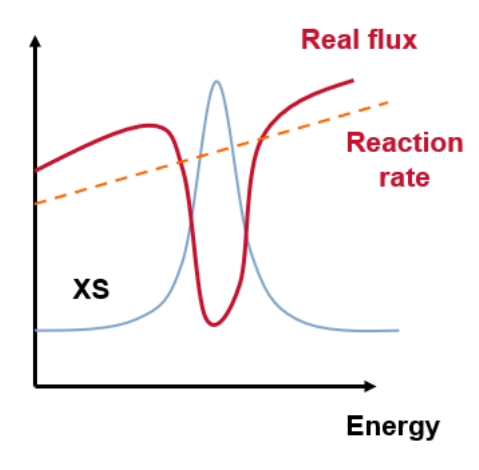


Figure 3.2: Depression of the neutron flux in resonance region

3.2.2 The neutron leakage model

The lattice calculation solves the transport equation in the frame of the assembly point of view, imposing the reflection and translation at the boundaries. The leakage model is the main algorithm use to consider all the leakage in the axial and radial directions that are not included in the boundary conditions, it depends on two different factor:

- Anisotropicity of scattering.
- Effects due to heterogeneity of the lattice.

In assembly calculations, an infinite lattice of repeated assemblies is assumed, which means that no information about the surrounding core environment is taken into account. In a real situation, inside the core there are different assemblies with different enrichment. In core calculation the core is critical $(k_{eff}=1)$ and over-reactive assemblies (fresh ones) gives neutron to less reactive assemblies (burn ones). It requires a dedicated treatment to account for the spatial leakage in the spectral code: flux spectrum must be modified before XS weighting. The assumptions are to consider critical conditions: each assembly is under steady-state conditions that means $k_{eff}=1$ and homogeneous in space.

- The flux is calculated for each assembly and it is solved considered reflective boundaries as it is done for the self-shielding model.
- The leakage model is introduced forcing the effective multiplication factor to one in the assembly, considering the neuron flux as:

$$\phi(\vec{r}, E, \vec{\Omega}) = \psi(\vec{r})\varphi(\vec{r}, E, \vec{\Omega}) \tag{3.7}$$

where $\psi(\vec{r})$ is the macroscopic distribution in space which represents an asymptotic curvature distribution for all the energies and directions and $\varphi(\vec{r}, E, \vec{\Omega})$ is the periodic flux or homogeneous flux.. This is *called fundamental approximation*. It is assumed that the macroscopic distribution is the solution of a Laplace equation:

$$\nabla^2 \psi(\vec{r}) + B^2 \psi(\vec{r}) = 0 \tag{3.8}$$

In this equation a new quantity is introduce, the buckling coefficient B^2 that have to modify the curvature of the distribution in order to get $k_{eff} = 1$. The model that uses the homogeneous mode states that the leakage rates are completely homogenized in each assembly. The generic solutions of the Laplace equation is:

$$\psi(\vec{r}) = \psi_0 e^{i\vec{B}\cdot\vec{r}} \tag{3.9}$$

where \vec{B} is chosen from $B^2 = \vec{B} \cdot \vec{B}$. Retrieving eq. 3.7, the neutron flux is then:

$$\phi(\vec{r}, E, \vec{\Omega}) = \varphi(\vec{r}, E, \vec{\Omega})e^{i\vec{B}\cdot\vec{r}}$$
(3.10)

In the case of the homogeneous fundamental mode the approach is to consider the curvature of the fundamental approximation homogenized in space, in this case the solution is:

$$\phi(\vec{r}, E, \vec{\Omega}) = \varphi(E, \vec{\Omega})e^{i\vec{B}\cdot\vec{r}} \tag{3.11}$$

Moreover, from this module are calculated diffusion coefficients that are mandatory in the second step, in full core calculation where the diffusion equation is solved.

3.2.3 Isotopic depletion

The topic discussed in the following sections is fundamental to the aim of this thesis. The neutron flux changes the isotopic concentration during the power cycle. Different isotopes are present inside the reactor, some of them can be not stable and the law that governs them it is the radioactive decay, the change of the density is the calculated using the *Bateman* equations, coupled systems of the ordinary differential equations, eq. 3.12

$$\frac{\mathrm{d}N_i}{\mathrm{d}t}(\vec{r},t) = -\sum_{k \neq i} \left[\lambda_{ki}^d + \int \phi(\vec{r},E,t) \sigma_{ki}^{tr}(E) \mathrm{d}E \right] N_i(\vec{r},t)
+ \sum_{k \neq i} \left[\lambda_{ik}^d + \int \phi(\vec{r},E,t) \sigma_{ik}^{tr}(E) \mathrm{d}E \right] N_k(\vec{r},t)$$
(3.12)

where:

- N_i is the concentration of isotope i,
- λ_{ki}^d is the decay constant from isotope *i* decays into isotope k [s⁻¹],
- $\sigma_{ik}^{tr}(E)$ is the transmutation cross section from isotope i to an isotope k.

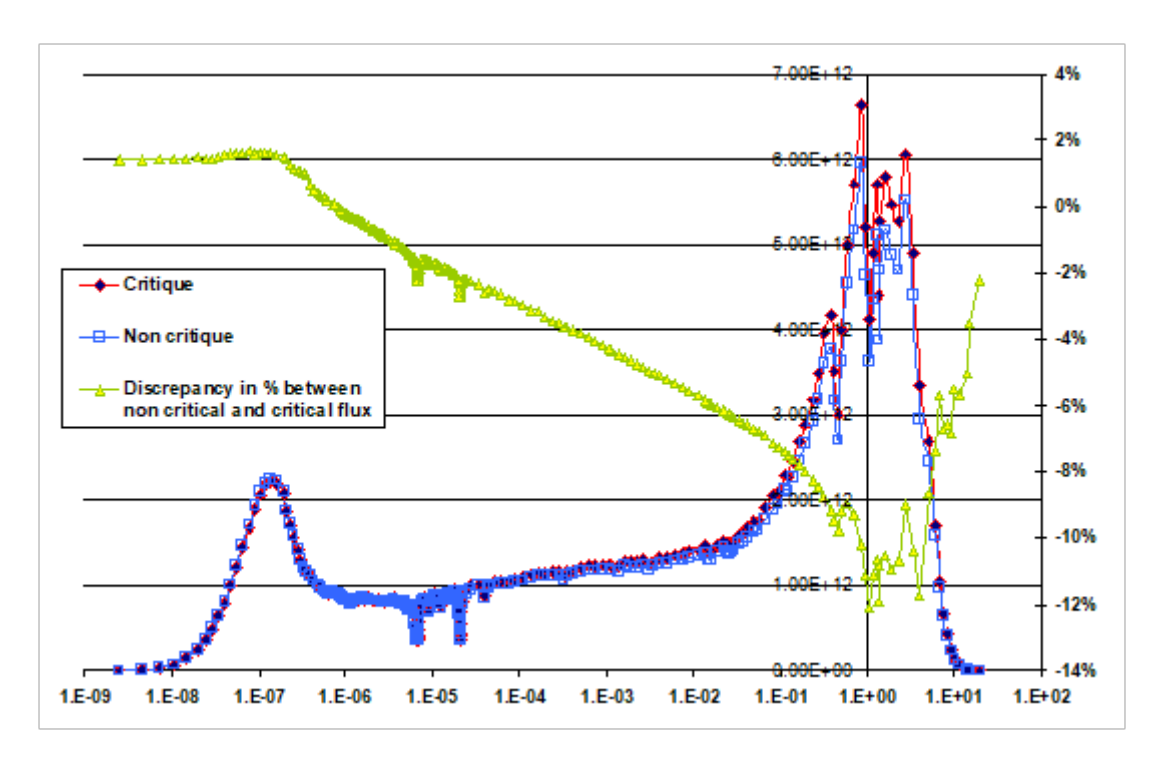


Figure 3.3: Case of study: 17x17 UOX 3.7%

The unit of measure of the power cycle and the energy released inside the reactor is the time-integrated parameter called burnup.

$$Bu(t) = \frac{V}{M_h} \int_0^t dt' < H\phi(t') >$$
 (3.13)

where V is the volume of the fuel $[m^3]$, M_h is the mass of heavy isotopes [t] at the beginning of the cycle, and H(E) is the recoverable energy from neutron-induced reactions [MW] with the primary contribution coming from the energy produced by fission.

The Bateman equations for the different isotopes are solved using databases known as cross-section libraries, which contain nuclear data such as thermal cross-sections, scattering matrices, decay modes, etc. The initial flux distribution is derived from previous neutron flux calculations.

Isotopic depletion is not calculated for all isotopes, but rather for those identified as heavy isotopes, which are typically found in the fuel. The uranium cycle, used in various types of nuclear power plants, such as pressurized water reactors (PWR), boiling water reactors (BWR), Canadian deuterium uranium reactors (CANDU), and liquid metal fast breeder reactors (LMFBR), plays a critical role in this process. When constructing the burnup chain, isotopes with a radioactive decay constant greater than their absorption rate can be treated as decaying instantaneously, thus being removed from the chain (for example ²³⁹U. and Np-239).

3.3 Core Calculation

The complexity in simulating the neutronics of the reactor core has led to the development of strategies that, through mathematical methods, have allowed the prediction of the most important parameters for reactor design. In the previous section, the first level of calculation, the lattice calculation, was introduced, which solves the transport equation by homogenizing the elements of a single assembly.

This section will briefly explain what is meant by core calculation by SCIENCE V2, the second level of calculation, two-group diffusion, and how the resolution of the neutron diffusion equation is used in this context.

The outputs generated by this second step include several key quantities: the neutron flux and the reaction rates throughout the reactor, from which the power distribution is calculated. Based on this, other important parameters are derived, such as fuel pellet temperatures and the coolant margin to departure from nucleate boiling (DNB). These two parameters are among the main quantities monitored during core design and safety evaluation.

3.3.1 The steady state diffusion equation

To solve the equation describing how neutrons behave within the core, several methods and mathematical formalisms have been employed to address complications such as energy treatment (multigroup formalism) the angular dependence of neutron motion (Pn, Sn models, etc.). 2

The full core calculation consists in solving a 2-D or 3-D (in SMART it is a three dimension simulation) of the diffusion equation of the neutrons that is an approximation of the transport equation replacing each assembly by the homogenized medium output of the first step. This means to do a simulation using a coarser mesh respect to the first step and it will cause a big difference between the two levels of the calculations. Unfortunately, homogenizing on a coarse mesh means loosing accuracy. So an equivalence intermediate step is mandatory, in Fig. 3.4 it is represented the idea behind the equivalence factors, considering O as the exact solution (the one that is aimed to be reached) and R and M as respectively a 2-D heterogeneous calculation and 2-D homogeneous calculation, the equivalence factor are computed between this two calculations. This equivalence factor is applied to F (3D homogeneous calculation) and O' it is obtained that is the approximation of the actual problem.

As mentioned before, an approximation of the transport equation in the diffusion equation that is based on the idea that neutrons are treated as a gas which diffuses within the core. The derivation of the Diffusion equation depends on the well-known Fick's law, it suggests that the neutron will move from an high concentration area to low concentration area.

The Pn method can be used to obtain the diffusion equation, in this method the direction of the flight is discretized and consists in project every term of the transport equation using specific function on the base of the domain of the problem (e.g. in 3D the angular direction is described by the surface of a sphere).

The equation is a system of coupled infinite ODE's for m that is a natural number. For the goals of this section just m = 0.1

$$\begin{cases}
\frac{d\phi_1(z)}{dz} + \Sigma(z)\phi_0(z) = \Sigma_s(z)\eta_0\phi_0(z) + S_0(z) \\
\frac{1}{3}\frac{d\phi_0(z)}{dz} + \frac{2}{3}\frac{d\phi_2(z)}{dz} + \Sigma(z)\phi_1(z) = \Sigma_s(z)\eta_1(z)\phi_1 + S_1(z)
\end{cases}$$
(3.14)

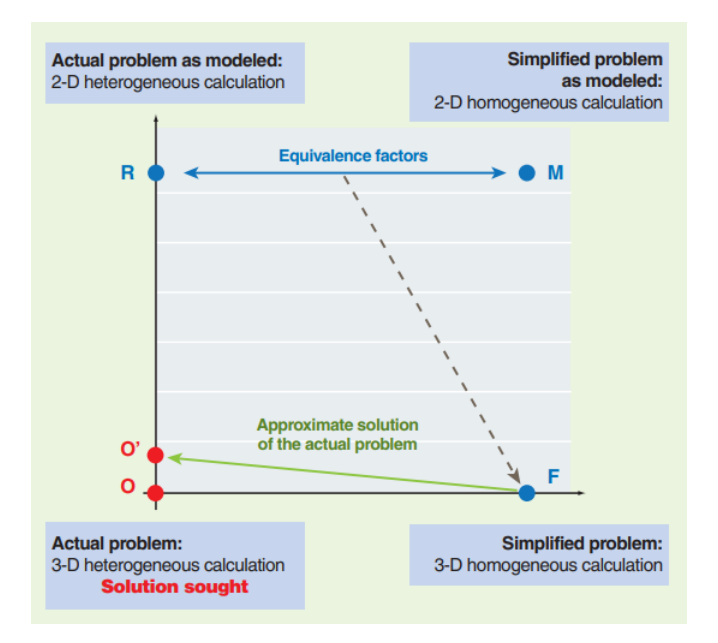


Figure 3.4: Principle scheme of equivalence for the example of a 3-D core calculation [1]

Since the focus is on m = 0.1 the second term of the second equation can be neglected

$$\begin{cases} \frac{d\phi_1(z)}{dz} + \Sigma(z)\phi_0(z) = \Sigma_s(z)\eta_0\phi_0 + S_0(z) \\ \frac{1}{3}\frac{d\phi_0(z)}{dz} + \Sigma(z)\phi_1(z) = \Sigma_s(z)\eta_1\phi_1 + S_1(z) \end{cases}$$
(3.15)

If the problem is totally isotropic the anisotropy source term $(S_1(z))$ can be cancelled and the equation system becomes:

$$\begin{cases}
\frac{d\phi_1(z)}{dz} + \Sigma(z)\phi_0(z) = \Sigma_s(z)\eta_0\phi_0 + S_0(z) \\
\frac{1}{3}\frac{d\phi_0(z)}{dz} + \Sigma(z)\phi_1(z) = \Sigma_s(z)\eta_1\phi_1
\end{cases}$$
(3.16)

In neutron transport theory, the current of neutrons represents the flow of neutrons in a particular direction and is a fundamental quantity in describing neutron flux within a reactor. The neutron current $\mathbf{J}(\mathbf{r})$ is expressed as neutrons/cm²/s and is connected to the neutron flux ϕ and the diffusion coefficient D expressed in cm, which quantifies the spread of neutrons in the medium, in addition the current is the first order moment of the angular flux. Coming back to the equation system, considering that the zero-th order moment of the angular flux is the total angular flux and the first order moment of the angular flux is the current.

$$\begin{cases}
\frac{dJ(z)}{dz} + \Sigma_a(z)\Phi(z) = S_0(z) \\
\frac{1}{3}\frac{d\Phi(z)}{dz} + \Sigma_{tr}(z)J(z) = 0
\end{cases}$$
(3.17)

Finally is possible to introduce the Fick's Law:

$$J = -D\nabla\phi \tag{3.18}$$

$$D = \frac{1}{3\Sigma_{tr}} \tag{3.19}$$

A general equation can be written for a large number of neutron energy intervals to

formulate the Multigroup Diffusion Equation, see 3.20

$$-\nabla \cdot [D(r,E)\nabla\phi(\vec{r},E)] + \Sigma_{tg}\phi_g(r) = \sum_{g'=1}^{N} [\Sigma_{sg'\to g} + \frac{\chi_g}{k_{eff}}\nu\Sigma_{fg}]\phi_g(\vec{r})$$
(3.20)

$$\Sigma_{xg} = \frac{\int_{E_g}^{E_g - 1} \Sigma_x(E) \phi(E) dE}{\int_{E_g}^{E_g - 1} \phi(E) dE}$$
(3.21)

Two Group Diffusion theory

In industrial reactor physics is very common to consider the two-group approximation. It consists in divide the energy domain in two regions and so two different categories, thermal and fast group. The cut energy that divide the interval is 1 eV as it is depicted in Fig. 3.5 Notice the diffusion equation considering the approximation:

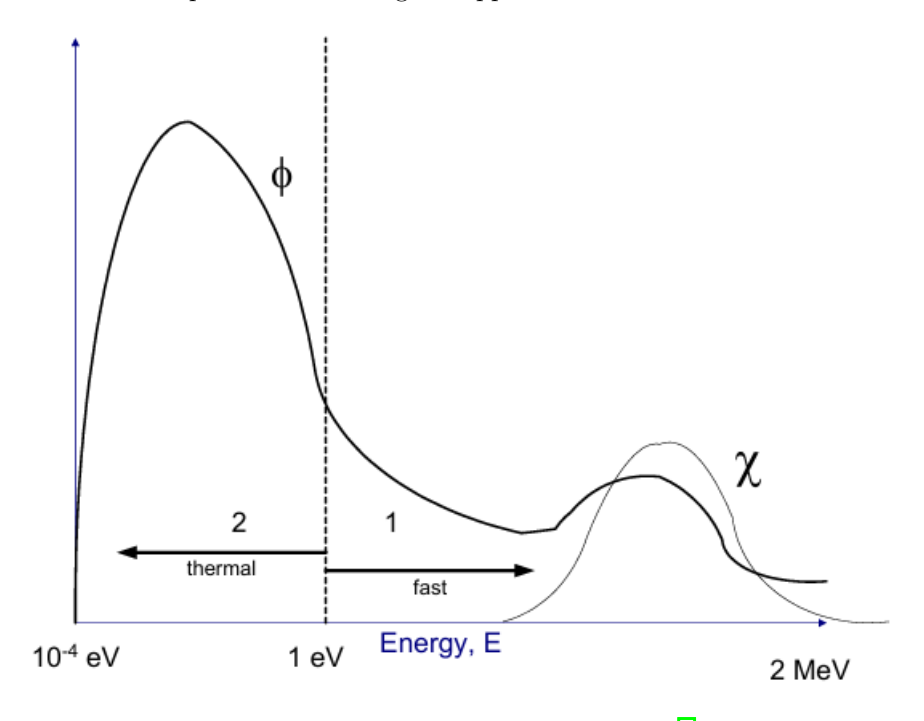


Figure 3.5: Two-group approximation [6]

$$\begin{cases}
\nabla \cdot D_{1}(\vec{r}) \nabla \phi_{1}(\vec{r}) - \Sigma_{1}(\vec{r}) \phi_{1}(\vec{r}) + \frac{1}{k_{eff}} (\nu \Sigma_{f1}(\vec{r}) \phi_{1}(\vec{r}) + \nu \Sigma_{f2}(\vec{r}) \phi_{2}(\vec{r})) = 0 \\
\nabla \cdot D_{2}(\vec{r}) \nabla \phi_{2}(\vec{r}) - \Sigma_{2}(\vec{r}) \phi_{2}(\vec{r}) + \Sigma_{1 \to 2} \phi_{1}(\vec{r}) = 0
\end{cases} (3.22)$$

• All secondary neutrons from fission are produced in group 1.

$$\chi_1(\vec{r}) = 1 \tag{3.23}$$

$$\chi_2(\vec{r}) = 0 \tag{3.24}$$

As follows the parameters of the equation are listed:

1.
$$D_1 = \frac{1}{\Sigma_1(\vec{r}) + \Sigma_{1 \to 1}(\vec{r})}$$

2.
$$D_2 = \frac{1}{\Sigma_2(\vec{r}) + \Sigma_{2\to 2}(\vec{r})}$$

3.
$$\Sigma_1(\vec{r}) = \Sigma_{a,1}(\vec{r}) + \Sigma_{1\to 2}(\vec{r})$$

4. $\Sigma_2 = \Sigma_{a,2}$, no up-scattering

In fig. 3.6 a schematic representation of the idea behind this approximation is represented, starting from the fast neutrons which have one source, the fission term. Instead thermal neutrons have a contribution for those fast neutrons that slowed down and enter in the thermal energy range. The fast flux is the source term for thermal neutrons, while the thermal flux is the source for fast through the fission event. Of course both of the two categories can be absorbed or diffuse. It follows that the fast flux is higher in fuel region

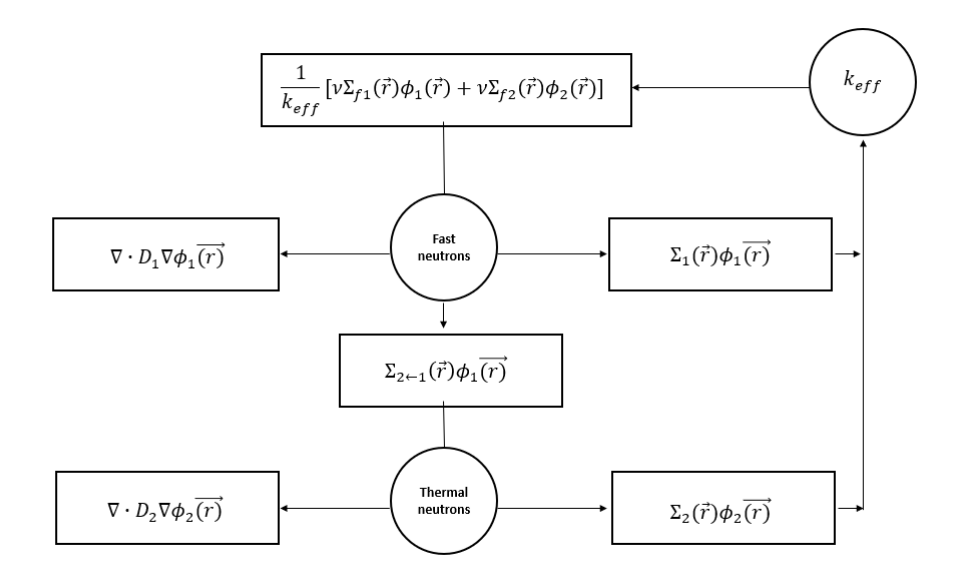


Figure 3.6: Two group full core calculations 6

where the fission occurs. Fast neutrons can diffuse through the moderator region and slow down 3.7.

3.3.2 Continuity and Boundary Conditions

The conception of boundary conditions between lattice calculation and core calculation is very different, in the first one the conditions imposed are reflection on all the faces of the assemblies to be coherent to the concept of infinite medium. In the second step the boundary conditions imposed considering the actual core boundary conditions. Due to its symmetry normally the core in divided considering one-quarter or one-eighth, in those case the continuity equation has to be applied.

The neutron flux is a continuous function of \vec{r} and due its direct relation as well the neutron current. Let's to considering an infinite plane in one of the three directions and a given point in this plane.

$$\phi_g(x_0^-, y, z) = \phi_g(x_0^+, y, z) \tag{3.25}$$

Also at the current can be applied the continuity equation using the normal unit vector $\vec{N} = (1,0,0)$:

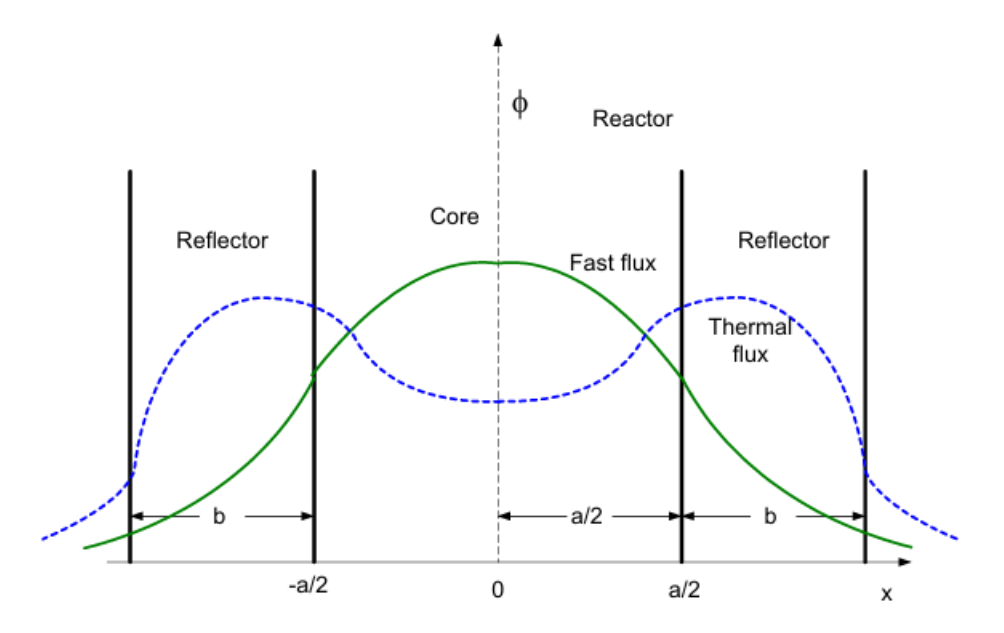


Figure 3.7: Spatial distribution of the flux 6

$$J_g(x_0^-, y, z) \cdot \vec{N} = J_g(x_0^+, y, z)$$
 (3.26)

Using the Fick's Law that was obtained previously:

$$-D_g(x_0^-, y, z) \cdot \nabla \phi_g(x_0^-, y, z) \vec{N} = -D_g(x_0^+, y, z) \cdot \nabla \phi_g(x_0^+, y, z) \vec{N}$$
(3.27)

In the borders of the reactor core the reflector is present, its function is to reflect all the neutrons that comes from the reactor, also this part has to be included in the assumption of the boundary conditions. Also a difference has to be done between real boundaries and artificial boundaries (symmetry boundaries).

The first type of boundary condition to impose at the real physical boundary is the zero incoming condition due to the fact that neutrons can escape from the reactor core but they can't be reflected back again, from the physical point of view the net current is zero.

$$J_{q}^{-}(r) = 0 (3.28)$$

This condition is the same for every energy group, it is possible to define the *albedo* parameter at position r, $\beta_g = 0$ represents the zero condition for the incoming current. In the industrial field in reality is usually to set the albedo not exactly to 0 but to a value slightly above 0, the value can change depending on the assumptions that are considered.

$$\beta_g(r) = \frac{J_g^-(r)}{J_g^+(r)} \tag{3.29}$$

The second type of boundary condition is the one to be imposed at the symmetry boundary $\beta_g = 1$:

$$J_q^+(r) - J_q^-(r) = 0 (3.30)$$

The definitions of the incoming and outcoming currents come from the P1 expansion

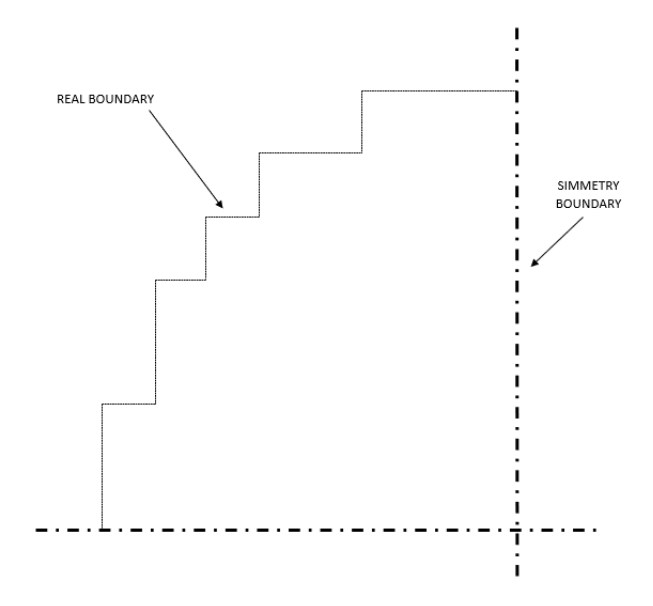


Figure 3.8: Spatial domain with symmetries

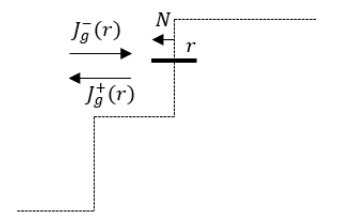


Figure 3.9: Symmetry boundary condition.

and are defined as:

$$J_g^-(r) = \frac{1}{4}\phi_g(r) - \frac{1}{2}(J_g^(r) - J_g^-(r)) \tag{3.31}$$

$$J_g^+(r) = \frac{1}{4}\phi_g(r) + \frac{1}{2}(J_g^(r) - J_g^-(r))$$
(3.32)

These boundaries conditions are used also in SMART, core code implemented in SCI-ENCE $\rm V2.$

3.4 Multiparametrized Homogenized Cross Section tables

In SCIENCE V2 the resolution of the multigroup diffusion equation Eq. 3.20 is done using nodal methods through a coarse mesh for spatial discretization, In this case cross sections and diffusion coefficients are nodal properties that are constant inside each nodes. Considering all the informations explained before the reactor simulation is a result of some

steps:

- Lattice calculation: perform of the 2D assembly simulations using fine meshes and results of these calculations are few-groups homogenized cross sections and diffusion coefficients, all of these results are stored in multiparametrized HXS tables.
- Reading of the HXS-libraries and it serves as an interface between the first and the
 second step. The library contains all the fuel properties in function of operational
 parameters and depletion. The selection of the parameters depends on the tools used
 during the simulation, usually the parameters selected are the thermophysical properties such as moderator density, fuel temperature, boron concentration, control rod
 presence, etc.
- Full-core calculations: parameters in XS-libraries are reading and before to be used they are interpolated in order to consider the local condition of each node.

Th formula used in SCIENCE V2 to generate HXS is presented below:

$$\Sigma = \Sigma_{ref} + \sum_{i}^{N=N_{tp}} \Delta \Sigma_{i}$$
(3.33)

where Σ_{ref} is the reference cross section at the nominal operation parameters, N_{tp} is the number of thermophysical parameters, $\Delta\Sigma_i$ are the corrective factors which represent the dependence of the cross sections on the operation parameters [8]. The explanation of the generation of the corrective terms will be the subject of the following chapter.

3.5 Limits of Two-step calculation and 3D direct calculation

The two-step calculation is one of the most used techniques in the industrial field for 3D simulations, but its results introduce several approximations that can be listed as follows:

- Starting from the lattice calculation, as explained before this step is dedicated to the simulation of one assembly through a 2D simulation, at the boundaries of the assembly reflection and translation are imposed. The environment of the assembly is not considered, it will affect the results since in real-world assemblies has different enrichments that can influence the spectrum of the neighbors in addition considering that in some assemblies control rods are inserted.
- The weighting spectrum is not the actual critical spectrum of the core. Instead, it is corrected using a leakage model to enforce approximate criticality $(k_{eff} = 1)$.
- In the lattice calculation there are actually two different kind of calculations. The assembly is depleted at some conditions that are considered nominal, at the end of this first calculation it will obtain all the isotopes nuclide concentrations at each burnup step, from this informations other calculations are performed just changing some parameter. These process is delicate and could introduce some inaccuracy, in fact, the conditions of the assembly during the depletion could be far from the experienced in the calculations. This introduce an error then in the creation of the HXS libraries: the history effect in two-step core modelling. To reach a high level of accuracy, the ideal situation is to perform as many depletion calculations as possible to cover all the

possible conditions in which the assembly can be in order to recalculate the reference reaction rates. Clearly, the size of the memory necessary to store all this informations is really to large, the approximation that is introduce is just to keep a selected set of values of the physical parameters, as discussed in [9]. In addition, the evolution of the assembly along the cycle is not possible to know a priori and this the reason because an history model can be necessary.

• At core level the approximation introduced regards the interpolation techniques necessary to reconstruct all the informations contained in the HXS libraries according to the node condition, see Appendix.

The necessity of using this kind of approach is because doing a 3D calculations or a Monte-Carlo will require an expensive cost in terms of computation and time. In the multi-physics applications there is the necessity to perform different simulation also for safety studies. The 3D direct transport core calculations is the other alternative option to the Two-step in which the full transport equation is solved to all the core with an high level of details in fuel pin. Different examples are reported in literature.

From Reference [10], we have the following considerations regarding large-scale 3D core calculations performed with the IDT solver of the APOLLO3® code:

3D MOSC core calculations were performed with the IDT solver of the code APOLLO3® for both the PWR and the experimental reactor EOLE. The former was computed with a P_3 26-energy-group cross-section library, where the problem was discretized using more than 10 million regions with linear volumetric and surface expansions for the flux and 80 directions in the unit sphere. This calculation was run using only MPI libraries with 28 nodes of 12 CPU cores, for a domain decomposition of 19×19 3D assemblies that include the axial reactor. The runtime with 336 CPU cores was 7.8 hours on an Intel Xeon L5640 2.26 GHz machine. The EOLE calculation, instead, has a smaller number of regions (648,434), since it is not a power reactor, but the problem contained 158,647 different materials for which a P_3 281-energy-group library was used. The angular flux was represented with a linear volumetric and surface expansion and using an S_8 quadrature formula. The calculation was performed with 900 CPU cores, one for each subdomain, producing a runtime of 46 minutes applying the new acceleration CMFD-RMA method.

Chapter 4

History effect in PWR modeling

As discussed in the previous chapter, the solution of the transport equations within the reactor core is approached using the two-step calculation method. The key step that links the calculation at the assembly level with those for the entire core is the creation of multiparametrized tables, which include, among other parameters, the homogenized cross-sections. It is important to note that this two step calculation scheme is one of the cause of discrepancies between these calculations and measurements on real plant.

The possible operating conditions of the reactor can vary over time, and therefore a single set of fixed values for the thermophysical parameters, during the depletion, may not be representative of the average reactor behavior. The main challenges are that, during the lattice calculation, constant values are imposed. Moreover, as also stated in Chapter 2, the outcome of the depletion in the first step is the isotopic concentrations. Setting fixed values could therefore introduce inaccuracies in the predicted concentrations. In the second step, an additional calculation is carried out using a different set of parameters from those adopted in the first calculation, however, this is not sufficient and represents the best that can be achieved. In addition, these simulations are performed under the assumption of an infinite medium, i.e., without considering the influence of the surrounding assemblies. The purpose of this chapter is to introduce the concept of a history model and to discuss its various aspects, while the study of the variations in neutron spectrum and the capture rates of $^{238}\mathrm{U}$ changing parameters serves to demonstrate these aspects. It is therefore important to emphasize that in the first step the depletion calculation is performed under fixed conditions, whereas in reality the node conditions within the assembly deviate from these assumptions while depleting, see Fig. 4.1. This discrepancy is referred to as the history effect within two-step modeling. In particular, variations in thermophysical parameters during the burnup process have been shown to strongly influence the cross sections. These fluctuations inevitably lead to differences in both isotopic concentrations and the neutron spectrum. A model is required to mitigate the issues in core scale calculation. In the following section, an overview on what is an history model will be presented, along with how it is treated in the literature.

4.1 Sensitivity Analysis

The reactor is made up of several assemblies, which are not subject to the same conditions; this is due to the initial characteristics of the assembly, such as the enrichment, but also to the conditions it is exposed to over time. In fact, in a reactor, the same assemblies may be exposed differently, for example, due to changes in water density or other changes such as

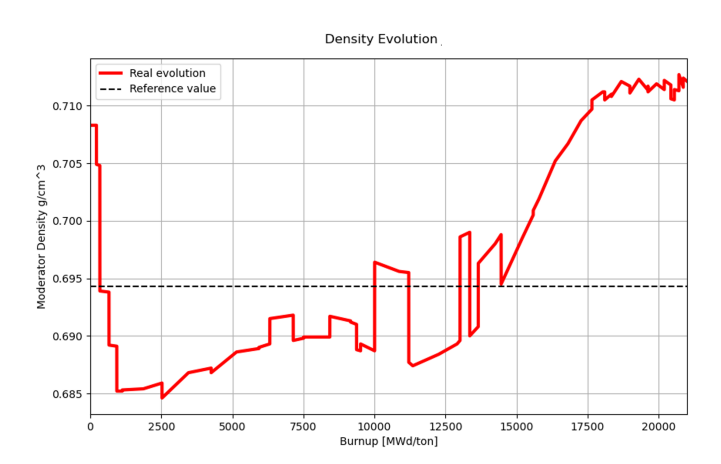


Figure 4.1: Evolution of the moderator density of a node during the cycle. It can be observed how it differs from nominal value used in the depletion

the presence of control rods.

In the two-step method, the first step consists of performing lattice calculations to generate homogenized cross sections. Finally, a core calculation is carried out using these pre-calculated homogenized cross sections from the first step. This method is not fully accurate because the conditions assumed in the depletion to generate the isotopic concentrations differ from the actual operating conditions of the assembly.

The sensitivity analysis has been carried out by considering the influence of water density on neutron spectrum, fuel temperature, boron concentration, and the presence of control rods. For each of these parameters, the reason for their importance and their effect on the spectrum will be discussed.

The analysis has been performed through lattice simulations of a fuel assembly, in which fixed values of the thermophysical parameters were initially imposed. Subsequently, after selecting a reference burnup value, each parameter was varied individually in order to assess its effect.

Below, data and histograms will be presented to demonstrate how, in the actual operating life of a reactor, assemblies can be subjected to very different conditions one to another. The parameters are distributed in a very different manner, and moreover, the thermophysical parameters are interdependent due to thermal and neutronical feedbacks.. The following analysis will examine how individual parameters can influence the neutron spectrum, which may help to identify which parameters have the greatest impact on it. In Fig. 4.2 shows four plots illustrating the distribution of the four parameters of interest. The data were extracted from a core calculation of a PWR, considering the first cycle. Only one assembly type was analyzed, with the purpose of demonstrating that even for a single assembly type the parameters exhibit a heterogeneous distribution. All axial points were taken into account.

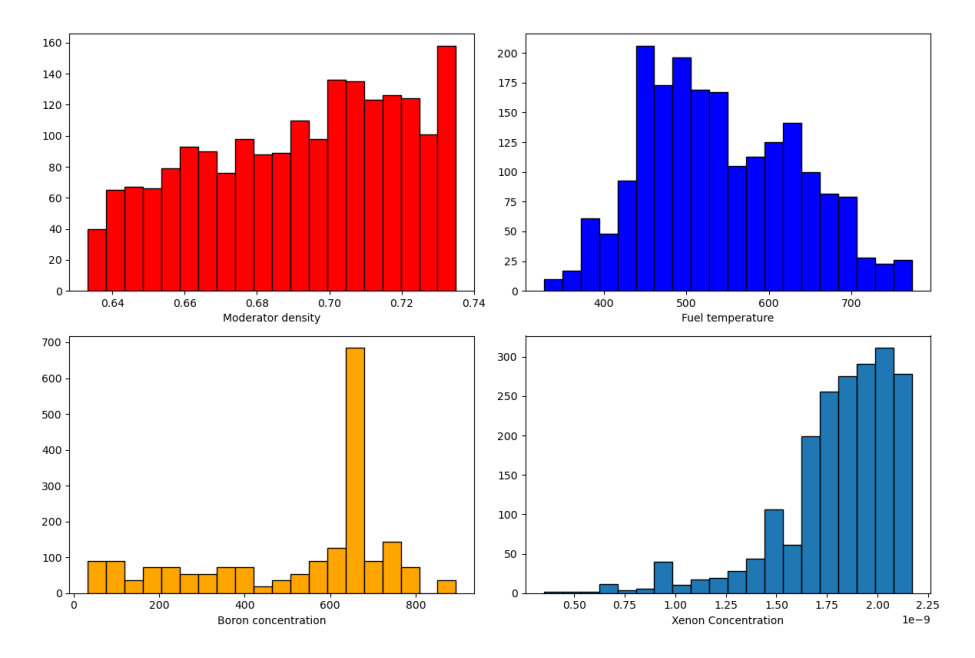


Figure 4.2: Representation of local data on an industrial fuel cycle depletion of density of the moderator, fuel temperature, boron concentration and xenon concentrations. Those realistic data are of one assembly type, as it is possible to see the distribution of each of them is not concentrated in a restricted range of values.

Moderator density effect

The first parameter presented is the moderator density. In the case of a LWR, the moderator is light water. The role of the moderator is to slow down neutrons so they can be used to induce as many fission reactions as possible.

In an LWR reactor, water serves as both the moderator and the coolant. It enters from the bottom side of the pressure vessel and rises towards the core, where it moderates the neutrons while simultaneously heating up. From the top side, depending on the reactor type, it may pass through intermediate circuits to generate steam or go directly to the turbine (for some BWR), after which it enters the condenser and returns once again to the bottom side.

If we focus on the core, the change in water density is as follows: since the temperature of the water increases on the top side of the core, the moderator density decreases, less denser water moderates neutrons less effectively. Therefore, the water density changes axially, with an higher value at the bottom of the core and a lower value at the top.

On the other hand, in the bottom side of the core, due to thermalization, the spectrum is softer. The lower temperature water moderates neutrons much more effectively, resulting in a greater thermal flux. A parameter that can help represent this information is the spectral index, which is defined as follows in the case of 2-group energy mesh:

$$SI = \frac{\phi_1}{\phi_2} \tag{4.1}$$

where ϕ_1 is the flux of fast neutrons while ϕ_2 is the flux of thermal neutrons.

$$SI_{bottom} < SI_{top}$$
 (4.2)

Since the water at the top is hotter and less dense, it moderates neutrons less effectively: therefore the spectrum is harder at the top.

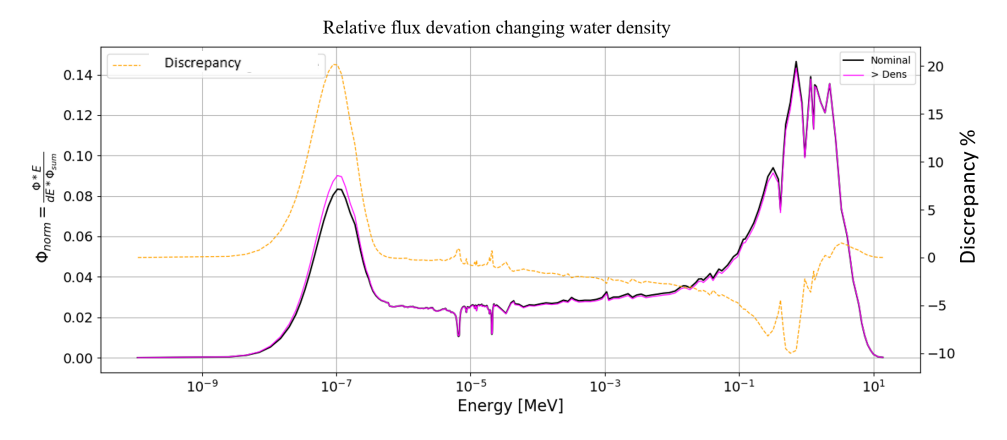


Figure 4.3: Effect on neutron spectrum changing water density. The higher value of water density is approximately 7% more than the reference value.

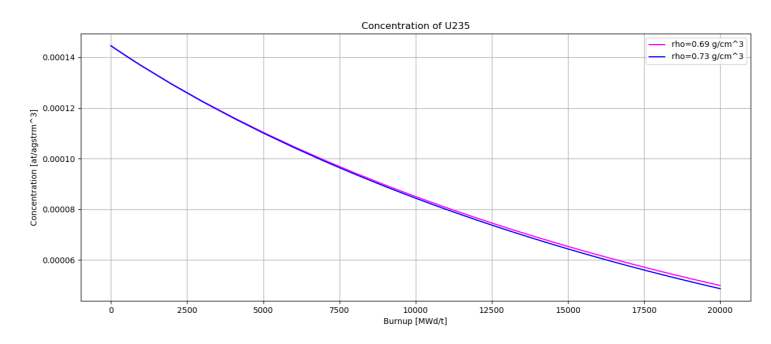
The results of several single assembly depletions with different moderator densities, calculated by APOLLO3®, illustrate the effects described above. From the figures, it is possible to see that different water density values are reflected in different nuclide contents, though the shape of the curves remains the same. In Fig. 4.3 are represented the neutron spectrum for two different water density values, black curve corresponds to the reference water density value, while the pink curve represents the case with the highest density. These values were selected based on the data extracted from the PWR core simulations, as previously discussed in relation to the histograms of the thermophysical parameters. The highest value of water density was chosen by selecting the highest value found at node level in the reactor. The nominal values is the one used in the first calculation in the first step. Considering that this is the upper bound in the range of densities. Finally, the yellow curve represents the difference in neutron flux between the two cases. As the water density increases, the discrepancy in the thermal range rises by approximately 20%, leading to a noticeable spectrum softening. Conversely, in the fast range, a reduction of about -10% is observed. This trend highlights the impact of water density on neutron energy distribution.

An important correlation has to be discussed, that is the influence of different water density values and production of some isotopes of uranium and plutonium. In Fig. 4.4a 4.4b 4.4c the evolution of the concentration along the cycle with the different values are depicted. In general if a closer condition to the inlet is considered, the water density is higher and the spectrum is thermalized. In this case, fewer neutrons are available to react with ²³⁸U so less ²³⁹Pu is produced, and more ²³⁵U is consumed. In terms of concentrations, at the inlet, the concentration of ²³⁵U and ²³⁹Pu will be lower, while ²³⁸U will be higher. On the opposite side, at the outlet, the spectrum is hardened, the concentration of ²³⁹Pu is higher along the cycle, and there is less ²³⁸U. At the bottom of the core, therefore, thermalization of the neutron spectrum has an higher impact. A softening condition in the neutron spectrum (e.g., increasing water density) leads to fewer neutrons being captured by ²³⁸U consequently resulting in lower ²³⁹Pu concentration and more ²³⁵U being burnt. It is therefore possible to state, that the water density strongly modifies the spectrum.

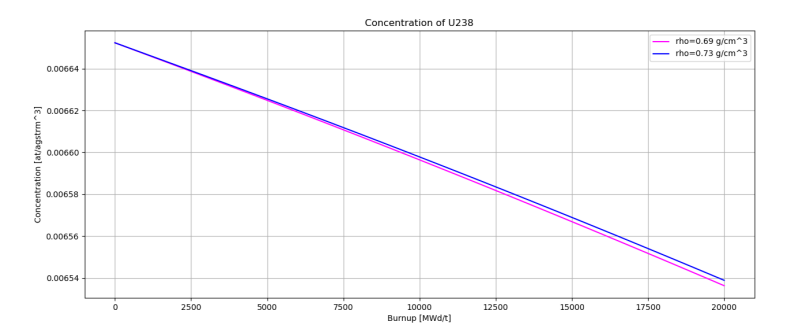
Fuel Temperature effect

The temperature of the fuel is another parameter that influences the neutron spectrum, but the predominant phenomenon in this case linking temperature variation to the spectrum is the Doppler effect. As can be seen in Fig. 4.5 the Doppler effect results in a broadening of the cross sections in the resonance region for fertile isotopes such as ²³⁸U. This effect is caused by the thermal motion of target nuclei.

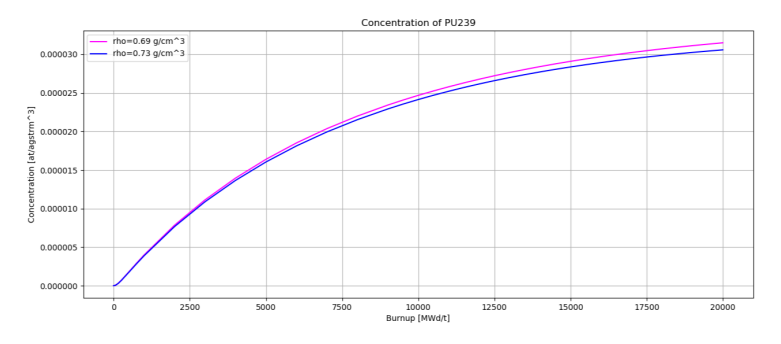
In the case of neutron capture, this interaction depends both on the energy of the neutron and the energy of the target. For a stationary nucleus to absorb an incident neutron, the energy must match the resonance energy. However, if the target is moving, this means that the neutron can have either lower or higher energy to be absorbed. The resonance area broadens, and the peak decreases. Therefore, an increase in temperature promotes higher thermal and kinetic energy. As the temperature increases, the spectrum is hardened. Also for this parameter the flux is calculated in a reference condition and considering the higher fuel temperature found with the data extraction (Fig. 4.6). The calculated discrepancy is not at all comparable to that observed with water density changes. As expected, some peaks appear in the resonance range, with a difference of -5% but the influence is significantly less impactful compared to water density effects. In Fig. 4.7a - 4.7b - 4.7c , the trends of 235 U, 238 U, and 239 Pu are shown. However, when the temperature changes, the isotopic concentrations do not vary significantly.



(a) Concentration of $^{235}\mathrm{U}$ along different depletion with two values of moderator density



(b) Concentration of $^{238}\mathrm{U}$ along different depletion with two values of moderator density



(c) Concentration of 239 Pu along different depletion with two values of moderator density

Figure 4.4: Moderator density effect on nuclide contents for some isotopes ${\cal C}$

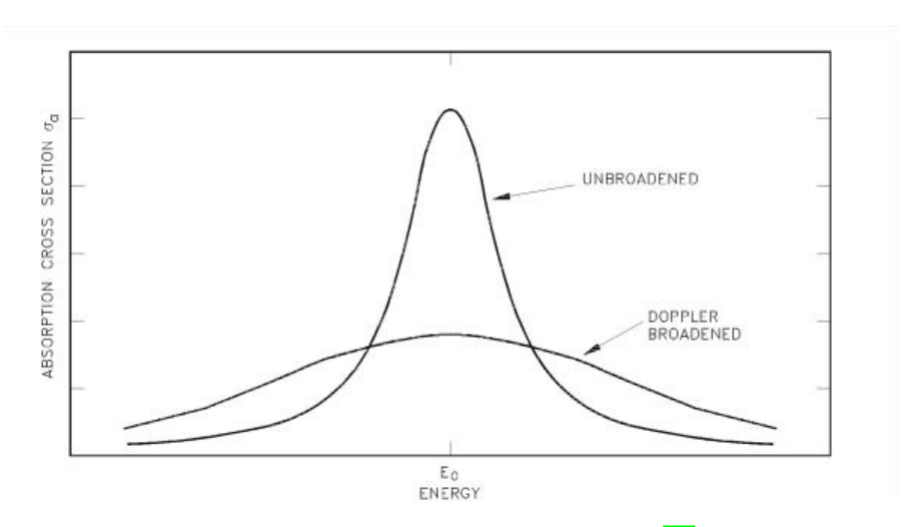


Figure 4.5: Doppler Effect Broadening [11]

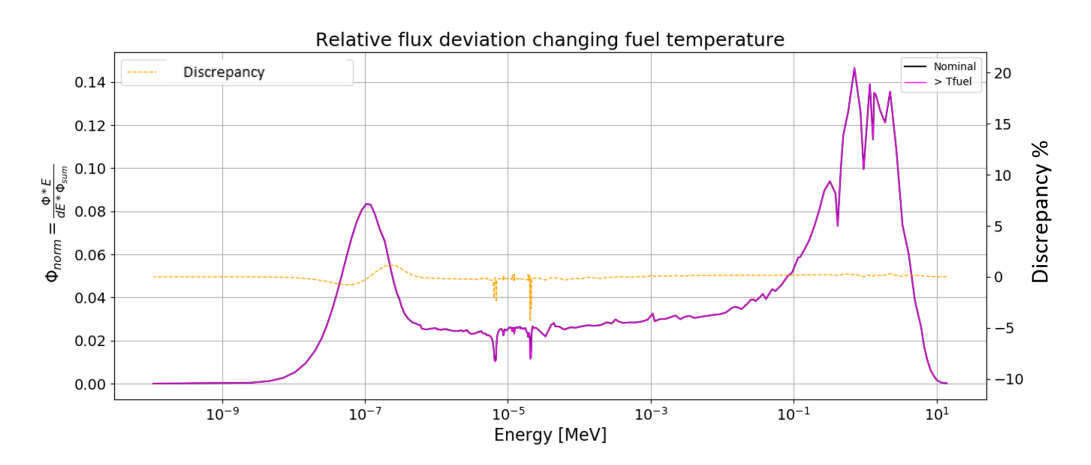
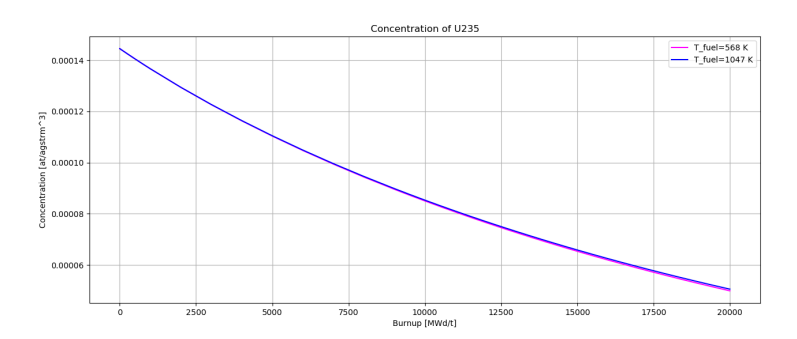
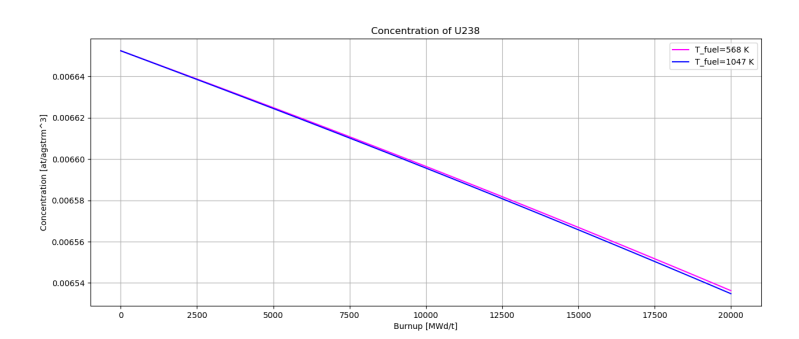


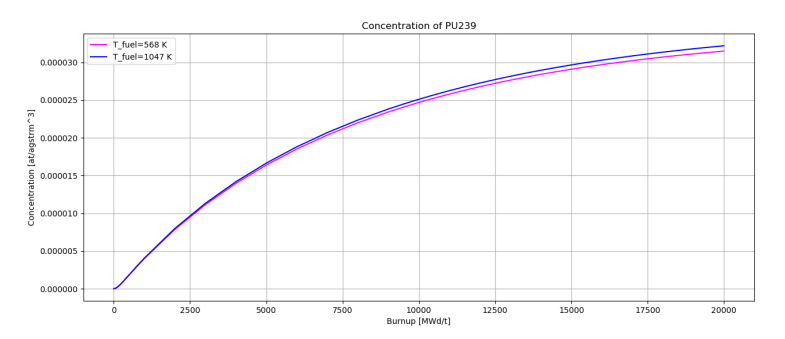
Figure 4.6: Effect on neutron spectrum changing fuel temperature. The higher value is 44% more than the nominal value.



(a) Concentration of U235 along different depletion with two values of fuel temperature



(b) Concentration of $^{238}\mathrm{U}$ along different depletion with two values of fuel temperature



(c) Concentration of ²³⁹Pu along different depletion with two values of fuel temperature

Figure 4.7: Fuel temperature effect on nuclide contents for some isotopes

Boron Concentration

Boron is dissolved in water and is one of the methods used to control reactivity in the reactor. The isotopes dissolved in the water are ¹⁰B and ¹¹B. As the fuel burns, the boron concentration is gradually reduced by the reactor control system in order to maintain criticality.

Boron is chosen because it has a high absorption cross-section in the thermal energy region. Since a higher boron concentration results in greater neutron absorption, the neutron

spectrum hardens, leading to a reduction in the thermal neutron flux.

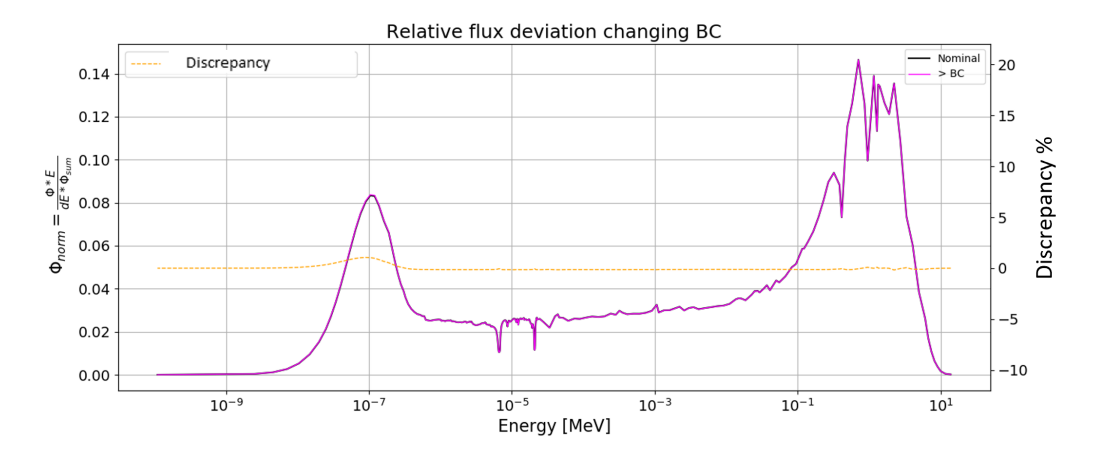


Figure 4.8: Effect on neutron spectrum changing boron concentration. The higher value is 27% more than the nominal value.

Control Rod Presence

The control of reactivity in a reactor, in addition to the use of borated water, also involves the use of control rods, which are made of materials with a high probability of neutron capture (boron, cadmium, hafnium, etc.) to control reactivity. Two different type of configurations are used: ARO (All Rods Out) and AIC (AgInCd rods). Normally, the control rods are not inserted all the way down to the bottom of the core, but only in the upper part, so it can be said that they have a greater influence on the outlet. Their presence has a significant effect on the concentration of isotopes and the neutron spectrum. When the control rods are inserted, they absorb neutrons, the flux in the thermal range decreases, and the spectrum hardens as is it possible to denote in Fig. [4.10]. In this picture two different curves are represented, the black one is the configuration with rods and the blue one is with rods inserted. The impact on the thermal range is strong.

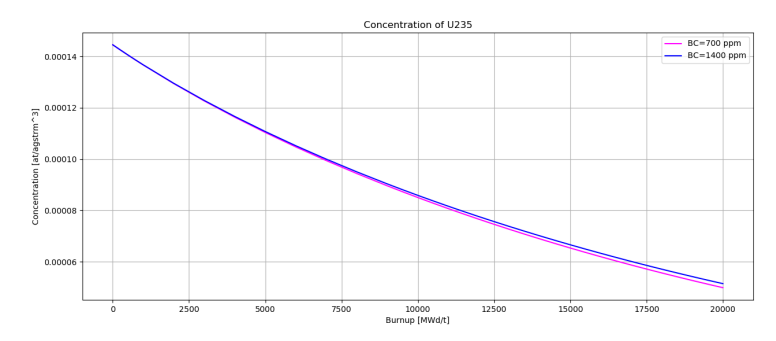
Capture rates of ²³⁸U

In this study, the capture rate of 238 U has been analyzed, as it plays a crucial role in plutonium production. The neutron capture reaction of 238 U leads to the formation of 239 Pu which is one of the main contributors to reactor reactivity through its subsequent fission process. The capture cross section of 238 U is larger in the resonance range. Understanding how different reactor parameters influence the capture rate of 238 U is essential for predicting plutonium buildup and its impact on long-term reactor behavior. This table presents the

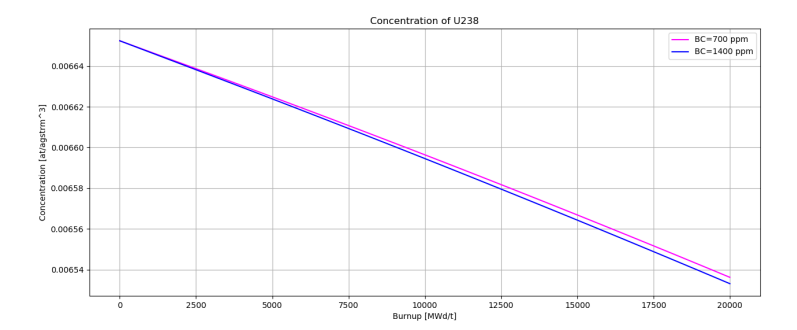
Calculation Parameter	Integrated deviation of capture rate
$\rho_{ref} - 0.10 * \rho_{ref}$	+6%
$BC_{ref} - 0.50 * BC_{ref}$	-2.6%
$Tfuel_{ref} - 0.20 * Tfuel_{ref}$	-0.6%

Table 4.1: Effect of different parameters on $^{238}\mathrm{U}$ capture rate compared with the reference value.

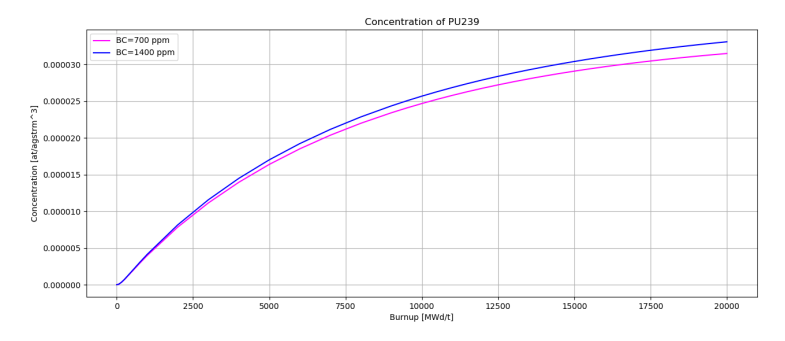
impact of variations in different reactor parameters (water density, boron concentration,



(a) Concentration of $^{235}\mathrm{U}$ along different depletion with two values of boron concentration



(b) Concentration of $^{238}\mathrm{U}$ along different depletion with two values of boron concentration



(c) Concentration of 239 Pu along different depletion with two values of boron concentration

Figure 4.9: Boron effect on nuclide contents for some isotopes

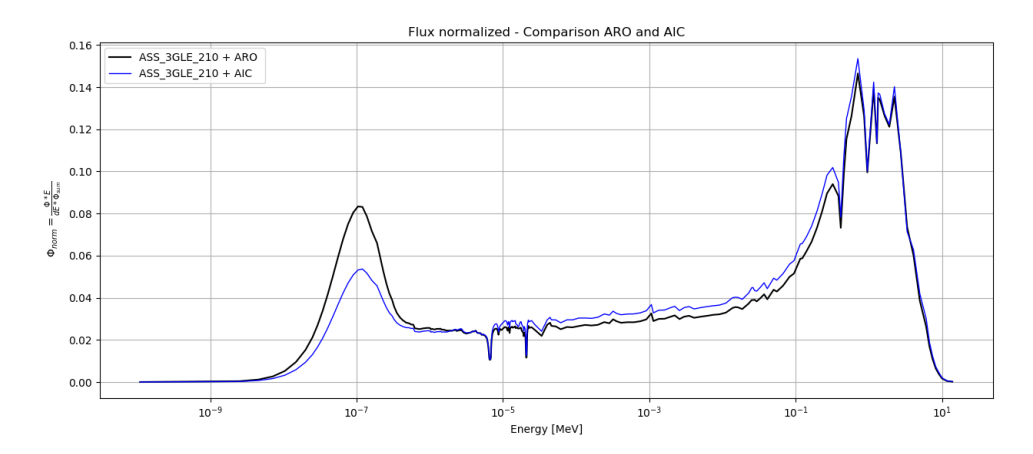


Figure 4.10: Neutron spectrum without control rod (ARO configuration) compared to control rods inserted (AIC)

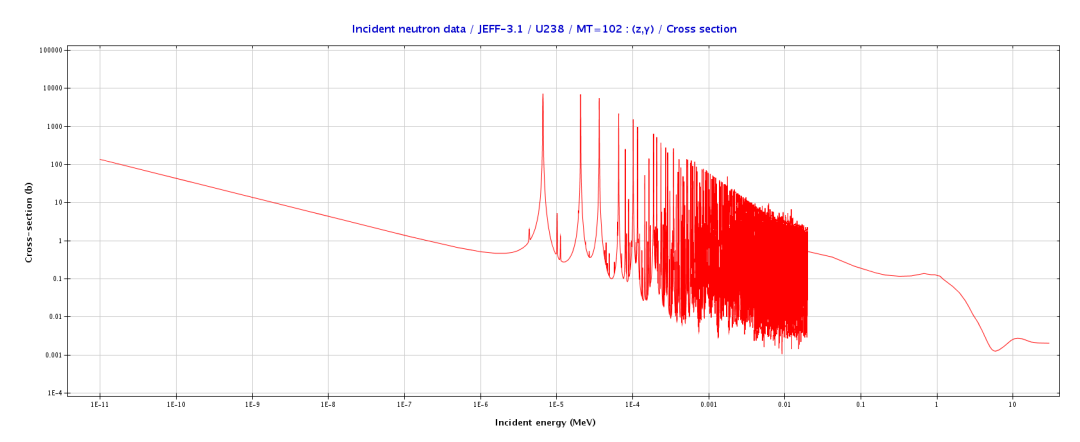


Figure 4.11: Capture cross section of 238 U $\boxed{12}$

and fuel temperature) on the integrated deviation of the neutron capture rate of $^{238}\mathrm{U}$ on all energy groups.

- Water density decrease: The capture rate increases by 6% in terms of microscopic cross sections, indicating that a lower water density leads to more neutron captures per nucleus. This effect is due to spectral hardening, as reduced moderation shifts the neutron energy spectrum towards higher energies. In this energy range, the relative contribution of ²³⁸U captures increases compared to ²³⁵U microscopic absorption (capture + fission). It should be noted, however, that in typical UOX fuel there is much more ²³⁸U than ²³⁵U, so the absolute impact on total absorption depends also on the isotopic abundances (see Fig. 4.12).
- Boron concentration decrease: The capture rate decreases by -2.6%, since boron is a strong neutron absorber. A lower boron concentration reduces neutron absorption, allowing more neutrons to remain in the thermal range, leading to a lower overall capture rate.
- Fuel temperature decrease: The capture rate decreases by 0.6%, showing a relatively

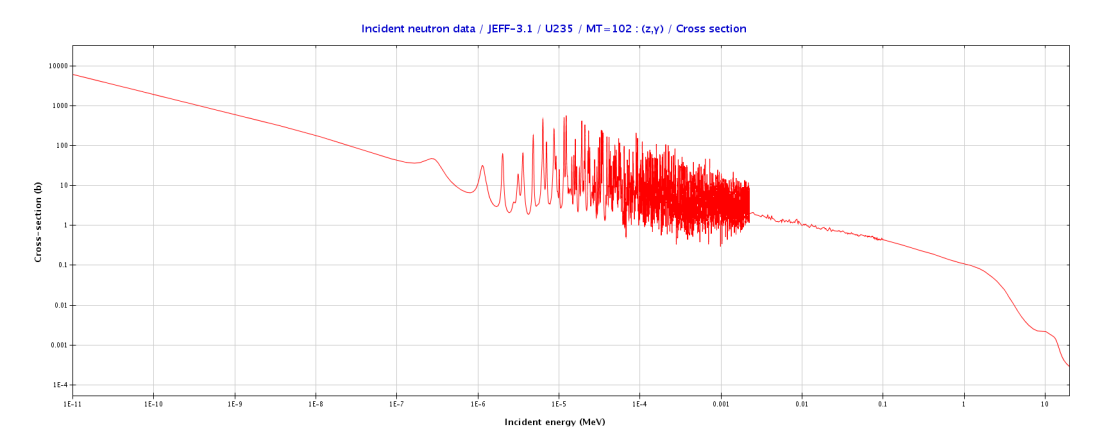


Figure 4.12: Capture cross section of 235 U 12

minor effect compared to the previous ones. This small change is likely due to the reduced Doppler broadening effect, which slightly decreases resonance absorption, leading to a slight reduction in the total capture rate.

Overall, the results highlight that water density variations have the most significant impact on the ²³⁸U capture rate, followed by boron concentration, while fuel temperature has a comparatively minor influence. The study of uranium-238 capture provides insights into plutonium generation, which is a key factor in reactor physics and fuel cycle management.

4.2 Spectral History Modeling

The idea behind the history model is the following. First, for each assembly a nominal depletion is carried out, in which certain values are fixed. Depending on the code used, one or more additional depletions are then performed, which differ from the nominal case in the fixed values.

The results of these evolutions are the isotopic concentrations, which are then used as the starting point for instantaneous evolutions. These are performed for each burnup step, where the variations of the spectrum as a function of the thermophysical parameters are taken into account.

The result of these instantaneous evolutions is the set of cross sections. In this way, cross sections are obtained from the instantaneous calculations based on both the nominal and additional evolutions. The history model focuses precisely on this point, namely the difference in the cross sections when considering the same instanteneous variations of the thermophysical parameters, but on several different depletion conditions. Thus, if there is a difference in spectrum, it is only due to the isotopic constitution resulting from different depletion conditions.

Subsequently, considering the instantenous and historical conditions (for example, those of a node), an interpolation is performed. This aspect will be discussed in the next section, where, based on findings from the literature, the available options for interpolation parameters will be analyzed and compared.

4.2.1 Interpolation parameters

In the literature, several interpolation parameters have been proposed, and in the following section a comparison among them will be presented.

In an early work the moderator history was used for computing empirical corrective terms stored in look-up tables. It is defined as a burnup-averaged quantity of the instantaneous moderator density δ [13].

$$MH = \frac{1}{Bu} \int_0^{Bu} \delta(Bu') d(Bu')$$
(4.3)

Later, in the code $\boxed{14}$, cross sections calculated at hot full power (HFP) condition were corrected, with additive terms presenting a quadratic dependence with the MH. Different parameters can be considered to model the history of the core, the difficult aspect to consider more than one is that more depletion calculations have to be considered so more computational cost. Nowadays a single history parameter was considering in PWR modeling $\boxed{13}$. Others define a spectral history parameter as the ratio between the actual SI and the one from the nominal calculation SI_N integrated over the burnup.

$$SH = \frac{1}{Bu} \int_0^{Bu} \frac{SI(Bu')}{SI_N(Bu')} d(Bu')$$

$$(4.4)$$

$$SI = \frac{\phi_1}{\phi_2} \tag{4.5}$$

The methods based on the use of the spectral index and the spectral history are called *Spectral Methods*.

The concentration of plutonium-239 can also be considered a strong candidate among historical parameters since, it is one of the isotopes leading to differences in the instantaneous spectrum after the depletion.. As observed in the analysis of various thermophysical parameters, plutonium concentration has proven to be a good representative of spectral differences. In [8], using the DYN3D code, a method is described that proposes plutonium-239 concentration as a potential history indicator.

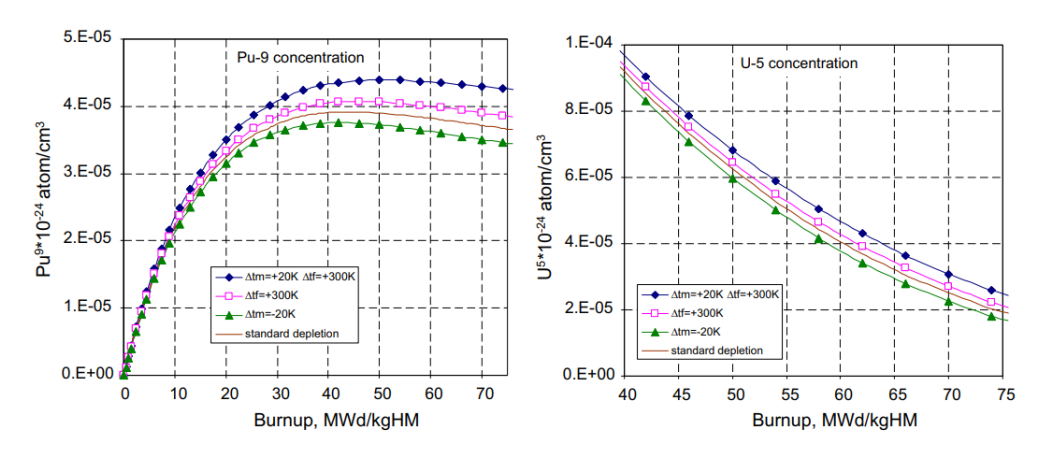


Figure 4.13: Nuclide concentrations in different depletion conditions, i.e. varying operation parameters ref. 8

In Fig. 4.13 is shown as the concentration of the isotopes (²³⁹Pu, ²³⁵U and ²³⁸U) change in different depletion calculations changing the temperature of the moderator and/or the fuel temperature comparing in the same figure with the standard depletion with reference conditions (red line).

It is possible to see that differences in fuel properties reflect differences in nuclide content: sequence of curves in figures remains the same, i.e. fuel depleted in hardest spectrum conditions has highest 239 Pu and 238 U concentrations, highest absorption and fission macroscopic

cross sections and the highest multiplication factor [8].

In Fig. 4.14, the deviation of homogenized cross-sections (HXS) is compared with the deviations in ²³⁹Pu concentration. This comparison aims to assess the correlation between spectral variations and plutonium buildup, reinforcing the potential of ²³⁹Pu concentration as a historical parameter.

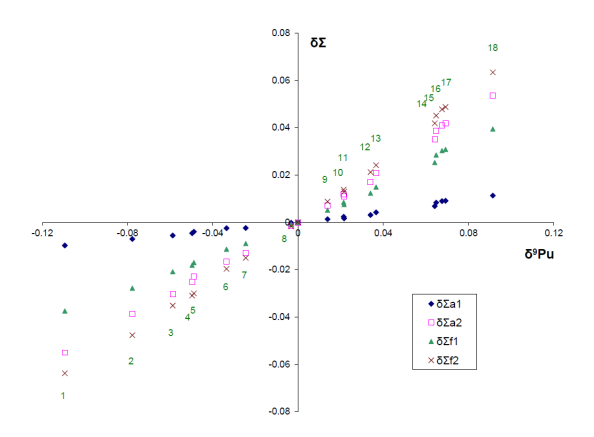


Figure 4.14: Correlation between relative change of macroscopic cross sections and ^{239}Pu concentrations in different depletions. $\boxed{8}$

Depletion	T_F , K	T_M , K	C_B, ppm	P, MPa
nominal	817	584	500	15.8
1	+58	+29	-	-
2	+683	-	-	-
3	-	+20	-	-
4	+458	-	-	-
5	+883	-20	-	-
6	-	-	+500	-
7	-	+10	-	-
8	-	-	-	14.2
9	+100	-	-	-
10	-	-	-300	-
11	-	-10	-	-
12	-253	-	-	-
13	-	-20	-	
14	-217	-20	-	
15	-	-44	-	-
16	-	-49	-	14.2
17	-	-49	-	-
18	-197	-49	-	-

Table 4.2: Correlation of the relative change of nuclide concentrations under different depletion conditions 8

$$\delta \Sigma = \frac{\Sigma - \Sigma_{ref}}{\Sigma_{ref}} \tag{4.6}$$

$$\delta N_{Pu239} = \frac{N - N_{ref}}{N_{ref}} \tag{4.7}$$

The analysis of the results demonstrates a correlation between the deviation of the cross-sections. What these figures show is that once the difference in ²³⁹Pu concentration is known, it is also possible to determine how much the macroscopic cross-section deviates from its nominal value.

In this work [8], results from a 3D core calculation with and without the use of the ²³⁹Pu coefficient were presented and compared with the results obtained from the lattice code. The findings indicate that if no correction is applied, the macroscopic cross-section values deviate from those of the lattice code as burnup increases. However, when the correction is applied, the discrepancy between the two calculations is eliminated. Referring to the work

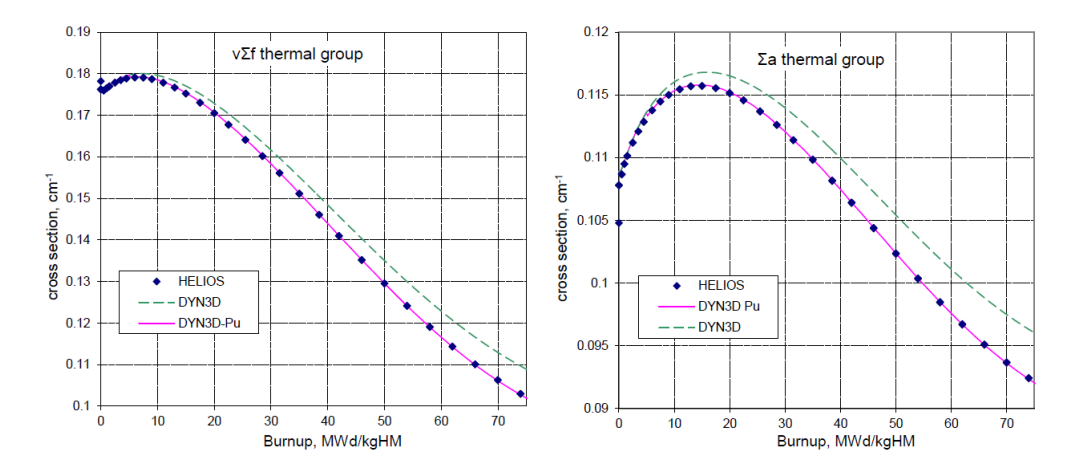


Figure 4.15: Homogenized macroscopic cross sections for the depletion with deviation in moderator temperature. DYN3D-Pu is regarding the core code with correction and DYN3D without correction.

conducted in [8], it was observed that the correlation between the macroscopic cross-section and Pu concentration followed a second-degree polynomial relationship. Therefore, to apply a linear proportionality, it was decided to use the square root of the concentration as the historical parameter.

$$P = \sqrt{239Pu} \tag{4.8}$$

Another parameter was introduced by the SCIENCE V2 code package by Framatome, which uses the ratio between the concentrations of all plutonium isotopes (Pu) and ²³⁸U to account for the history 13.

$$PU = \frac{Pu}{^{238}U} \tag{4.9}$$

4.2.2 Performance of the methods

Several parameters have been considered, some based on moderator density, others on the spectral index, and others on plutonium concentration. In [13], various depletion histories were analyzed to reproduce different historical effects and to test and compare the different parameters proposed in the literature.

In order to compare the different methods proposed in the literature, various depletion conditions are considered. These conditions are denoted by the letter B in Table 4.3 with subscripts indicating specific conditions. It is important to note that a new irradiation history with a different moderator density introduces an additional off-nominal calculation for the parameterization. $\boxed{13}$. In Tab 4.4 is described the history effect parametrization, for

	Description	Tf	ρ_M	CR
		[°C]		
B_N	Nominal condition	600	0.72	OUT
B_I	Inlet condition	600	0.75	OUT
B_O	Outlet condition	600	0.66	OUT
B_F	High fuel temperature	1200	0.72	OUT
B_{c1}	CR in the 1° cycle	600	0.72	IN [0,15] [GWd/t]
B_{c2}	CR in the 2° cycle	600	0.72	IN [15,30] [GWd/t]

Table 4.3: Depletion histories considered to test the different history parameters in literature. [13]

each method is referred an equation and the combinations between off nominal history and instantaneous parameters which are used to performed branch calculations.

Method	History parameters	Off-nominal history	Instantaneous parameter	
P1	Eq.4.8	B_I	B_I	
P2	Eq.4.8	D_I	B_N	
P3	Eq.4.8		B_O	
P4	Eq. <mark>4.8</mark>		B_N	
PU	Eq. <mark>5.5</mark>	B_O		
SI	Eq. <mark>4.5</mark>		B_O	
SH	Eq. <mark>4.4</mark>			
MH	Eq. <mark>4.3</mark>			

Table 4.4: 13

A way to compare the performances of the methods in the different uses is the burnup averaged error, it is defined in a generic interval (BU_1, BU_2) as:

$$\bar{\varepsilon}_{\mathcal{B},\theta} = \frac{1}{\Delta Bu} \int_{Bu_1}^{Bu_2} |\varepsilon_{\mathcal{B},\theta}(Bu)| \, dBu', \tag{4.10}$$

and presented in the Fig. 4.16 where for B_I, B_O and B_f is considered a complete burnup interval [0,45] GWd/t, in the case of B_{c1} and B_{c2} are separated per cycle. From this figure, it is possible to observe that, since the inlet conditions are close to the nominal ones, the error associated with the uncorrected microscopic cross section is lower than in the other cases (see the light blue square). As expected, the best results are obtained with B_I and B_O because they were used to compute the off-nominal calculations. In the third case, with high fuel temperature, SI and SH reduce the error from 0.8% to 0.6%, exhibiting poor performance, whereas PU achieves better results.

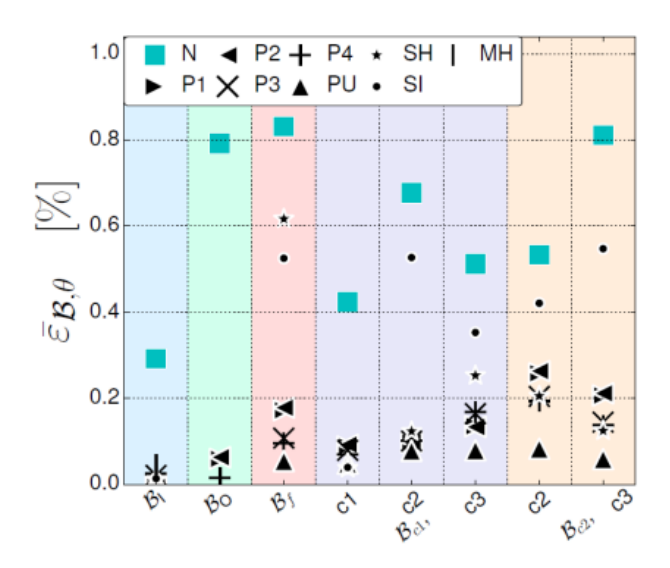


Figure 4.16: Burnup-averaged error with all the history parameters and for the given use cases $\boxed{13}$

4.3 Multi-Parametrized Libraries and History Model of SCIENCE V2

The main goal of this step is to generate a multiparametrized library necessary for SMART calculation containing homogenized cross sections and fine reconstruction parameters. Nuclear data used in SCIENCE V2 are supplied by CEA93 multigroups library with 99 energy groups, based on the JEF2.2 evaluations.

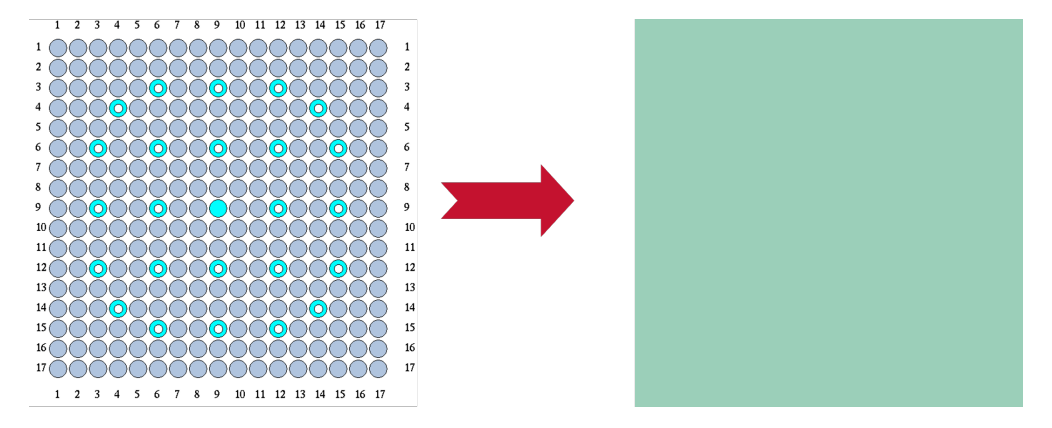


Figure 4.17: Homogenization of all the elements inside an assembly

In this step a detailed calculation is provided in both space and energy for an assembly and the transport equation is solved in 2D geometry, assuming a infinite medium. This calculation address to provide, as mentioned before, the microscopic and macroscopic cross sections of homogeneous equivalent medium (Fig. 4.17).

Preparing the cross sections taking this homogenization into account is by no means a simple step, but requires a careful and delicate approach. The first point to clarify is that when solving the transport equation for an assembly, one cannot refer to just a single configuration, as in the real-life operation of a reactor, it faces various situations in which the parameters, and consequently the densities of isotopes, change. To better understand the influence of these changes on the cross section values, the definition of the microscopic cross section homogenized in space and collapsed in energy is introduced.

$$\sigma_{i,r,g} = \frac{\int_{v} \int_{g} \sigma_{i,r}(\vec{r}, E) n_{i}(\vec{r}) \phi(\vec{r}, E) dE d\vec{r}}{\int_{v} \int_{g} \phi(\vec{r}, E) n_{i}(\vec{r}) dE d\vec{r}}$$
(4.11)

Inside this definition, the neutron flux is included, which is subject to changes in the thermo-physical parameters, see Section [4.1] In SCIENCE V2, parameters such as boron concentration, water density, fuel temperature and the insertion of the control rods are considered. All of these parameters are differently distributed from BOL (Beginning of Life) to EOL (End of Life), and they also depend on the specific fuel assembly being considered, as these can have different enrichment. Since the history of a real depletion is subject to various changes, it is important to identify the parameters that best represent these deviations in order to properly prepare the cross-sections for use in the second step of the process, the standard approach for preparing it is to divide the lattice calculation in two sub-steps.

The first step is the fuel depletion calculation, which determines the properties of the fuel in a heterogeneous representation as it undergoes depletion. This process allows for the generation of tables containing the isotopic concentrations required for the next step. In this sub-step:

Restart calculation



Figure 4.18: Graphical visualization of depletion and restart calculations. The parameters inside the boxes are the ones that change during the restart calculations

- The **Bateman equations** are solved, governing the evolution of nuclide concentrations during irradiation, as previously explained.
- Two different step are involved:
 - Nominal depletion: The core state parameters remain fixed at their nominal values.
 - Table generation: Different values of cross sections are collected inside this library at different conditions.
- In the case of **SCIENCE V2**, a history model is then introduce using the perturbed depletion obtained by modifying the **water density** and table D.

Finally, the result of this first sub-step consists of the isotope concentrations n_i at each burnup step, chosen based on the discretization. These values are then used in the second sub-step.

"Branch" calculations, also known as restart calculations, use n_i as the initial value. For each burnup step, different branches are performed to capture all possible deviations from the nominal values varying instantaneously the operating parameters. Ideally, all variables should be modified simultaneously to obtain the most realistic results.

In SCIENCE V2, the process is approximated by varying all the parameters, two at a time, while keeping the burnup constant. The overall effect is then estimated as the sum of the contributions of all parameter pairs. Consequently, for the spatial mesh, isotope concentrations are retrieved from the depletion burnup point.

With reference to SCIENCE V2, the process involves initiating instantaneous calculations based on the nominal depletion, simultaneously modifying multiple parameters, and considering the microscopic cross-section as a function of these variations. In summary, for each burnup point, multiple calculations are carried out, and the corresponding cross-sections are stored.

$$\sigma(Bu, \rho, T_f, CR, CB, CXe, Pu/U) \tag{4.12}$$

This tabulation that born from the instantaneous calculation is structured as follows:

- Table A: inside this table are collected the branches for each burnup step at the "reference" conditions. The branches in this table are calculated from the isotope concentrations in the nominal evolution.
- Table B: correction of σ from the base evolution considering the impact of the boron concentration and the density of the water.

- Table C: correction of σ from the base evolution considering the impact of the temperature of the fuel, these corrections are tabulated in function of the density of the water.
- Table P: correction of σ from the base evolution considering the presence or not of the control rods. These correction are tabulated in function of the boron concentration and water density.
- Table D: the most important data for this study are collected inside this table, in this case all the results are calculated by the perturbated evolution. Branches are calculated for each burnup step with the same "reference" conditions that are used in Table A. From each branch inside the table D the microscopic cross sections are saved and compared in order to see which is the history impact.

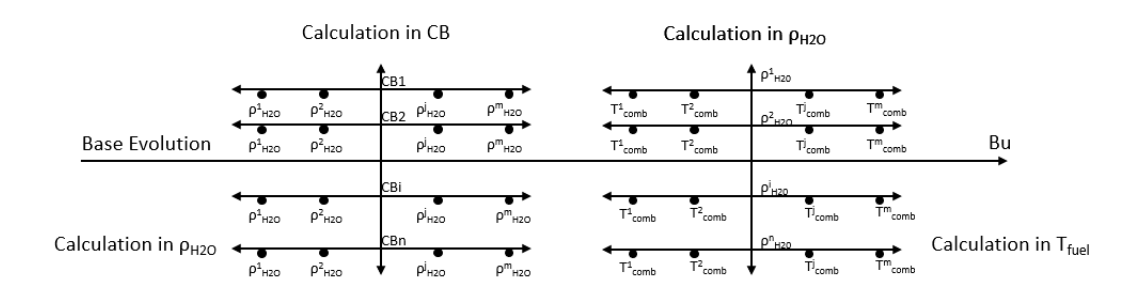


Figure 4.19: Representation of the base evolution

A different criteria is then applied to the perturbated evolution where the only change is in the value of the moderator density. This choice is motivated by the fact that, as shown in the neutron spectrum analysis, the water density has the strongest effect on the isotope concentrations. This parameter should be critically assessed and potentially reconsidered at the conclusion of the project, as its influence on the results could be significant.

As a result, for a given burnup step, two different branches are obtained: one from the nominal depletion and one from the perturbed depletion.

This approach significantly reduces computation time but introduces approximations. The time and memory required for lattice calculations in this step may limit the ability to represent multiple scenarios accurately.

The uranium depletion chain used in the core calculation of SCIENCE V2 is presented in Fig. 4.20. The chain used in the lattice calculation is more complex than the one used in the core calculation.

In a typical PWR, ²³⁵U is the main fissile material within the fuel, capable of undergoing fission when it absorbs a neutron. ²³⁸U in contrast, is a fertile material that has a minor contribution to the fission process. As depicted in the figure, ²³⁵U following neutron absorption that results in the production of ²³⁶U, which then undergoes further neutron absorption, producing Np-237. Np-237 subsequently undergoes beta decay, forming ²³⁸U. Neutrons originating from ²³⁵U fission are often absorbed by ²³⁸U which transforms into ²³⁹U. ²³⁹U decays into Np-239, which is unstable and undergoes beta decay to form ²³⁹Pu.Like ²³⁹Pu the most probable fate of ²³⁹Pu is fission, allowing it to contribute to the fuel cycle. The conversion ratio of ²³⁸U to ²³⁹Pu varies depending on reactor type. As the fuel continues to

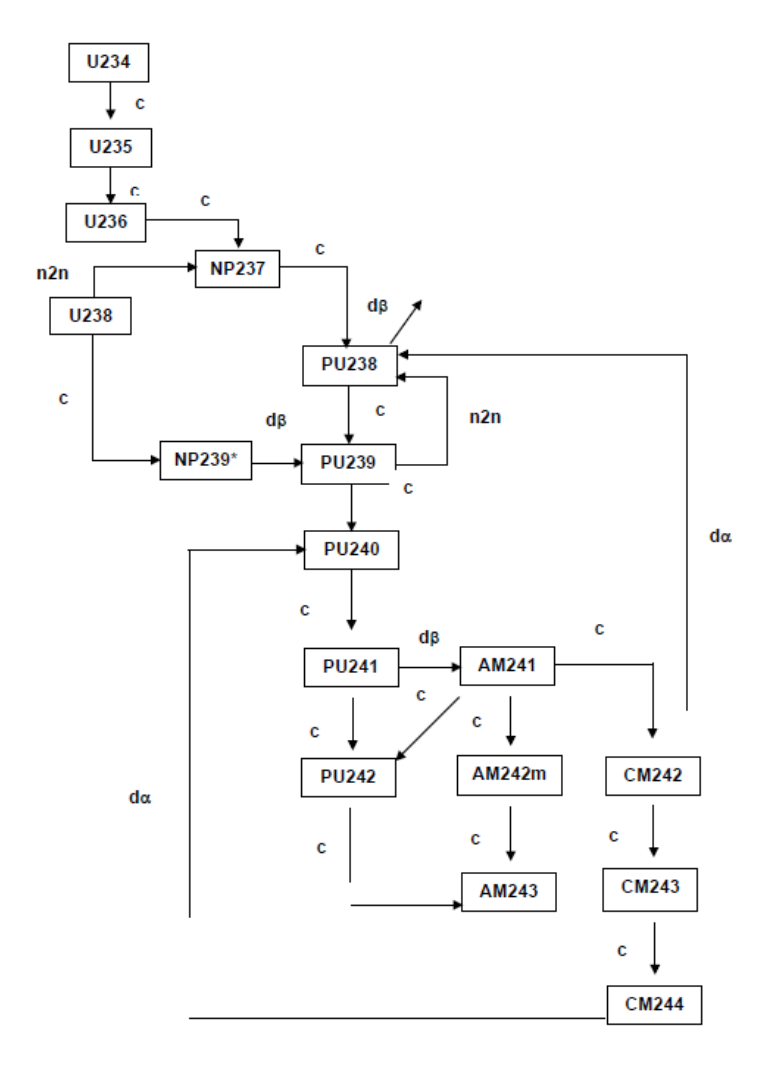


Figure 4.20: Heavy product depletion chain in SCIENCE V2 in SMART

burn, additional isotopes, including other plutonium and curium isotopes, are produce. The isotopic depletion calculation is also presented in the full core calculation. As explained previously, in lattice calculation the restart calculations aim to produce homogenized cross section to be used by SMART. Multi-parametrized libraries are generated by APOLLO2-F and they depend on different parameters. The objective of SMART at this point is to interpolate homogenized cross sections considering the actual node condition. In this way it obtains the microscopic sections of the various isotopes that are followed in the core calculation, where the density of each isotope is considered. Isotopes which are not followed in the second step are collected in a generic cross section called "residual", for these the density used in the core calculation is the same of the lattice evolution. Combined with the isotopic densities, they provide the means of calculating the macroscopic sections.

Chapter 5

Data Analysis

The aim of this thesis is to verify whether the hypotheses underlying the history effect model used in SCIENCE V2 are capable of adequately solve the problems related to the inability to predict the real reactor conditions. In order to conduct this analysis, it is necessary to analysing the variability of the local condition along a fuel cycle. To this end, data from the Taishan 2 reactor were used, and through these data, it was possible to identify various patterns within the reactor influenced by different parameters and operating conditions. A key aspect of this chapter is the identification of nodes characterized by significantly higher or lower plutonium production compared to other areas of the reactor. These nodes will be analyzed in more detail in the following sections.

5.1 Taishan Reactor

The data used in this thesis to perform the necessary analyses were extracted from the simulation of the TAISHAN Unit 2 reactor. This reactor is an EPR 1750, like the one studied in 15, with the first cycle simulated as shown in Fig. 5.1 The nuclear power plant is located in Taishan, China. Unit 1 was commissioned in 2018, while Unit 2 began operations in 2019. The reactors in question are, as mentioned before, EPRs (European Pressurized Reactors), which are considered among the most advanced designs in terms of both safety and efficiency. These reactors are equipped with advanced passive safety systems and other innovative technologies aimed at reducing risks and improving performance. The plant consists of two reactors, each with an electrical capacity of 1750 MWe. 16

As mentioned earlier, the data were extracted from simulations of Unit 2. Specifically, the reactor is a PWR 17x17 configuration, with 241 fuel assemblies. The fuel assemblies are identical in design but differ in their enrichment levels and the number of fuel pins that contain Gadolinium, as shown in Fig. 5.1 The addition of gadolinium to the fuel rods is essential due to its high neutron absorption cross-section, which significantly aids in controlling reactivity, especially in reducing thermal flux on some pins, so reducing fission reactions locally. This is particularly useful during the reactor's operation to maintain stability and prevent excessive reactivity at the BOL, to reach long cycle depletions. Additionally, the reactor uses a heavy reflector made of a substantial amount of stainless steel, along with a small amount of moderator, to reduce the geometrical neutron leakage and improve the neutron flux and enhance the reactor's efficiency. The loading pattern followed is the first core.

In addition to burnable absorbers (Gadolinium) for reactivity control, dissolved boron in the moderator is also used, and the control rods are inserted only partially along their

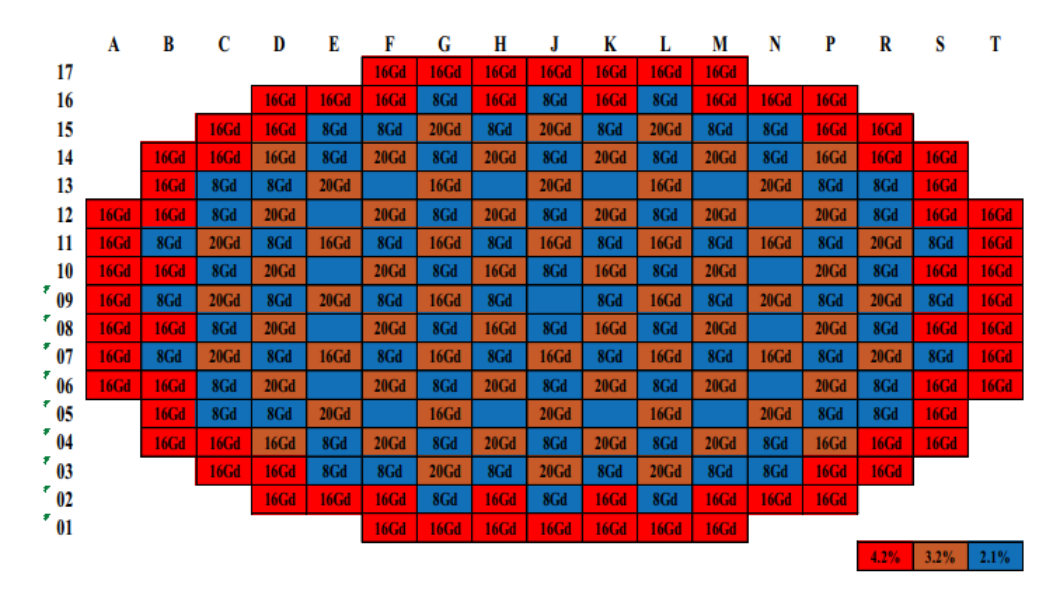


Figure 5.1: Fuel assembly loading of the EPR1750 core

length and only in some assemblies. Control rods are made of different materials: some are AIC (silver-indium-cadmium), others are stainless steel, and others are B_4C (boron carbide). The more absorbent rods are used for SCRAM (rapid shutdown), while the others are employed for fine reactivity control. There are also mixed rods, such as AIC + stainless steel, or AIC at the bottom and B_4C at the top.

In this chapter will be used many times the term "node", in this context it refers to a portion of a given assembly, of a certain axial height.

5.2 Historical Analysis from SCIENCE V2 data

The results presented below were obtained from a core simulation conducted with SCI-ENCE V2 and subsequently analyzed using Pyxtrac, a Python-based tool that allows data extraction at both the core and assembly levels. To proceed with the data analysis, all burnup substeps, moderator density, fuel temperature, and boron and xenon concentrations were extracted for each node.

5.2.1 Data distribution within the Core

The first key analysis was to identify the data distribution within the core. To achieve this, the data was categorized based on the type of fuel assembly (Fig. 5.2 Fig. 5.6). These figures illustrate the distribution of moderator density and fuel temperature across five different families of assemblies considering all the first fuel cycle. It is interesting to observe how all the families, at certain points, deviate from what are considered the nominal conditions, i.e., those used in the base evolution. In our case, the nominal conditions are: $\rho = 0.6943 \, \text{g/cm}^3$, fuel temperature = 568 °C, BC = 700 pm and xenon concentration = $2.5 \times 10^{-9} \, at/angstrom^3$.

First Assembly Family: UOX 2.1 (Assembly 1)

Starting with Fig. 5.2 the water density graph shows that only a small portion of the nodes within this assembly family are near the nominal value. The remaining nodes are fairly evenly distributed across the entire range, with a fraction of the population shifted towards higher densities, close to the maximum water density of the range. A similar trend is observed for temperature, where many nodes fall outside the nominal range. The red line in the graphs represents the nominal value, while the magenta line indicates the average temperature and water density values. Despite the relatively uniform distribution, the average values remain fairly close to the nominal conditions.

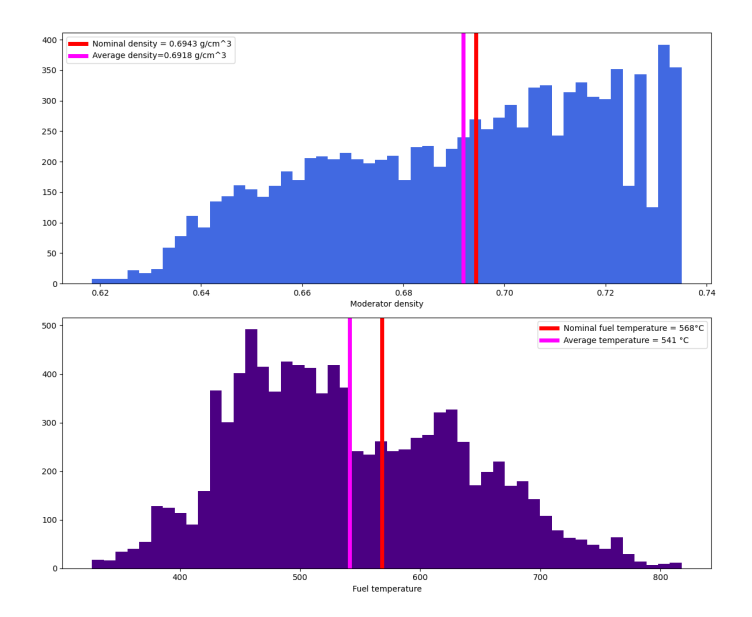


Figure 5.2: Histogram of the distribution for the assembly UOX 2.1 (Assembly 1)

Second Assembly Family: UOX 2.1 + 8 Gd pins (Assembly 2)

The second fuel assembly family exhibits a behavior similar to the first one, but with some key differences:

- Moderator density: A larger population of nodes falls above the nominal water density value. Consequently, the average water density is higher than in Assembly 1 and is closer to the nominal value.
- Fuel temperature: The distribution is similar to the first case, but a higher concentration of nodes is found to the left of the nominal value. Specifically, the average temperature for this assembly is 527 °C (as shown in Table 5.1), which deviates more from the nominal value compared to Assembly 1.

Third and Fourth Assembly: UOX 3.2 + 16 Gd pins (Assembly 3) and UOX 3.2 + 20 Gd pins (Assembly 4)

For the third and fourth fuel assembly families, the distributions of moderator density and fuel temperature follow a similar pattern. This is expected since these two assemblies share the same enrichment, differing only in the amount of gadolinium present. Interestingly, their average temperatures are very close to, or even overlapping with, the nominal value.

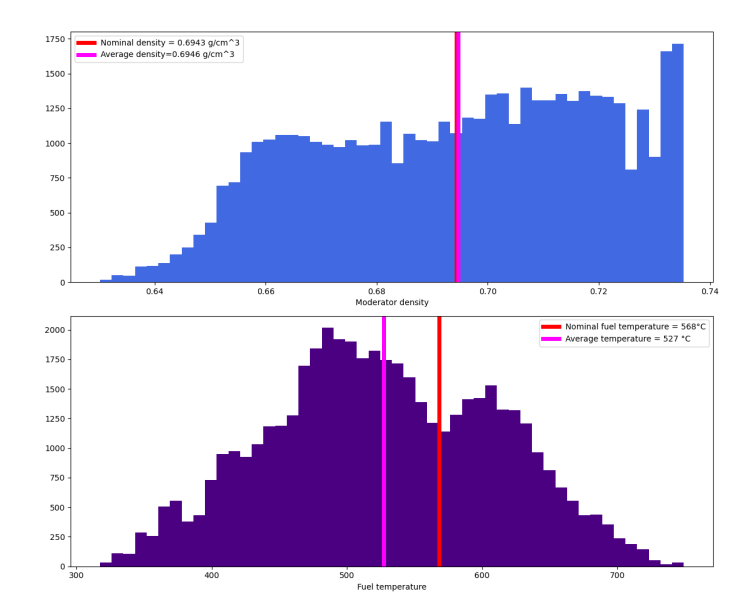


Figure 5.3: Histogram of the distribution for the assembly UOX 2.1+8 Gd pins (Assembly 2)

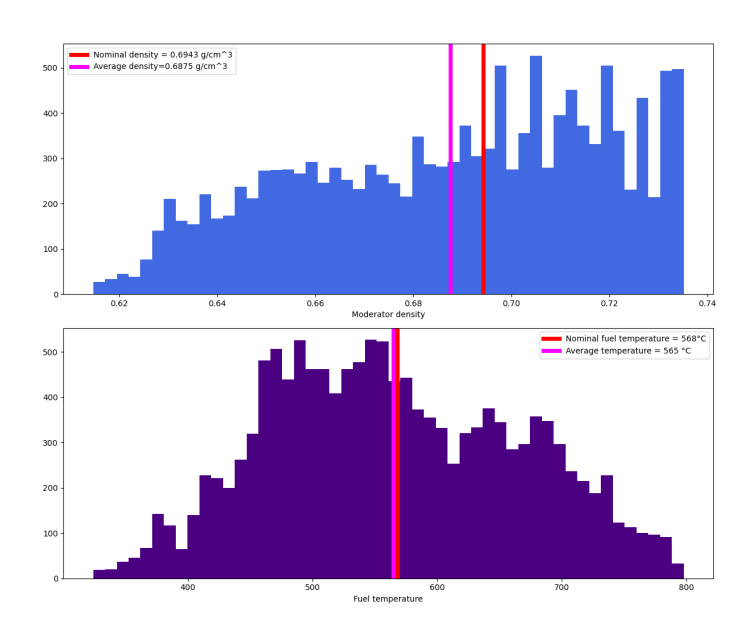


Figure 5.4: Histogram of the distribution for the assembly UOX 3.2 \pm 16 Gadolinium pins (Assembly 3)

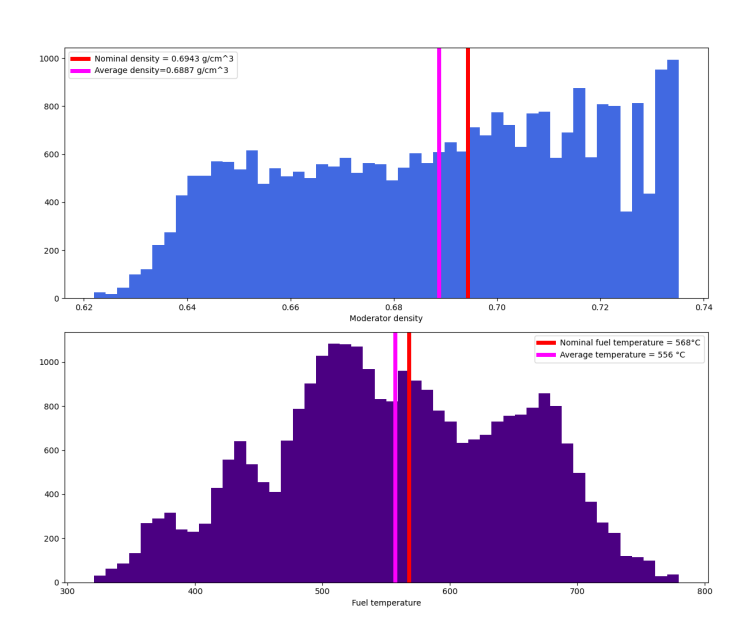


Figure 5.5: Histogram of the distribution for the assembly UOX 3.2 \pm 20 Gadolinium pins (Assembly 4)

Fifth Assembly: UOX 4.2 + 16 Gd pins (Assembly 5)

For the last assembly, the average water density is generally around the nominal value, but the situation is different for temperature. Most of the nodes are to the left of the nominal value, deviating from it. Considering that, in general, the cross-sections are influenced by operational parameters, this type of situation could lead to inaccuracies during the lattice calculations.

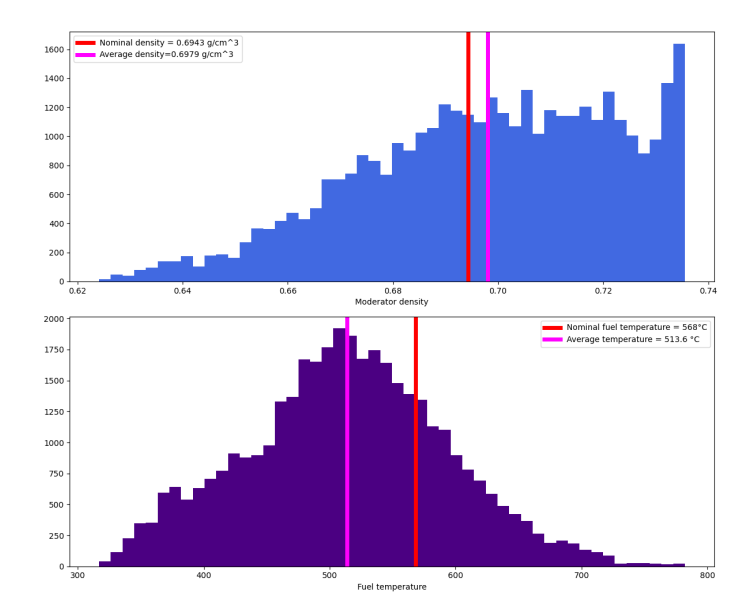


Figure 5.6: Histogram of the distribution for the assembly UOX 4.2 + 16 Gd pins (Assembly 5)

Assembly	Average moderator density	Average Fuel Temperature
1	$0.6918 \ g/cm^3$	541.0 °C
2	$0.6946 \ g/cm^3$	527.0 °C
3	$0.6875 \ g/cm^3$	565 °C
4	$0.6887 \ g/cm^3$	556 °C
5	$0.6979 \ g/cm^3$	513.6 °C

Table 5.1: Average values for each assembly used in TSN reactor

5.3 Deviations of the state parameters

From the previous section, the average trend of parameters such as water density and temperature for the assembly families was analyzed. It was found that the average values of the parameters are close to the nominal ones selected for standard depletion. However, it is essential to identify the nodes that deviate the most, from these conditions. These fluctuations could influence the plutonium quantity, making it necessary to investigate and find a way to quantify them.

A new indicator is introduced: the deviation from nominal condition averaged along depletion, which will be calculated for each state parameter as follows:

$$\epsilon_{\rho}(Bu) = \frac{\sum_{c=Bu_{i}}^{Bu_{f}} (\rho_{c} - \rho_{nom})(Bu_{c} - Bu_{c-1})}{\rho_{nom} * Bu_{av}}$$
(5.1)

$$\epsilon_{T_f}(Bu) = \frac{\sum_{c=Bu_i}^{Bu_f} (T_c - T_{nom})(Bu_c - Bu_{c-1})}{T_{nom} * Bu_{av}}$$
(5.2)

$$\epsilon_{Xe}(Bu) = \frac{\sum_{c=Bu_i}^{Bu_f} (Xe_c - Xe_{nom})(Bu_c - Bu_{c-1})}{Xe_{nom} * Bu_{av}}$$
(5.3)

$$\epsilon_{BC}(Bu) = \frac{\sum_{c=Bu_i}^{Bu_f} (BC_c - BC_{nom})(Bu_c - Bu_{c-1})}{BC_{nom} * Bu_{av}}$$
(5.4)

These deviations quantify how much the values deviate throughout the burnup cycle, acting as a sort of relative error compared to the nominal value averaged over the burnup.

In Fig. 5.7 the distribution of these deviations is shown. A significant observation is that only a small number of nodes exhibit a deviation equal to 0%, meaning that many nodes accumulate deviations during the burnup cycle. The calculated deviations provide a quantitative value but serve mainly for a qualitative study in selecting nodes for the next steps.

Starting from the cumulative deviation of water density, a range of approximately -10% to +10% is observed. For temperature deviations, the range extends from -20% to +30%. For completeness, histograms of boron and xenon deviations are also included.

The primary objective of this analysis is to determine how to select the nodes for further investigation. The first question to address is which parameter has the most significant influence on table generation, as an incorrect modeling of this parameter could lead to substantial errors.

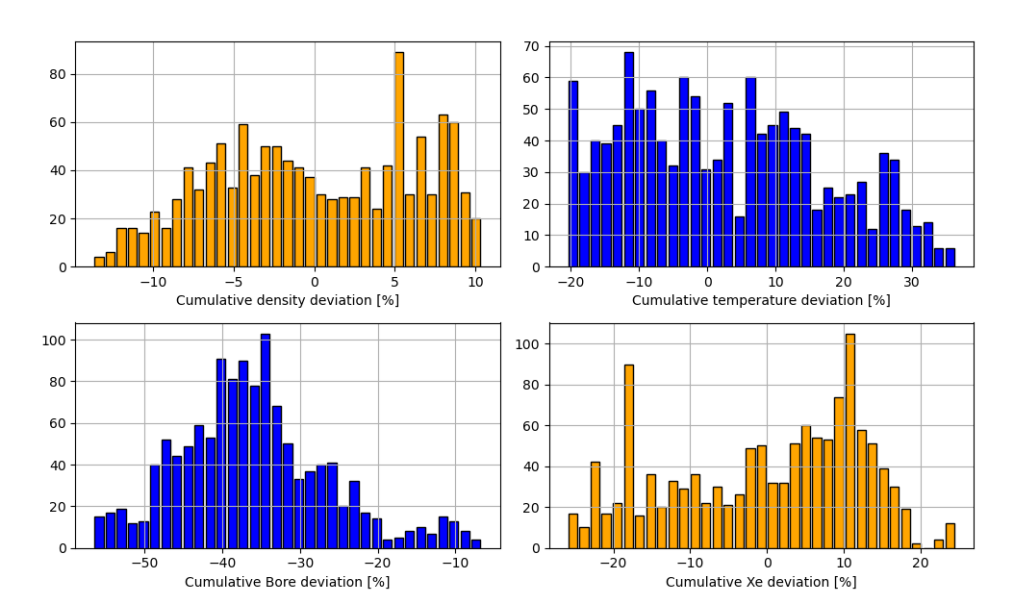


Figure 5.7: Histogram of the cumulative deviation for all nodes for each state parameter.

As explained in Section 4.2.1, the parameter PU is one of the best among others because

is capable to collect the history of a node.

$$PU = \frac{Pu}{^{238}\text{U}} \tag{5.5}$$

Through it, an information on the previous life is given and so on the variation of the parameters along the cycle. Therefore, in addition to calculating deviations for the state parameters, the deviation of PU can also be determined. Pu isotopes is interesting also due to its role in the fission process.

The only difference introduced is that, while for state parameters we want to see how the deviation accumulates throughout the cycle, for PU, the deviation is calculated only at the end of the cycle—at the last burnup step—without considering historical contributions.

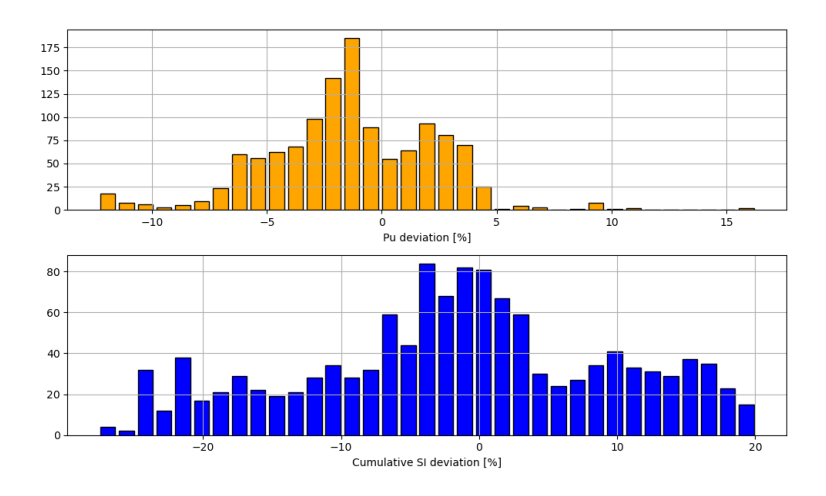
$$\epsilon_{PU}(Bu = last) = \frac{PU_c - PU_{nom}}{PU_{nom}}$$
(5.6)

Additionally, the variation of the spectral index is calculated to observe the cumulative effect of each node over the entire cycle. The spectral index is defined as:

$$SI = \frac{\phi_1}{\phi_2}$$

The corresponding deviation is given by:

$$\epsilon_{SI}(Bu) = \frac{\sum_{c=Bu_i}^{Bu_f} (SI_c - SI_{nom})(Bu_c - Bu_{c-1})}{SI_{nom} * Bu_{av}}$$
(5.7)



5.4 Correlations

In this chapter, the correlations between different variables will be analyzed to understand their mutual effects and identify any significant dependencies. The objective is to assess how variations in one quantity influence the others, thus providing a quantitative basis for interpreting the obtained results. Statistical methods will be employed to compute correlation coefficients, such as the Pearson coefficient, to assess if you two variables are linearly correlated. This analysis is essential for validating the developed model and gaining a deeper understanding of the system's behaviour.

The pearson coefficient is a measure of the linear association between two variables, this

value is between -1 and +1, where:

$$r = \frac{\sum_{i} (x_i - \bar{x})(y_i - \bar{y})}{\sqrt{\sum_{i} (x_i - \bar{x})^2 \sum_{i} (y_i - \bar{y})^2}}$$

- -1 indicates a perfectly negative linear correlation, if one variable increases than the other decreases linearly.
- 1 indicates a perfectly positive linear correlation, the increasing of the two variables is simultaneously.
- 0 indicates no linear correlation between the two variables.

Besides the Pearson coefficient, the p-value is also used to determine statistical significance. Typically, the obtained p-value is compared to a predefined significance level of $\alpha = 0.05$.

- if p > 0.05 the result is statistically significant
- if p < 0.05 the result is not statistically significant

The Spearman coefficient, denoted as ρ_s , is a non-parametric measure of the strength and direction of a *monotonic relationship* between two ranked variables. If d_i is the difference between the ranks of the two variables for observation i, and n is the total number of observations, then Spearman's coefficient (in the case of no tied ranks) is calculated as:

$$\rho_s = 1 - \frac{6\sum d_i^2}{n(n^2 - 1)}$$

Value range:

- $\rho_s = 1$: perfect increasing monotonic relationship
- $\rho_s = -1$: perfect decreasing monotonic relationship
- $\rho_s = 0$: no monotonic correlation

Spearman's coefficient is particularly useful when:

- the data do not follow a linear relationship
- the variables are ordinal
- the presence of outliers may distort other correlation measures

Parameter	Pearson r	P-value	Spearman s	P-value
Density	-0.47	0.000	-0.5	0.000
Fuel Temperature	0.14	0.000	0.16	0.000
Boron Concentration	-0.08	0.003	-0.1	0.000

Table 5.2: Pearson and Spearman correlation coefficients

The obtained results show that:

The water density deviation exhibits a moderate negative correlation and is statistically significant. The relationship is not perfectly linear, likely due to the presence of some outliers.

• The fuel temperature and boron concentration exhibit a weak positive correlation with minimal impact.

In Fig. 5.8, the graphical representation of the correlations between the deviations of state parameters, PU deviation, and SI deviation is shown. In particular, this figure represents cumulative deviations, meaning the final deviation value at the end of the cycle, also considering any compensations (positive and negative deviations), for all core nodes. The nodes are grouped according to their axial elevation (z-coordinate), ranging from light pink at the bottom of the core to dark purple at the top.

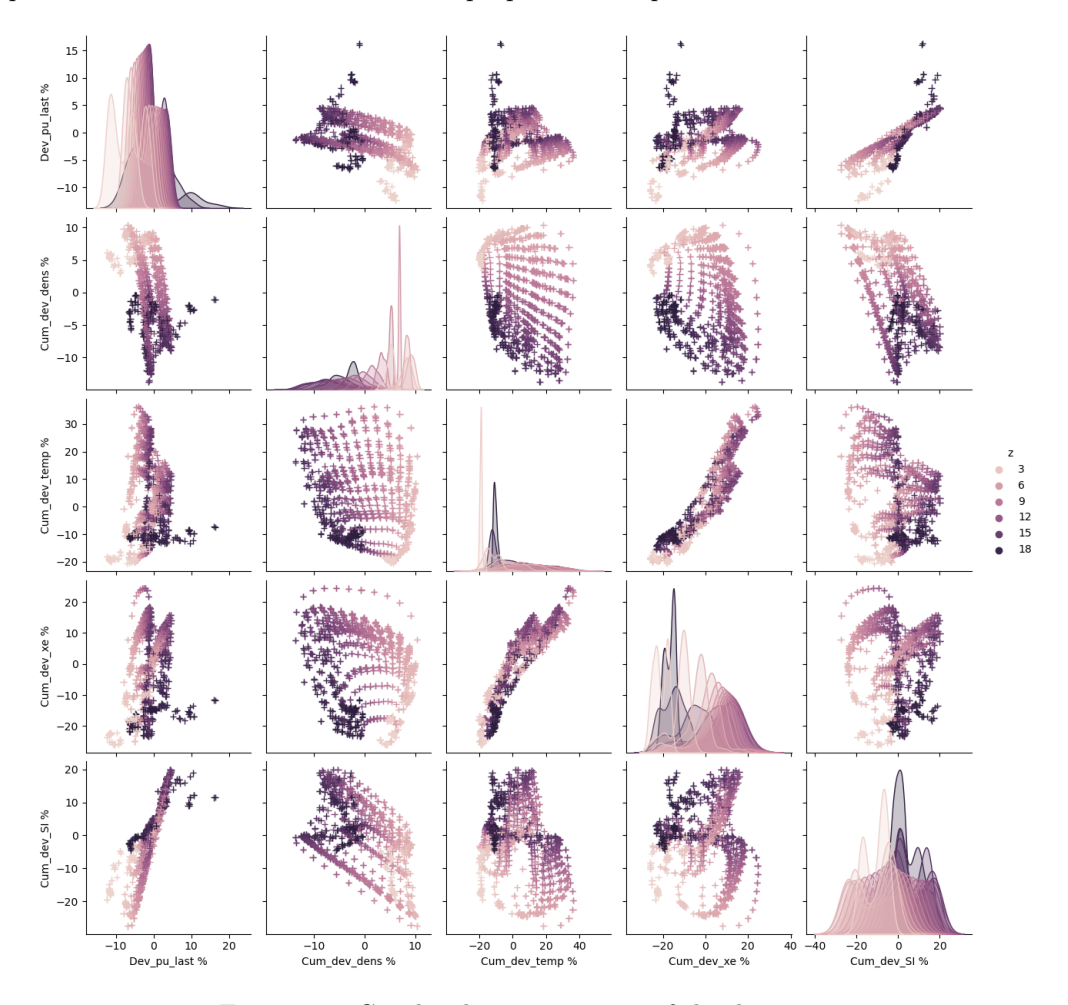


Figure 5.8: Graphical representation of the deviations.

The first row is of primary interest as it represents the correlation with ϵ_{PU} , eq. 5.6 In Fig. 5.9 a zoomed view of the first row is provided, illustrating the correlation between PU deviation and other deviations.

The first graph from the left shows the distribution of PU deviation, highlighting axial nodes with different shades. The second graph is arguably the most important in this chapter, as it presents the real correlation between plutonium formation and water density, considering actual core data from simulation. The theoretical expectation was to observe a strong correlation between water density and plutonium. Specifically, at the top of the core, a decrease in water density was expected to result in neutron spectrum hardening and increased plutonium production, whereas at the bottom of the core, an increase in water density was expected to soften the neutron spectrum and decrease plutonium production.

Analyzing the figure, the expected general trend is observed, but some outliers are present, particularly at the top and bottom of the core. Investigating these outliers, it was found that they are associated with two distinct physical factors: control rods and the reflector. Control rods (present at the top of the core) significantly alter plutonium production, especially since they do not remain in a fixed position throughout the cycle. The presence of control rods hardens the neutron spectrum, leading to higher plutonium buildup. Conversely, the reflector at the bottom of the core softens the neutron spectrum, reducing plutonium accumulation.

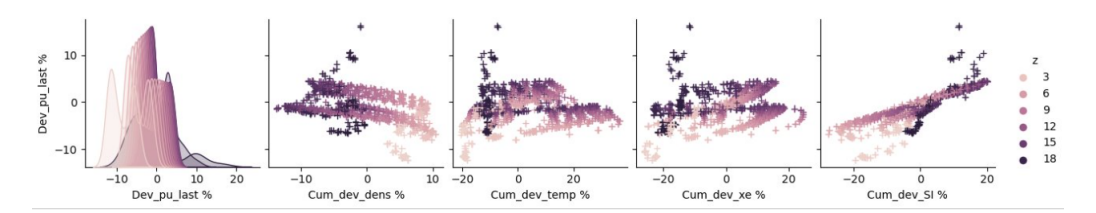


Figure 5.9: Zoomed-in view of the first row.

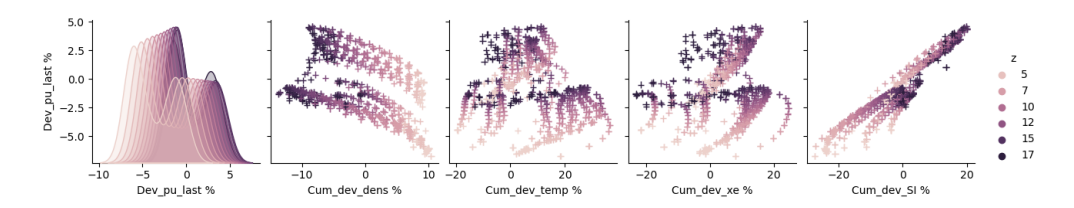


Figure 5.10: Zoomed-in view of the first row without top and bottom core nodes.

By filtering out data from the top and bottom of the core, where control rods and the reflector are present, Fig. 5.10 is obtained. As expected, some outliers are no longer present, and the plutonium deviation now ranges between [-5%, +5%].

Despite filtering the data, correlations remain unclear. For instance, when observing the correlation between the spectral index and plutonium, distinct node families can be identified. If the same figure is filtered based on assembly type rather than axial coordinate, the result is shown in Fig. [5.11].

This final figure reveals an interesting finding: plutonium formation is not solely influenced by state parameters but also by something else. To better evaluate the correlations considering these insights, Pearson and Spearman coefficients are recalculated. Comparing the values in Table 5.2 and Table 5.3 an increase in correlation strength is observed. This indicates that when considering each case separately, the correlations are stronger and more dependent on each other.

Coefficient	Assembly 1	Assembly 2	Assembly 3	Assembly 4	Assembly 5
$r(\epsilon_{PU}, \epsilon_{dens})$	-0.83	-0.89	-0.92	-0.95	-0.76
$s(\epsilon_{PU},\epsilon_{dens})$	-0.84	-0.9	-0.94	-0.98	-0.82
$r(\epsilon_{PU}, \epsilon_{tfuel})$	0.57	0.66	0.6	0.74	-0.02
$s(\epsilon_{PU}, \epsilon_{tfuel})$	0.24	0.53	0.22	0.55	0.03
$r(\epsilon_{PU}, \epsilon_{cb})$	-0.45	-0.34	-0.37	-0.34	0.08
$s(\epsilon_{PU},\epsilon_{cb})$	-0.43	-0.39	-0.45	-0.41	0.04

Table 5.3: Pearson and Spearman correlation coefficients for each assembly without considering the top and the bottom

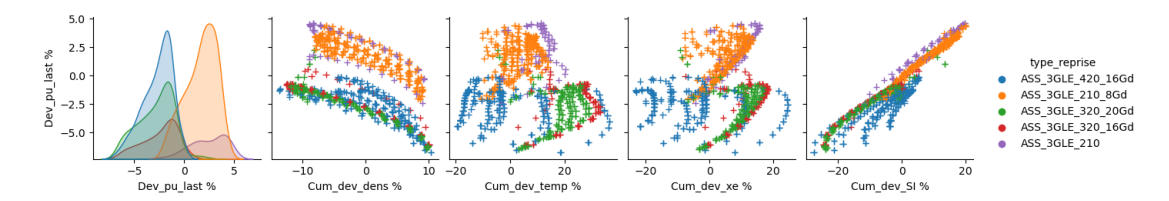


Figure 5.11: Correlation representation considering different assembly types.

In the following section, correlations will be examined in detail for each assembly type.

5.4.1 Correlations in each case study

To investigate the origin of the different families, the data are separated by assembly, so that each assembly can be considered as a distinct case study. It is not possible to analyze them globally since they operate under different conditions and exhibit unique behaviors in terms of plutonium formation. The following figures provide a graphical representation of the deviations along the x-direction, this direction is labeled with letters).

In Fig. 5.12, the second graph presents two distinct trends. The red line represents column J (Fig. 5.1), which shows a significantly different plutonium formation pattern compared to other assemblies of the same type. However, despite this deviation in plutonium, the water density variation remains identical to that of the other assemblies. The curve appears to be systematically shifted, and in some nodes, the plutonium deviation is even negative, indicating lower plutonium production. A similar trend can be observed in the temperature and boron deviations in relation to plutonium.

The relationship between ϵ_{SI} and plutonium reveals a spectral softening effect specific to assembly J. Upon further investigation, it becomes evident that, despite being of the same type, these assemblies experience different surrounding conditions. Assemblies E, F, and H share the same neighboring assemblies, whereas assembly J is located at the center of the core, surrounded by different neighbors. This observation leads to the hypothesis that plutonium production is influenced not only by state parameters but also by the surrounding environment, which must be considered when analyzing these correlations. Assembly type

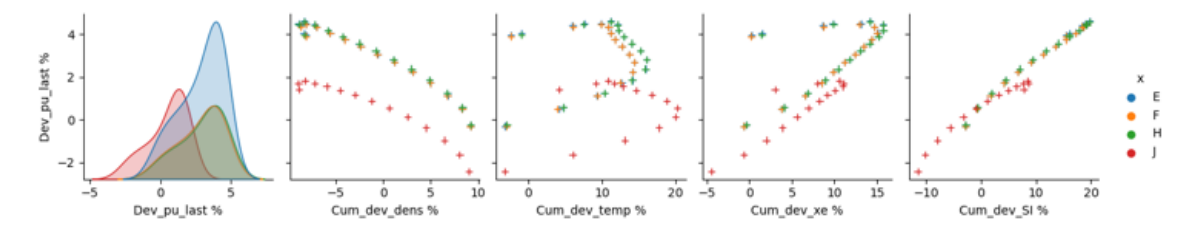


Figure 5.12: Representation of the correlations the assembly 1

2 exhibits a similar behavior, with the key difference that these assemblies are more widely distributed within the core. Some are located near higher-enriched assemblies, leading to a hardening of their neutron spectrum. This difference in distribution is evident in the graph, as all curves are shifted despite having the same water density deviation. Once again, this demonstrates the presence of an additional key parameter influencing plutonium production beyond the state parameters. As in the previous case, the spectral index correlation with PU deviation follows the same linear trend.

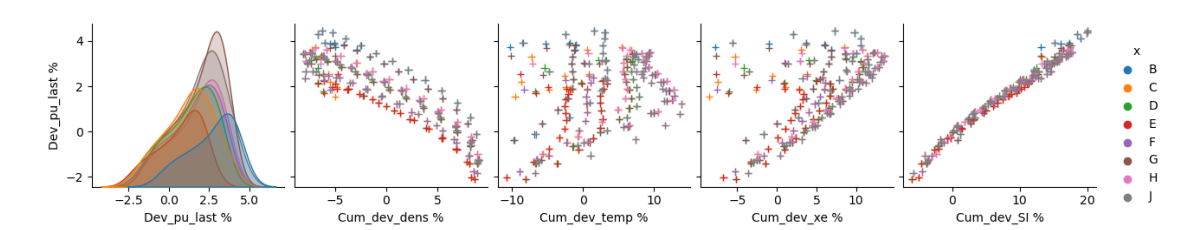


Figure 5.13: Representation of the correlations for assembly type 2

Assembly type 3 presents two distinct curves in the second graph. The blue curve corresponds to assembly D, which differs from others of the same type due to its proximity to an assembly with a higher enrichment. The data and plots clearly highlight the significant influence of the surrounding environment on plutonium production. The fact that the plutonium deviation is consistently negative indicates that this assembly produces less plutonium throughout the entire cycle than during the nominal depletion in lattice calculation.

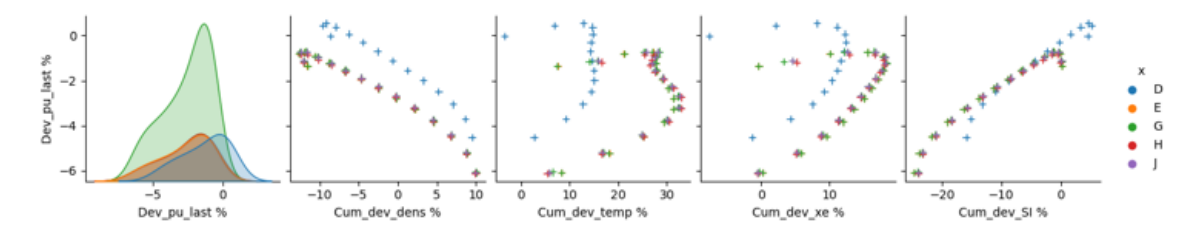


Figure 5.14: Representation of the correlations for assembly type 3

All assemblies of type 4 are evenly distributed throughout the core. As a result, all curves overlap, indicating a uniform behavior.

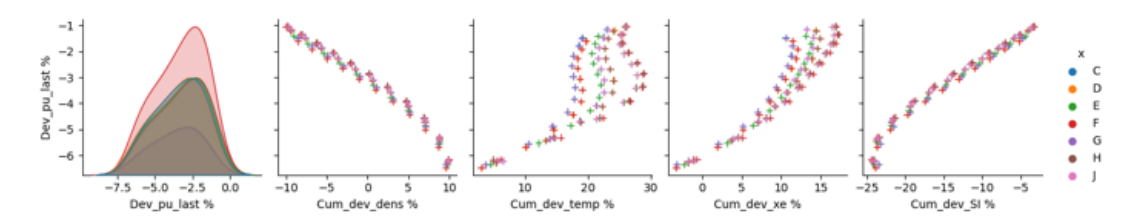


Figure 5.15: Representation of the correlations for assembly type 4

Assembly type 5 represents an interesting case, as it is located at the core's periphery. Here, another important parameter significantly affects the results. Unlike the other cases, where all curves were simply shifted with different plutonium production levels, this assembly exhibits a distinct water deviation. The correlation between plutonium production and water density is weaker, which is also reflected in the spectral index. This pronounced difference in behavior is likely due to its proximity to the reflector.

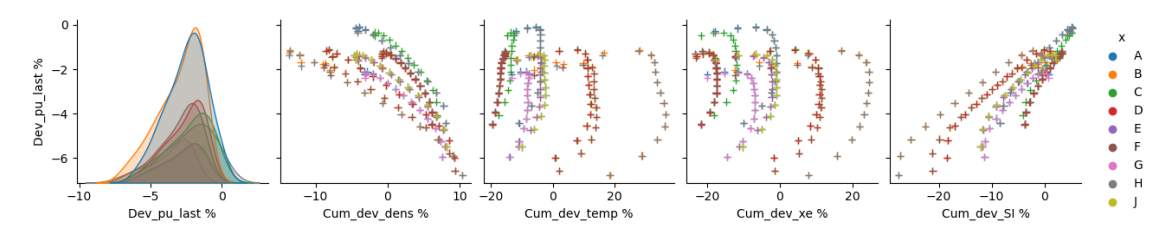


Figure 5.16: Representation of the correlations for assembly type 5

One of the main and unexpected findings of the study is that the analysis became significantly more complex than anticipated. The history effect model of SCIENCE V2, infact, accounts only for water density as the driver of spectrum shifts, whereas the results clearly indicate that the surrounding environment also exerts a strong influence on both the spectrum and the isotopic concentrations. The following step will be to validate the history model used in SCIENCE V2, using the analysis done in this chapter to select the best candidates for the process.

Chapter 6

Validation

This final chapter presents the results of the study. The adopted methodology consisted in replicating table A conditions implemented in SCIENCE V2 framework in order to reconstruct the homogenized cross sections (HXS) assuming the nominal depletion conditions. Once the macroscopic cross sections were obtained, they were subsequently used to reconstruct infinite medium multiplication factor multiplication factor (k_{∞}) . It is worth emphasizing that the main objective is to assess the validity of the correction method applied by SCIENCE V2 to the microscopic and residual macroscopic considering the history effect described above related to the two-step calculation. To validate the proposed approach, the results obtained by reproducing the calculations performed between the first and second steps in SCIENCE V2 will be compared against reference values derived from full-core simulation and the parameter used will be as mentioned before k_{∞} . The results are obtained through the new code APOLLO3®. It is the new deterministic nuclear code for lattice and core calculation under development in a common project between CEA, Framatome and EDF with the objective of improving accuracy, flexibility and architecture of it. The advancement in the code architecture leads to a less computation effort in terms of time and memory sizes in according to the necessities of the actual nuclear industry. It will also provide enhanced algorithms and the future developed methodology in neutronics deterministic modelling. Moreover the interface of this new code is more user friendly thank to the Python interface that leads to easily perform a new calculation.

- APOLLO3® has two different type of output files:
 - Multi-parametric Output (MPO) with a fixed structure (HDF5 format);
 - File in hdf format that contains the information chosen by the user.

The user has to define a priori the cell geometries, properties of materials, lattice configurations and working parameters but it is needed to define also the meshes for self-shielding and flux calculation, the options of all solvers and the sequence of calculation.

The flexibility of APOLLO3[®] was exploited for the goals of this thesis, since it was necessary to run different simulations for the same assembly changing different conditions.

6.1 Selection of the nodes

Following the preliminary analysis, the subsequent step involves selecting the most significant nodes for inclusion in the validation process.

6.1.1 First case

The first candidate is the 2.1% assembly without gadolinium, which, as previously explained, exhibits a distinctive behavior. As shown in Figure 6.1 two different curves are present: one of them represents only the assembly in position J, which appears to produce less plutonium compared to its counterparts.

An interesting observation emerges: for the same axial coordinate (i.e., at equal water density and so equal water density deviation), plutonium production varies depending on the assembly's position within the core. This effect is clearly represented by ΔPU_{env} . Looking at the figure on the right, it is evident that the difference in plutonium production is closely correlated to spectral variations.

Given these considerations, the selected candidate is the assembly that is least affected by environmental influences (J09), allowing us to isolate the effects of water density differences. The central node and another node located in the upper part of the core, where water density is lower, have been chosen for further analysis.

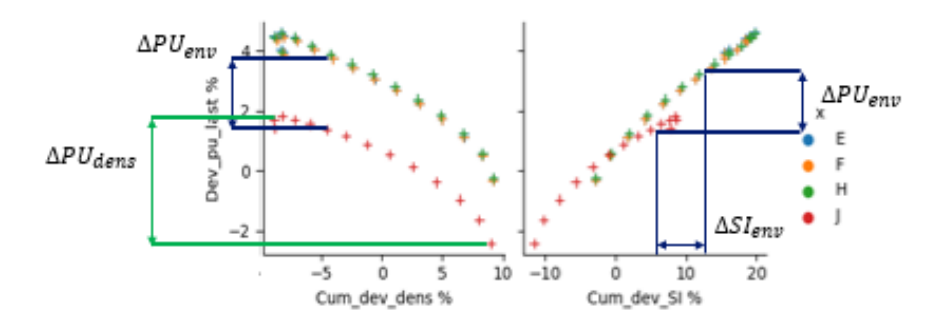


Figure 6.1: First case: Deviation in plutonium correlated to different density and the environment

The selected nodes and corresponding burnup points are listed below. For this assembly, the simulation will be conducted under an infinite medium approximation:

- J09 axial node 9 (middle of the core):
 - Middle of cycle
 - End of cycle
- J09 axial node 13 (upper part of the core):
 - Middle of cycle
 - End of cycle

6.1.2 Second case

The second selected candidate belongs to the assemblies with 3.2% enrichment and 16 gadolinium pins, which exhibit a behavior similar to the first case but with gadolinium: this is the purpose of having almost the same behavior and analysis but on a different assembly design. Once again, one assembly stands out from the others—this time, the one positioned along column D.

Due to its proximity to assemblies with higher enrichment, this assembly produces more plutonium compared to its counterparts, as its neutron spectrum is harder. The other assemblies in positions E, G, H, and J share the same distribution. Among these, the assembly in position G has been selected because it is surrounded entirely by similar assemblies, making it more suitable for simulation.

Additionally, for one of these nodes, the environment will also be simulated in the next phase. As in the previous case, a central axial coordinate has been chosen, along with a node located at the bottom of the core.

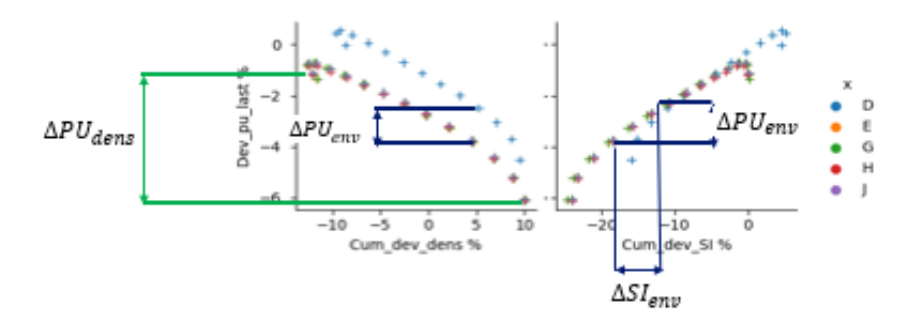


Figure 6.2: Second case: Deviation in plutonium correlated to different density and the environment

The selected nodes and corresponding burnup points are as follows:

- G11 axial node 9 (middle of the core):
 - Middle of cycle
 - End of cycle
- G11 axial node 5(bottom of the core):
 - Middle of cycle
 - End of cycle
- G11 axial node 9 (middle of the core) + environment:
 - -6200 MWd/t

6.2 Methodology for comparison

In order to validate properly the history model the process chosen is to reproduce the method implemented in SCIENCE V2, in particular in APOLLO2-F, during the reconstruction of the multiparametrized libraries.

In Chapter 5 a detailed analysis of the TSN core was carried out, identifying several key fuel assemblies that exhibit distinct characteristics.

- One assembly without gadolinium pins and an enrichment of 2.1%.
- One assembly with gadolinium pins and higher enrichment 3.2%.

For each of these assemblies, a specific node was chosen. Multiple simulations were then performed using APOLLO3[®] in order to replicate the reconstruction previously done with SCIENCE V2.

A main difference has to be considered: in APOLLO2-F is implemented the nuclear library JEF2.2, while in APOLLO3[®] the library is JEFF3.1.1. Furthermore, the difference in the calculation scheme involves a difference in isotopes concentrations and as a result a difference in microscopic cross sections. During the validation process we handle with differences between microscopic cross sections and isotope concentrations so the difference between the two libraries is not a problem. The comparison method will be explained more in details below.

6.2.1 Detailed procedure

The reconstruction of the history model in SCIENCE V2 is performed in several steps:

- First step: two different fuel depletion of the assembly imposing two different set of physical parameters.
 - Base or nominal assembly depletion: simulation that starts with a fixed set of physical parameters (water density, fuel temperature and boron concentration).
 - Perturbated assembly depletion: also in this case the simulation starts with fixed set of parameters but they are different from the "base" case, considering that the SCIENCE V2 is simulate only a difference in water density is considered.
- Second step: restart calculations also called "branches", these simulations starts considering the results of the depletions (isotope concentrations) at each burnup steps. They have to capture the differences considering instantaneous variation of the parameters.
- Third step: interpolation according the real node conditions. The interpolation is a mandatory step in core simulation since every node (refer to the different axial coordinate in z-direction) is in a different condition and it is depleted in a different way.
- Last step: generation of a dataframe where is collected a set of HXS for a single node in a given burnup point. They contain HXS for each energy group.

6.2.2 Fuel depletions

This is the initial step from which the HXS reconstruction begins. For the selected assembly, two different simulations are performed, as previously mentioned. The parameters chosen for the base simulation are reported in Table [6.1] in this case, the assembly is depleted starting from conditions considered the most likely during the plant's operational life. For the same assembly, a second simulation is also performed, the perturbed one Tab.[6.2] in which only the water density is modified. The water density is assumed to be the main driver of variations in the neutron spectrum.

The other parameter to set is the burnup mesh. For the assemblies with gadolinium the burnup mesh has to be finer. The mesh used is the same as in SCIENCE V2, however the predictor corrector method is used in order to obtain results that are independent from the burnup. Once all the parameters are imposed, the simulation can be performed; the results from this first step that are necessary from this second step are the isotope concentrations

	Parameter	Value	
	Water density	0.6943	g/cm^3
	Fuel temperature	835.21	K
Ī	Boron Concentration	700	ppm

Table 6.1: Operating conditions of the base depletion.

Parameter	Value	
Water density	0.7377	g/cm^3
Fuel temperature	841	K
Boron Concentration	700	ppm

Table 6.2: Operating conditions of the perturbated depletion.

Step	Burnup [MWd/tU]
1	0
2	150
3	500
4	1000
5	2000
6	4000
7	6000
8	8000
9	10000
10	12000
11	14000
12	16000
13	18000
14	20000
15	22000
16	24000
17	26000

Table 6.3: Burnup values for each simulation. Note that this mesh is used only for visualization of the results and does not correspond to the calculation mesh.

for each burnup step. In Fig. 6.3 it is possible to see a graphical representation of the first step where two different two parallel simulations are performed with the same burnup mesh but with different fixed values. The main key point at this moment is to catch the differences between the isotopes concentrations considering that the fixed values in the simulations are different.

6.2.3 Restart calculations

The objective of the second step is to prepare the homogenized cross sections (HXS) required by the core code to perform bilinear interpolation. From the previous step, the isotope concentrations are obtained. To properly generate the HXS for the next step, it is essential to estimate the instantaneous effect of varying one or more state parameters. Each burnup point defined in the first step, associated with a specific isotopic composition serves as the starting point for a set of calculations known as "branches". To perform these calculations, it is necessary to specify the burnup step at which the branches should be evaluated. Once the burnup step is selected, APOLLO3® retrieves the isotope concentrations corresponding

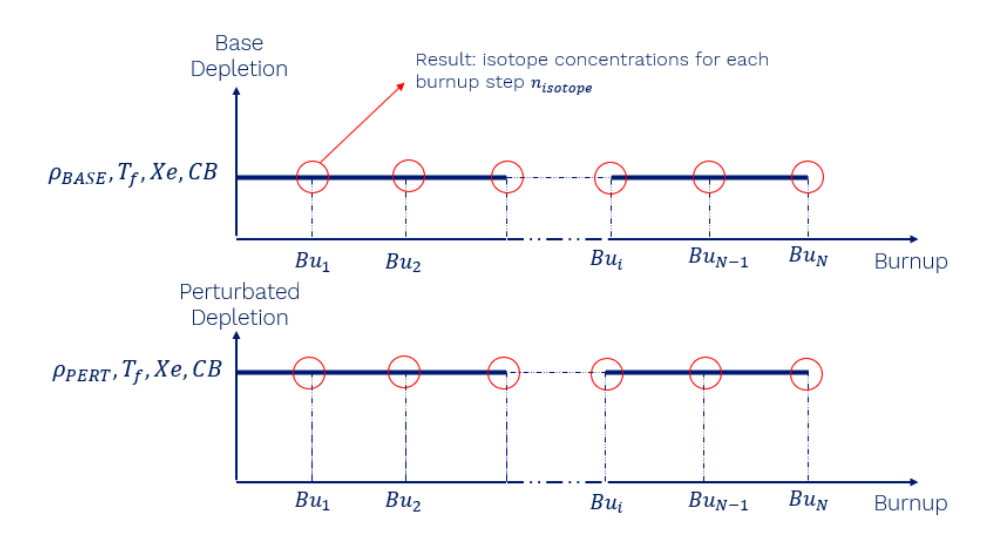


Figure 6.3: Representation of the base and perturbed depletion

to that step. At this stage, the user must indicate how the state parameters should be perturbed in order to generate the required cross sections for interpolation. The results that are obtained can be use as follows.

In SCIENCE V2, accurate HXS results are obtained through an approach that sums multiple contributions, each calculated by varying a single parameter, such as temperature, for example. To obtain these different contributions different branches are performed for each burnup point. Considering the table decomposition implemented inside SCIENCE V2 in order to consider only the history effect has to be considered a common working point (density, temperature, boron concentration and xenon) between the base depletion and the perturbated depletion, S_0 . This working point is one of point of branch "A".

Parameter	Value	
Water density	0.7046	g/cm^3
Fuel temperature	835.21	K
Boron Concentration	700	ppm

Table 6.4: S_0 conditions imposed for each burnup point

From Fig. 6.4 the representation of the common working point in the two branches is shown. In general it states that the HXS at the node level is the sum of the microscopic

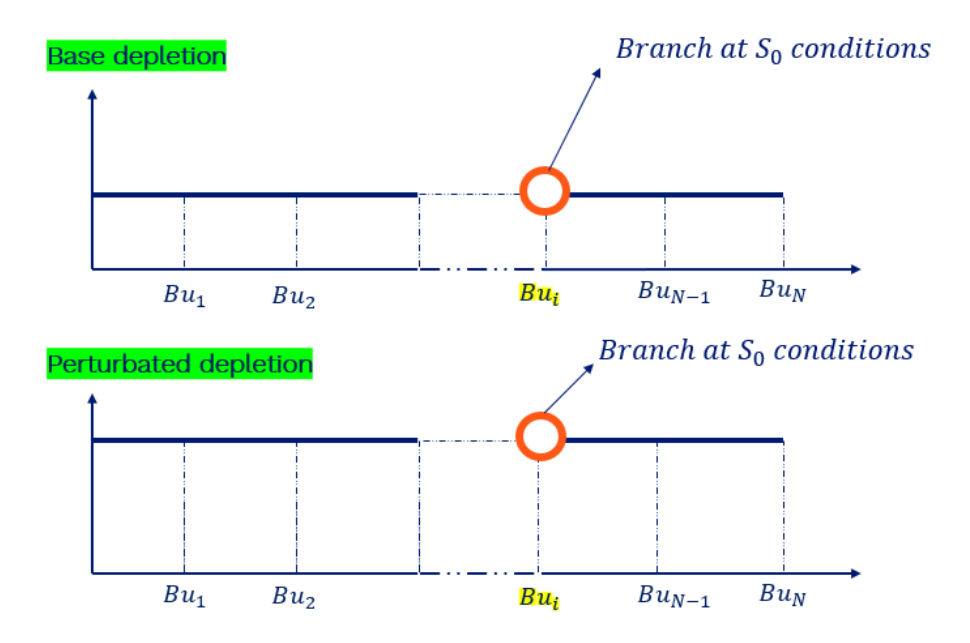


Figure 6.4: Representation of the branches for base and perturbated depletions.

cross section from the branch calculating at the base depletion σ_{A,S_0} and a correction called $\Delta\sigma_{D,S_0}$ which is the result of the history model used in SCIENCE V2 (corresponding to the D table in the SCIENCE V2 cross sections tables framework), and is computed using a bilinear interpolation (Pu/U and BU).

$$\sigma = \sigma_{A,S_0} + \Delta \sigma_{D,S_0} \tag{6.1}$$

This second step is necessary to reconstruct $\Delta \sigma_{D,S_0}$, for each burnup point are provided the microscopic cross sections for each isotope, reaction (absorption and fission) and group (1

and 2) as shows in Fig. 6.5. If a generic burnup is consider Bu_i from branches in base and perturbated depletion the following cross sections result $\sigma_{BASE,S_0}^{Bu_i}$ and $\sigma_{PERT,S_0}^{Bu_i}$.

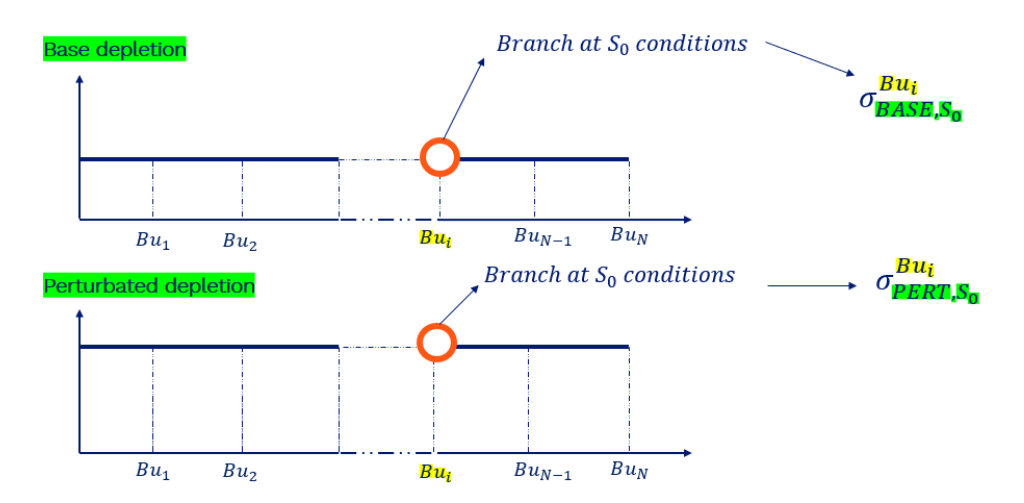


Figure 6.5: Representation of the branches for base and perturbated depletions. σ at S_0 conditions is necessary for the validation.

Finally, it is possible to calculate the $\Delta \sigma_{D-A}^{Bu_i}$:

$$\Delta \sigma_{D-A}^{Bu_i} = \sigma_{PERT,S_0}^{Bu_i} - \sigma_{BASE,S_0}^{Bu_i} \tag{6.2}$$

6.2.4 Third step: Bilinear interpolation

All the previous step are performed for each assembly type (in TSN reactor there are 5 different type of assembly), considering that each node in the reactor have different conditions is necessary to interpolate the results previously calculated. The interpolation step is performed by SMART (the core code) where the interpolation method used is a bilinear interpolation. The interpolation parameter used in SCIENCE V2 is Pu/U (eq. 5.5). It is a ratio between concentrations coming from branches, it is the second result from the branches along with $\sigma_{BASE,S_0}^{Bu_i}$ and $\sigma_{PERT,S_0}^{Bu_i}$, Fig. 6.6 The result of this step is the correction of the HXS interpolating according the local node condition. Assuming the real depletion known by the core calculation (as in Fig. 6.7) the burnup point (Bu_{real}) and the corresponding PU are considered (PU_{real}). The burnup selected by the real depletion falls between two burnup points within the mesh. After identifying these two points, the $\Delta \sigma$, PU values and BU for each of them are used for interpolation. The informations of point that has to be interpolated are PU and BU.

Now it is possible to calculate the correction that emulate the SCIENCE V2 history model considering the local conditions.

$$\Delta \sigma_{D}^{Bu_{real}} = f(Bu_{real}, PU_{real}, Bu_{i}, \Delta \sigma_{D-A}^{Bu_{i}}, Bu_{i-1}, \Delta \sigma_{D-A}^{Bu_{i-1}}, PU_{BASE}^{Bu_{i}}, PU_{BASE}^{Bu_{i}}, PU_{BASE}^{Bu_{i-1}}, PU_{PERT}^{Bu_{i}})$$
(6.3)

Finally is possible to reconstruct the HXS $(\sigma_{H-MODEL})$ considering the definition:

$$\sigma_{H-MODEL} = \sigma_{BASE,S_0}^{Bu_{real}} + \Delta \sigma_D^{Bu_{real}}$$
 (6.4)

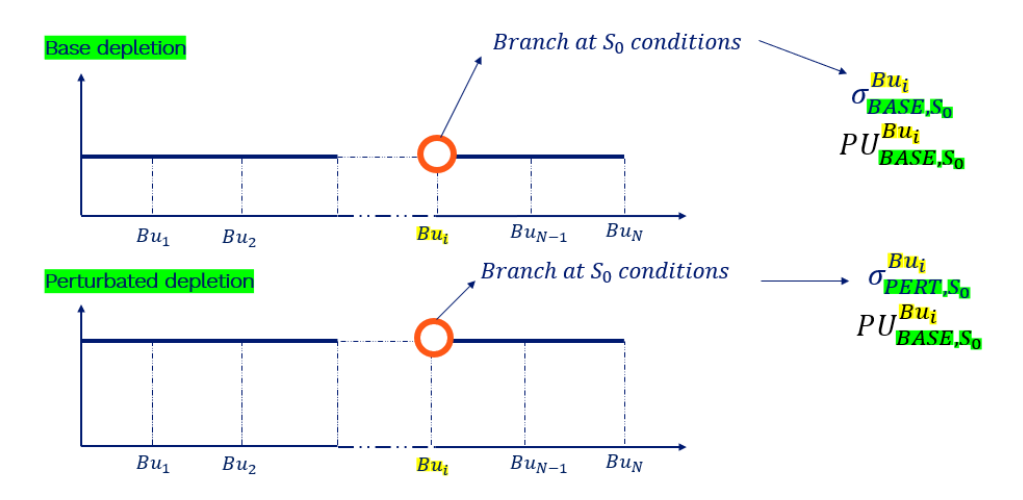


Figure 6.6: Representation of the branches for base and perturbated depletions. PU at S_0 conditions is necessary for the validation.

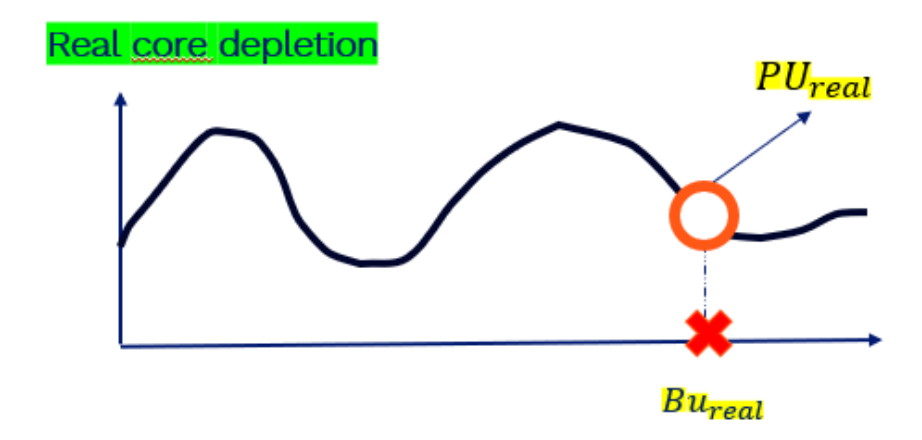


Figure 6.7: Graphical representation of the real core depletion

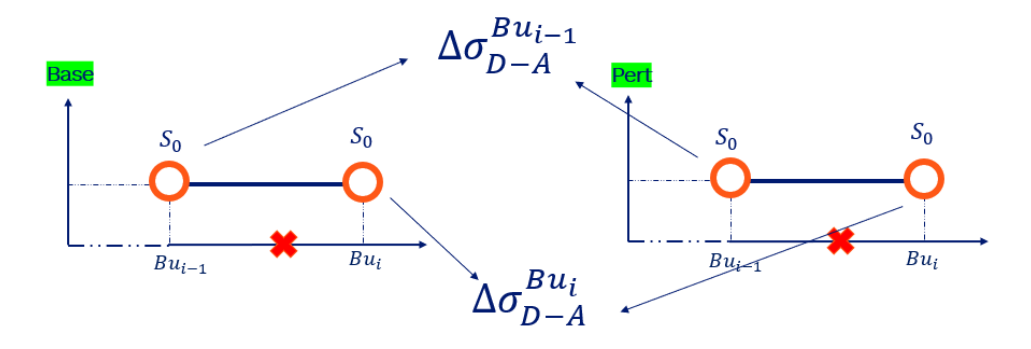


Figure 6.8: Burnup interval considered for the interpolation

Then it is trivial the reconstruction of the macroscopic cross section $(\Sigma_{H-MODEL})$:

$$\Sigma_{H-MODEL} = \sum_{is=1}^{n_{is}} N_{is}^{Bu_{real}} \sigma_{H-MODEL}$$
(6.5)

Comparison method

During the core data analysis process, all values of moderator density, fuel temperature, and boron concentration were collected at each burnup step. These data were obtained from a previous full-core simulation of the TSN reactor, furthermore they had been used in the previous chapter. Specifically, these parameters can be set in APOLLO3[®] through an "realistic depletion" approach, where the corresponding values of density, fuel temperature, and boron concentration are fixed at each burnup step. This method ensures that the depletion process

precisely replicates that of the core simulation. Once the depletion data, including isotope concentrations, have been collected, it becomes possible to perform a branch calculation (similar to what was done for the base and perturbed depletion). Now the focus is to follow the real evolution in the core (an example in Fig. 6.9) with APOLLO3[®]. This procedure

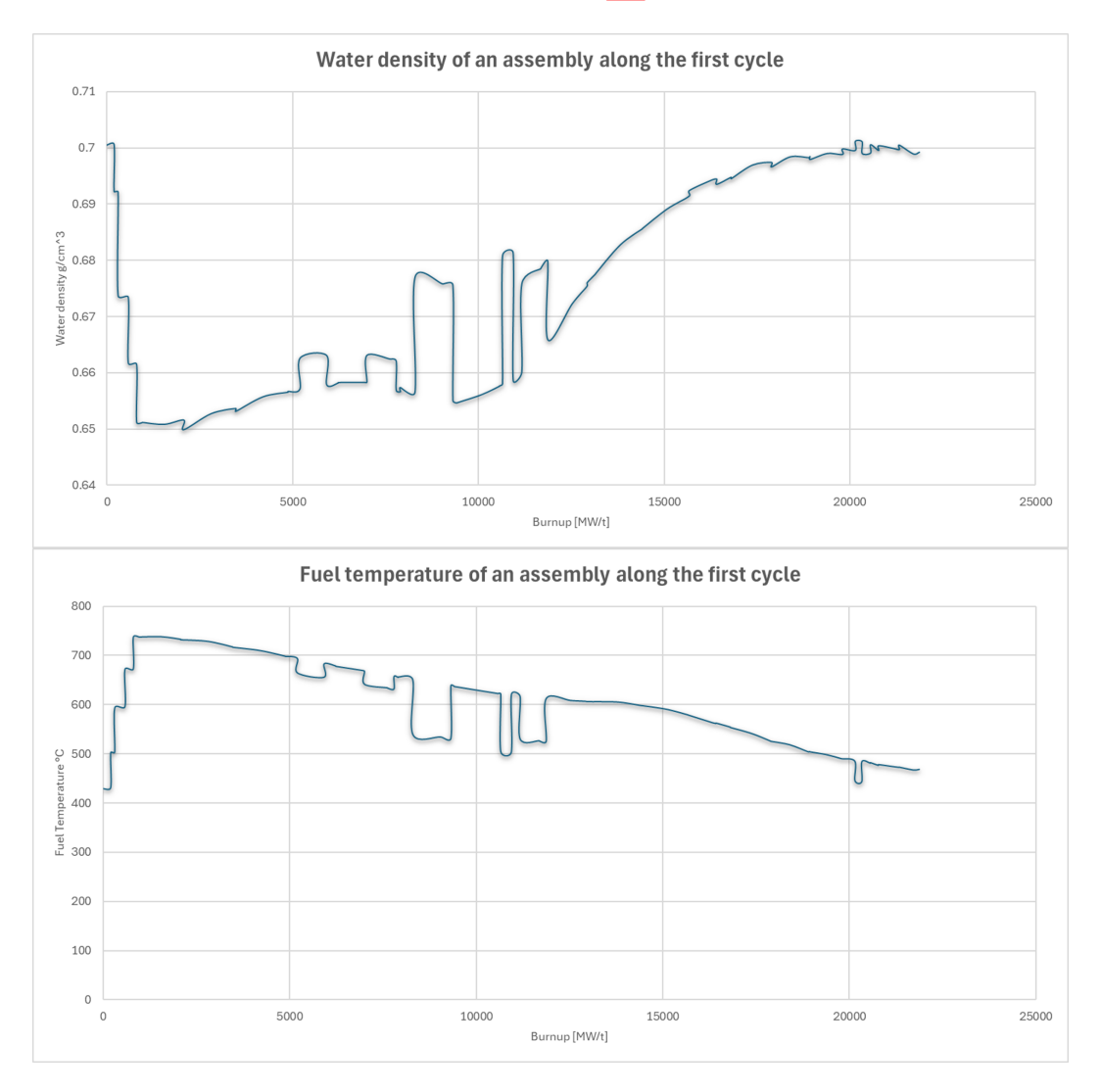


Figure 6.9: Real evolution of water density and fuel temperature along the cycle on a node ones of the 3D core coarse mesh.

enables a highly precise comparison between real depletion values and those derived from the spectral history model implemented in SCIENCE V2, replicated in APOLLO3®. This is possible because, once the branch calculations are performed, the microscopic cross-section data for each isotope, reaction, and energy group $(\sigma_{AP3,S_0}^{Bu_{real}})$ can be easily extracted. From these microscopic cross-sections, the macroscopic cross-sections for each reaction and energy group $(\Sigma_{AP3,S_0}^{Bu_{real}})$ can be computed. To further assess the impact of the correction term $\Delta\sigma_D^{Bu_{real}}$ the infinite multiplication factor k_∞ is calculated in order to have just one value for the comparison. The equation for k_∞ is derived from the neutron diffusion equation:

$$k_{\infty} = \frac{\nu \Sigma_{f1} + \frac{\nu \Sigma_{f2} \Sigma_{1 \to 2}}{\Sigma_{a2}}}{\Sigma_{a1} + \Sigma_{1 \to 2}}$$

$$(6.6)$$

In this section, the different results for the various nodes will be shown. For the microscopic cross sections, four different figures are presented, in which the results for absorption and fission for each isotope are shown for every energy group. In each figure, the realistic values, represented as deltas, are compared with the values obtained from the spectral history modelling as implemented in SCIENCE V2.

$$\Delta \sigma_{real,rel} = \frac{\sigma_{real,S_0}^{Bu_{real}} - \sigma_{A,S_0}^{Bu_{real}}}{\sigma_{A,S_0}^{Bu_{real}}}$$
(6.7)

$$\Delta \sigma_{real,abs} = \sigma_{real,S_0}^{Bu_{real}} - \sigma_{A,S_0}^{Bu_{real}} \tag{6.8}$$

The same approach for the macroscopic cross sections.

$$\Delta\Sigma_{real,rel} = \frac{\Sigma_{real,S_0}^{Bu_{real}} - \Sigma_{A,S_0}^{Bu_{real}}}{\Sigma_{A,S_0}^{Bu_{real}}}$$
(6.9)

$$\Delta\Sigma_{real,abs} = \Sigma_{real,S_0}^{Bu_{real}} - \Sigma_{A,S_0}^{Bu_{real}}$$
(6.10)

The global parameter chosen to be included in the validation is k_{∞} , which, also in this case, is not considered as an absolute value but rather as the difference in k_{∞} . In particular, the comparison will be made between:

No correction:
$$k_{\infty}^{real,S_0} - k_{\infty}^{A,S_0}$$
 (6.11)

With correction:
$$k_{\infty}^{real,S_0} - k_{\infty}^{HM,S_0}$$
 (6.12)

6.3 Case study: Assembly 1

The first candidate selected for validation is the assembly without gadolinium. Referring to Figure 5.1, which shows the positioning of the assemblies within the core, this corresponds to the assembly located at position J09. The neighboring assemblies are not exactly identical, but the assumption of similarity is adopted. For this specific case, it was decided, thanks to the analysis performed in previous chapter, to exclude the influence of the surrounding environment, which translates into a simulation where the assembly is placed in an infinite medium. Furthermore, given the geometrical symmetry of the assembly itself, only half of it was considered, as illustrated in Figure [6.10] As discussed in detail in previous chapters, significant axial variations exist within a single assembly, both in terms of material density and neutron spectrum. At the top of the assembly, the presence and movement of control rods throughout the fuel cycle introduce spectral perturbations. A similar situation occurs at the bottom due to the presence of the reflector, which also has a notable influence on the neutron spectrum—although this effect is not addressed in the current thesis. To account for this axial inhomogeneity, a representative axial node was selected, from which real operational data were extracted using SMART for the first fuel cycle. The chosen node is located at the mid-plane of the assembly to minimize external influences. Figures 6.11 and 6.12 show the actual behavior of the two selected axial nodes, including the evolution of density, temperature, and boron concentration over time, each plotted with respect to the reference value.

As previously mentioned, the depletion analysis was performed using SMART data. For each selected axial node, the results will be evaluated at mid-cycle and end-of-cycle conditions. For each node, the $\Delta \sigma$ values will be presented for both the fast and thermal energy ranges, in terms of absolute and relative differences, for both fission and absorption

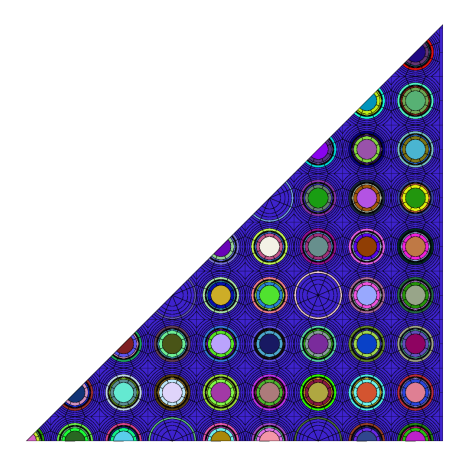


Figure 6.10: Graphical representation of the geometry implemented in APOLLO3 $^{\circledR}$.

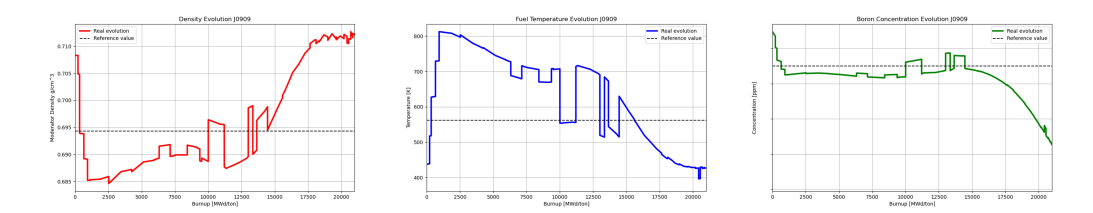


Figure 6.11: Real depletion for node J0909.

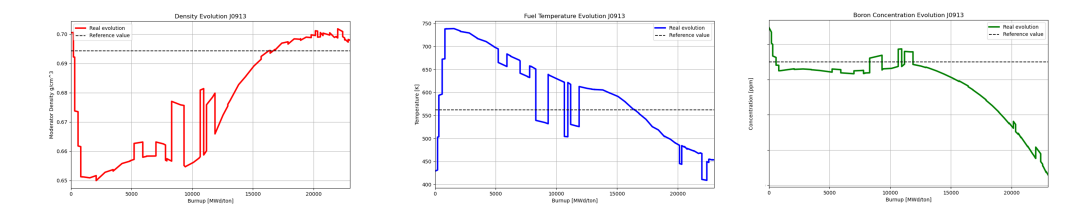


Figure 6.12: Real depletion for node J0913.

 ${\it cross \ sections.}$

However, the most relevant quantity to be considered for reactor analysis is the $\Delta\Sigma$.

6.3.1 J0909: middle of cycle

From Fig. 6.13 to 6.20 the spectral history modelling proves to be effective in reproducing the microscopic cross sections for each isotope, regardless of the reaction type and energy group considered. This result is evident in both the relative and absolute representations. In particular, the absolute representations allow us to identify the isotopes that contribute the most to the macroscopic cross sections. For absorption and fission reaction, where the relative weight of the main isotopes becomes more apparent compared to the relative representation.

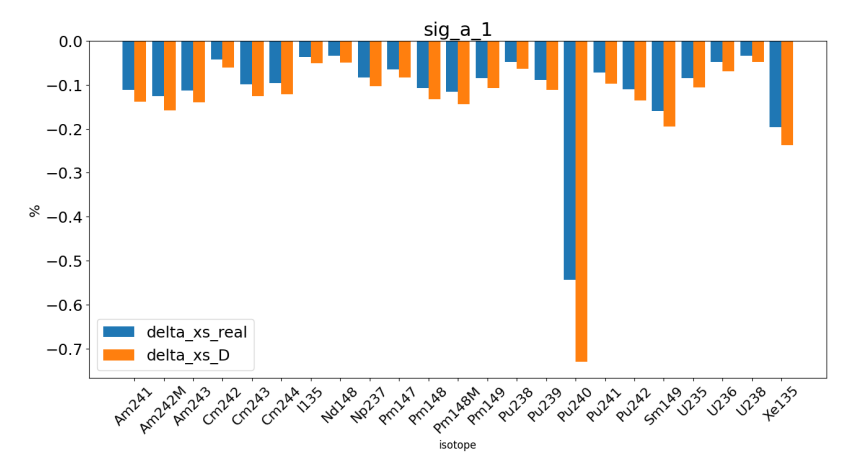


Figure 6.13: Fast group absorption cross sections - relative for assembly J0909 middle of the cycle.

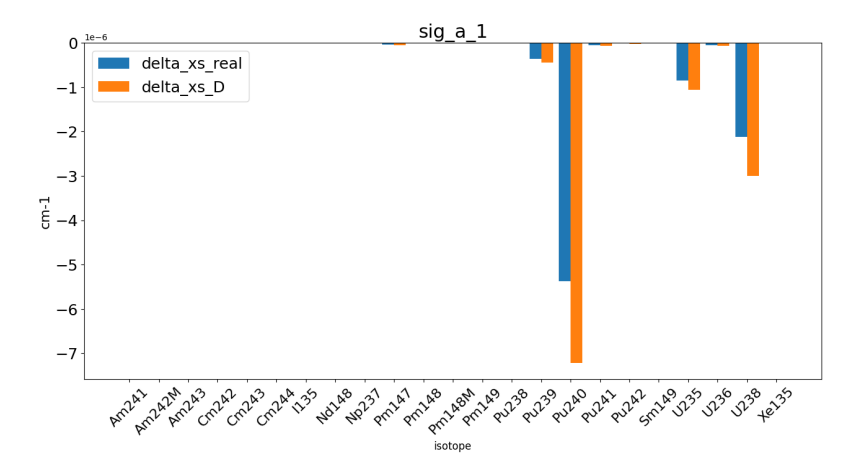


Figure 6.14: Fast group absorption cross sections - absolute for assembly J0909 middle of the cycle.

For the fission reaction, a consistency between the spectral history modelling predictions and the expected values of the node can be observed.

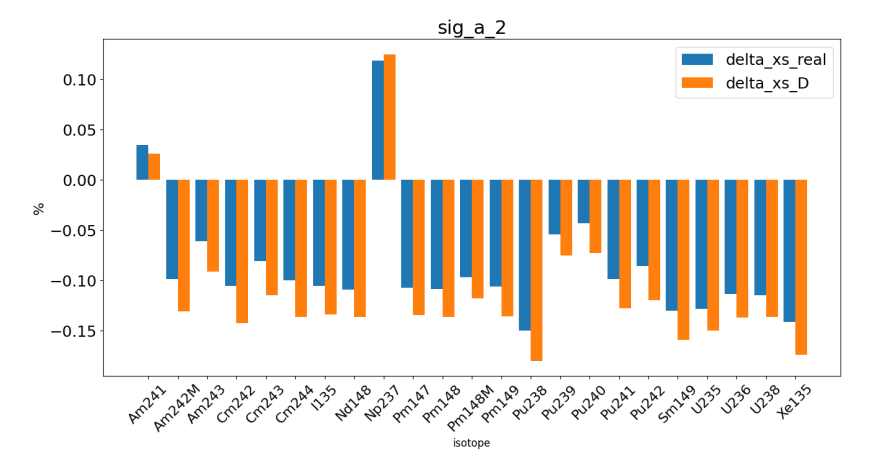


Figure 6.15: Thermal group absorption cross sections - relative for assembly J0909 middle of the cycle.

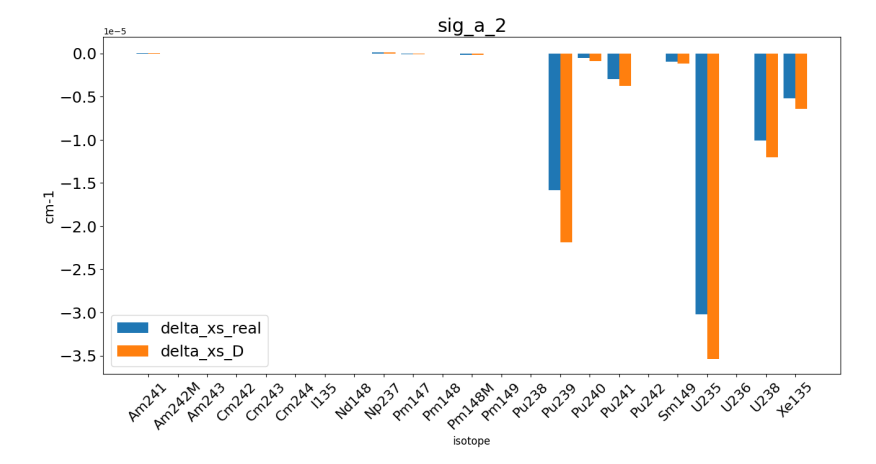


Figure 6.16: Thermal group absorption cross sections - absolute for assembly J0909 middle of the cycle.

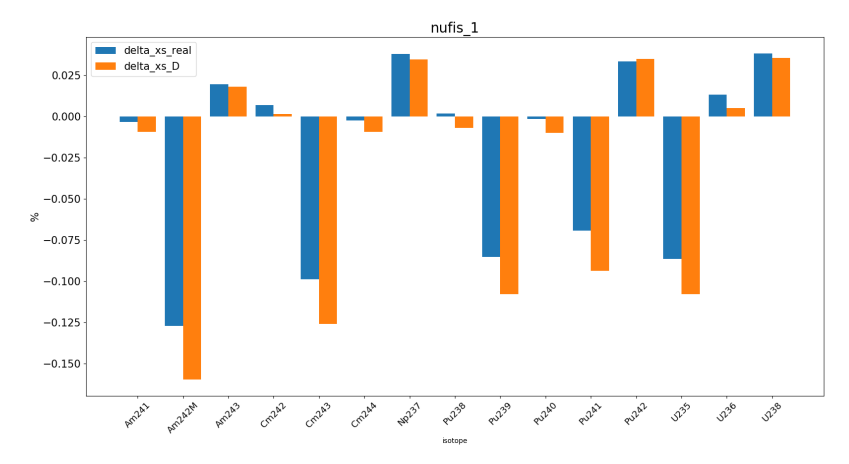


Figure 6.17: Fast group fission cross sections - relative for assembly J0909 middle of the cycle.

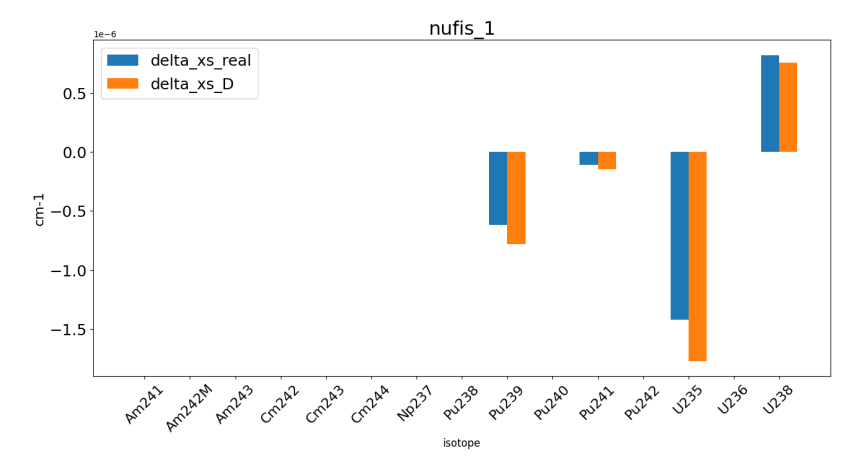


Figure 6.18: Fast group fission cross sections - absolute for assembly J0909 middle of the cycle.

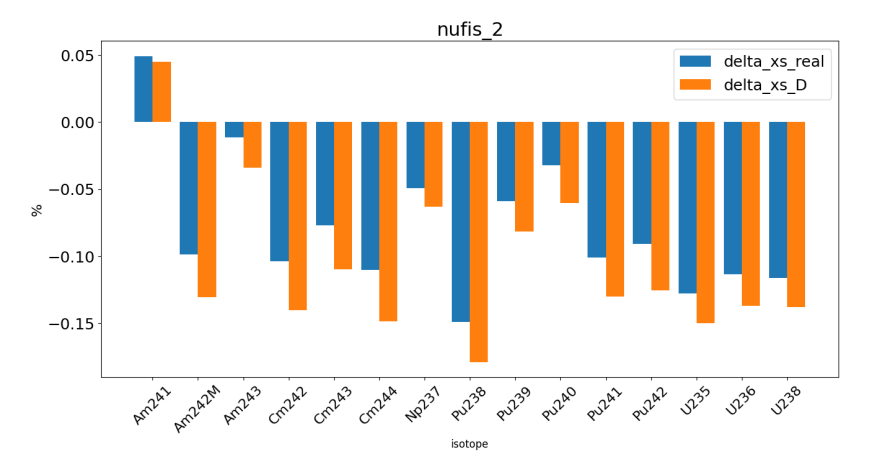


Figure 6.19: Thermal group fission cross sections - relative for assembly J0909 middle of the cycle.

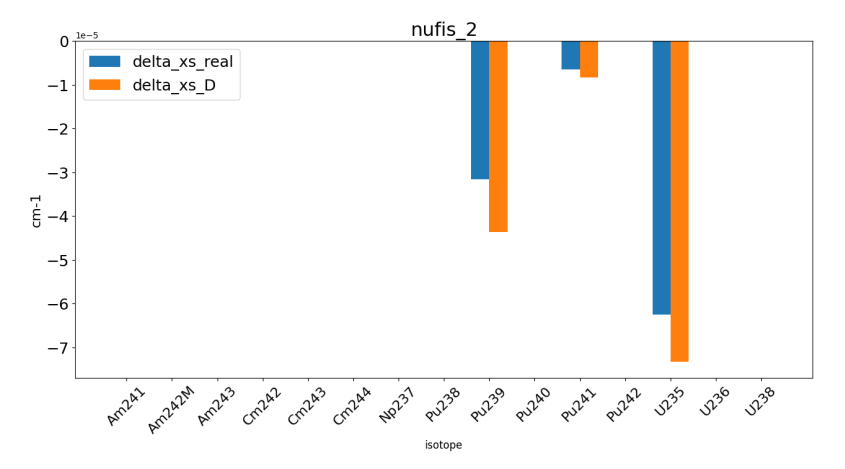


Figure 6.20: Thermal group fission cross sections - absolute for assembly J0909 middle of the cycle.

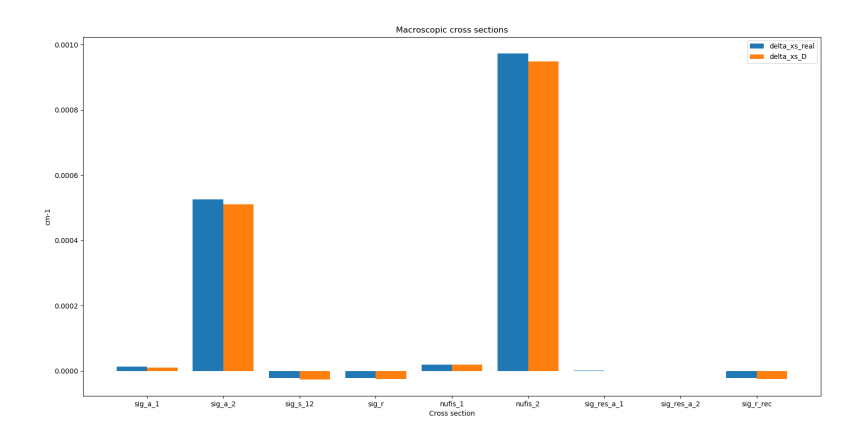


Figure 6.21: Absolute Macroscopic Cross Section correction for assembly J0909 middle of the cycle.

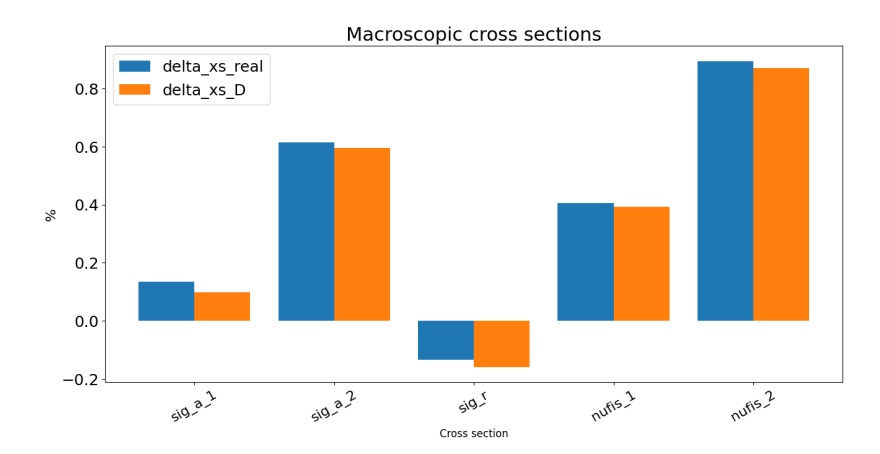


Figure 6.22: Relative Macroscopic Cross Section correction for assembly J0909 middle of the cycle.

Fig. 6.22 6.21 present the macroscopic cross sections in both absolute and relative values. The observed trend is consistent with that of the microscopic cross sections, confirming that the spectral history modelling is capable of providing corrections to the macroscopic cross-section values so that they better reflect the physical reality of the system. Therefore, at least for this node, the obtained results appear reliable when compared to a realistic simulation.

Moreover, the improvement introduced by the spectral history modelling is also clearly visible in the k_{∞} values. Without applying the spectral correction, the reactivity difference compared to the reference value is on the order of 200 pcm. However, with the introduction of the spectral history modelling, this discrepancy is significantly reduced, leading to an improvement in the k_{∞} value of 2.8 pcm, as reported in the table.

Condition	Δk_{∞} [pcm]
Without correction	-216.6
With correction	2.8

Table 6.5: Effect of correction on Δk_{∞}

6.3.2 J0909: end of cycle

Microscopic cross sections for the same node but at the end of the cycle (near 24000 MWd/t) appear to be less accurate compared to the middle of the cycle. In general, the results for the fast group seem to be less accurate (Fig. 6.23 and 6.24) than for the thermal group (Fig. 6.25 and 6.26). This behavior is particularly evident in the absorption cross sections, where deviations appear more pronounced in the fast energy range. In the case of fission, the situation follows the same trend: the discrepancies at the end of the cycle are noticeably larger than at the middle of the cycle. This is consistent across both absolute and relative differences, highlighting the increased difficulty in accurately capturing the spectral history effects towards the end of the cycle (from Fig. 6.27 to 6.30).

Despite the discrepancies observed in the microscopic cross sections, very good agreement is achieved in the macroscopic cross sections. This suggests that possible compensations occur when summing up all microscopic contributions, effectively reducing the overall error at the macroscopic level. The compensation effect is particularly relevant when looking at reactivity corrections: at the end of the cycle, applying the spectral history modelling leads to a more than 500 pcm correction.

From Tab. 6.6 it is clear that without the spectral correction, the infinite multiplication factor deviation is 526.2 pcm, whereas with the correction applied, the deviation is reduced to -31.1 pcm, bringing the results much closer to the expected values. This significant reduction highlights the effectiveness of the spectral history modelling in mitigating biases introduced in the cross section calculations.

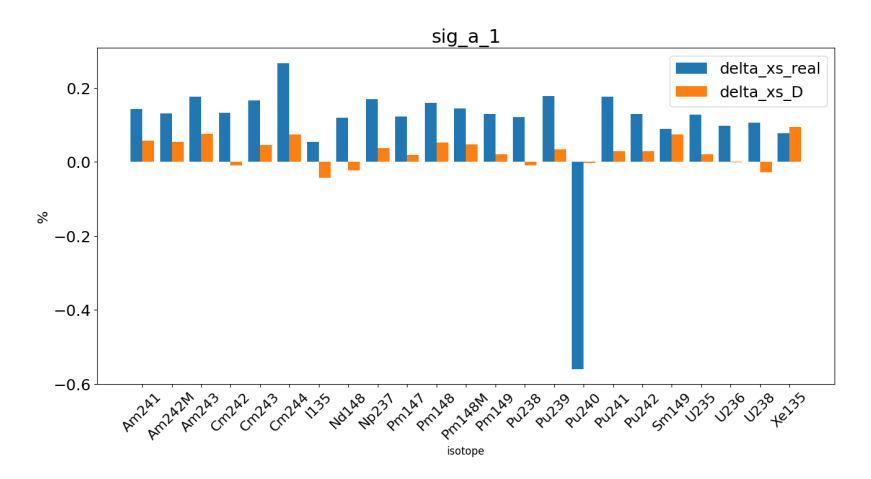


Figure 6.23: Fast group absorption cross sections - relative for assembly J0909 end of the cycle.

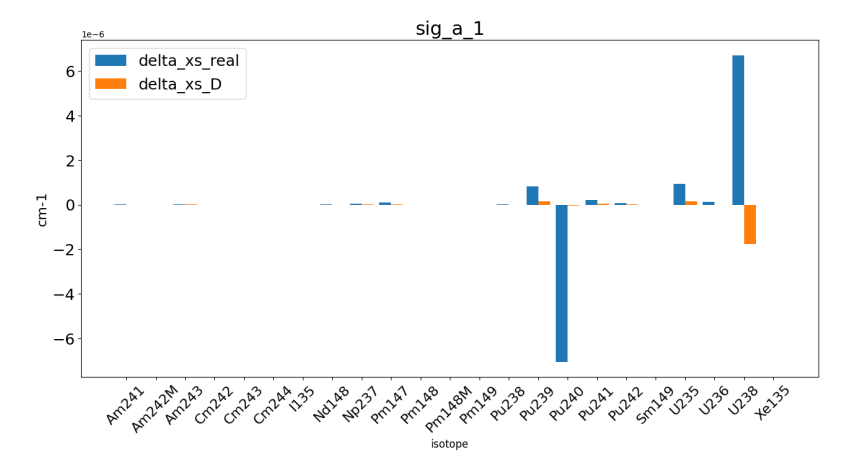


Figure 6.24: Fast group absoprtion cross sections - absolute for assembly J0909 end of the cycle.

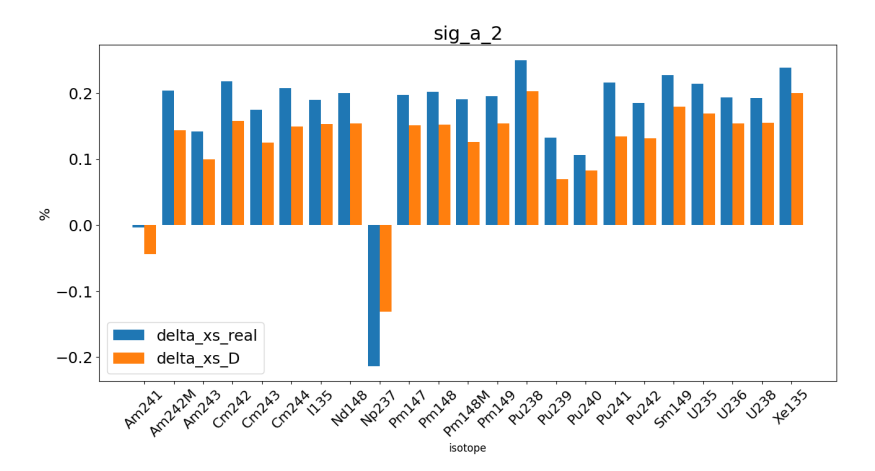


Figure 6.25: Thermal group absorption cross sections - relative for assembly J0909 end of the cycle.

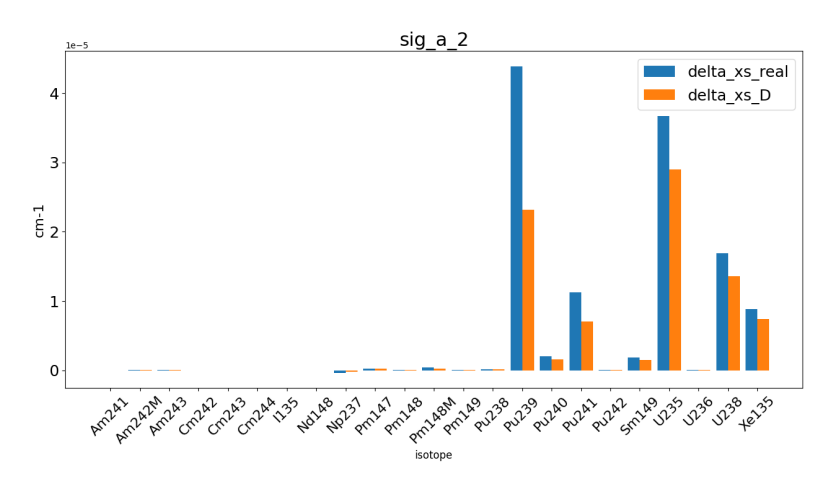


Figure 6.26: Thermal group absorption cross sections - absolute for assembly J0909 end of the cycle.

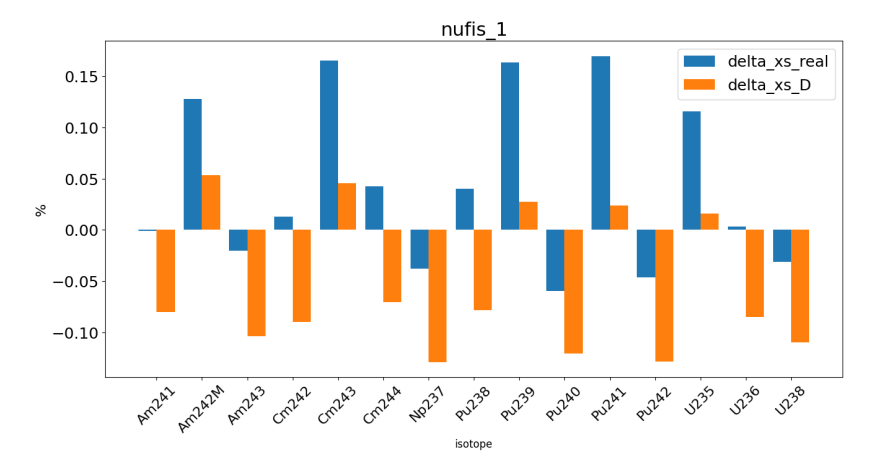


Figure 6.27: Fast group fission cross sections - relative for assembly J0909 end of the cycle.

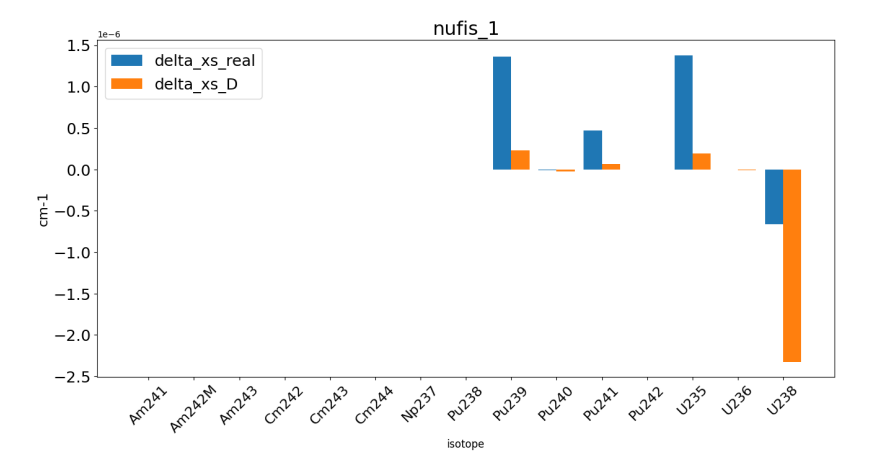


Figure 6.28: Fast group fission cross sections - absolute for assembly J0909 end of the cycle.

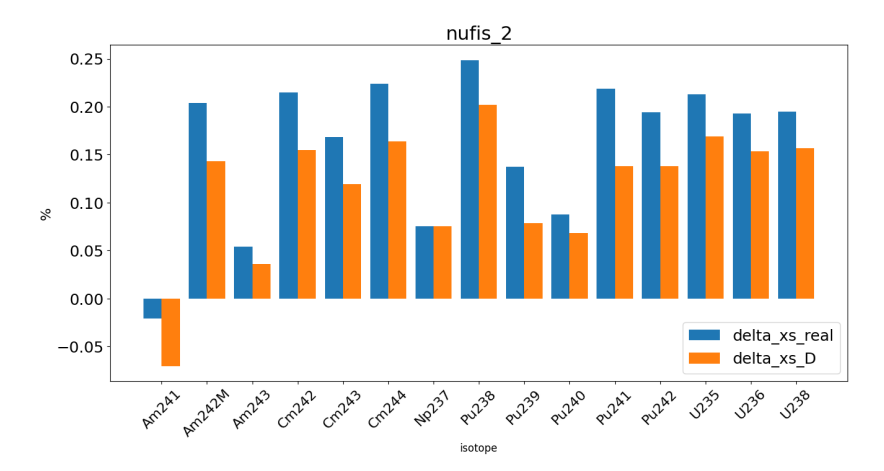


Figure 6.29: Thermal group fission cross sections - relative for assembly J0909 end of the cycle.

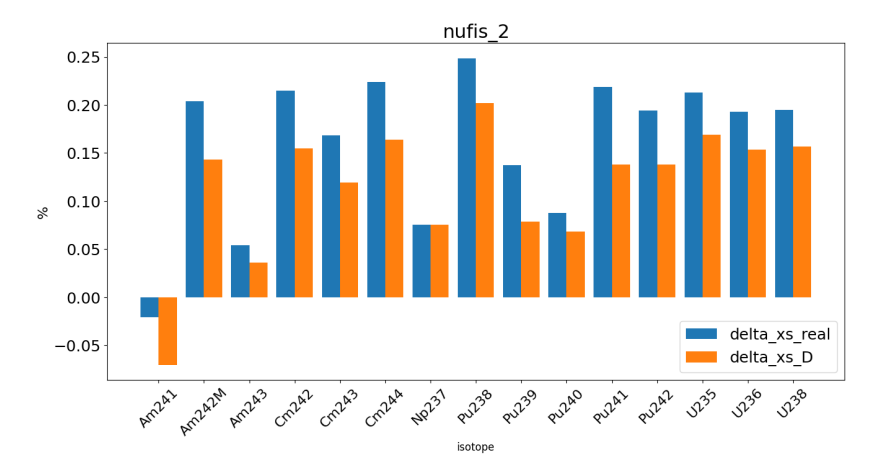


Figure 6.30: Thermal group fission cross sections - absolute for assembly J0909 end of the cycle.

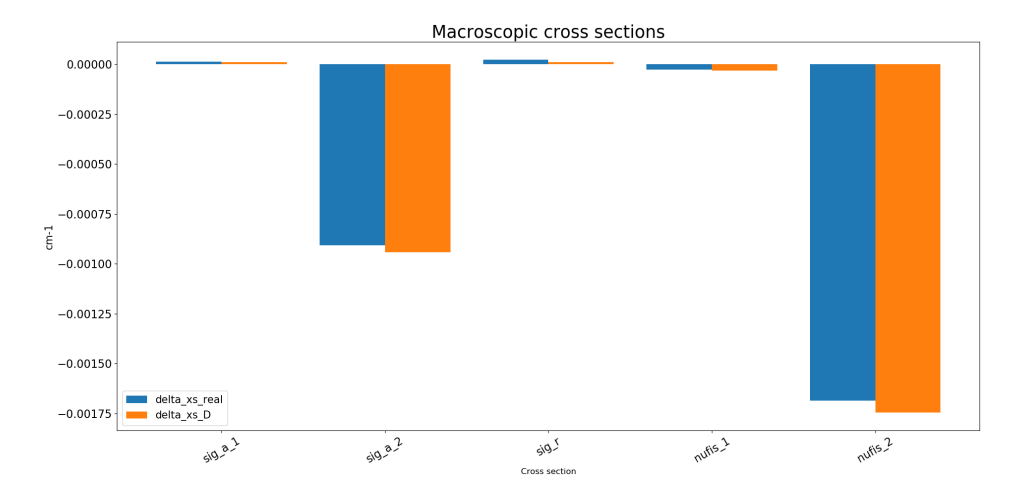


Figure 6.31: Absolute Macroscopic Cross Section for assembly J0909 end of the cycle.

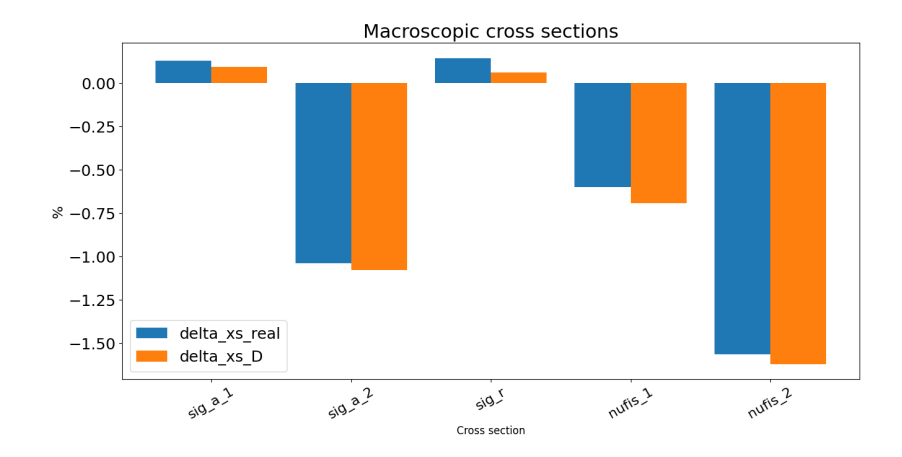


Figure 6.32: Relative Macroscopic Cross Section for assembly J0909 end of the cycle.

Condition	Δk_{∞} [pcm]
Without correction	526.2
With correction	-31.1

Table 6.6: Effect of correction on Δk_{∞}

6.3.3 J0913: middle of cycle

The node analyzed in this section is the one characterized by the lowest water density value. The analysis of the microscopic absorption cross sections shows generally satisfactory results. In absolute terms, the most significant contribution comes from Pu-240, which is well modeled, at least from the microscopic point of view. For some isotopes the results calculated through APOLLO3® follows opposite trends for the real one, as before a concrete overview is given by the results from the macroscopic cross section. Looking at the macroscopic absorption cross section in the fast group, the result is accurate, both in terms of absolute and relative differences. Of greater importance are primarily the thermal absorption and fission cross sections, which are modeled with satisfactory precision when comparing the reference data with the model predictions. The reactivity deviation without applying the history model remains very small for this node at mid-cycle. Nevertheless, an improvement is still obtained when the correction is applied.

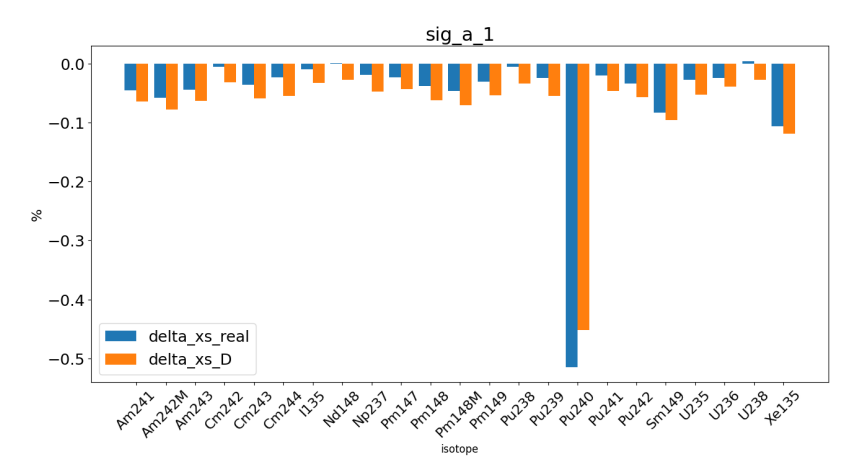


Figure 6.33: Fast group absorption cross sections - relative for assembly J0913 middle of the cycle.

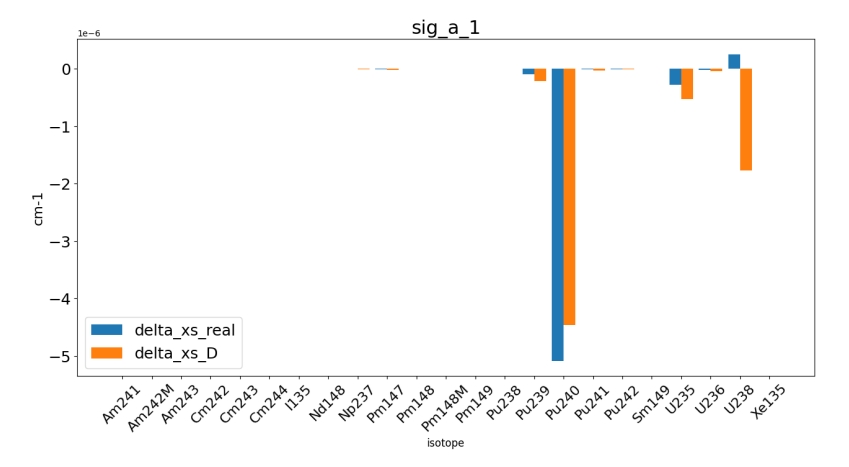


Figure 6.34: Fast group absorption cross sections - absolute for assembly J0913 middle of the cycle.

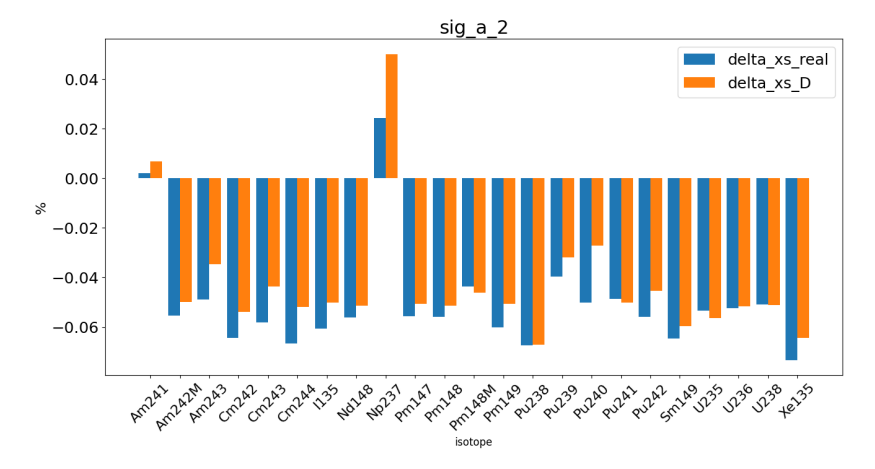


Figure 6.35: Thermal group absorption cross sections - relative for assembly J0913 middle of the cycle.

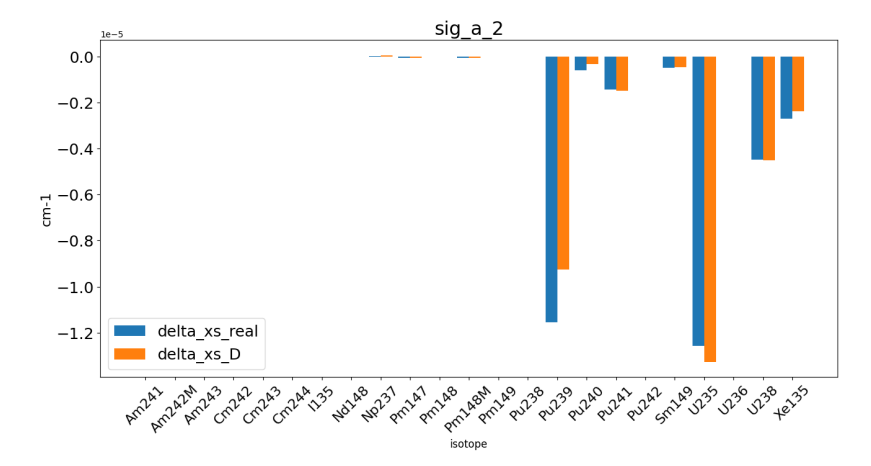


Figure 6.36: Thermal group absorption cross sections - absolute for assembly J0913 middle of the cycle.

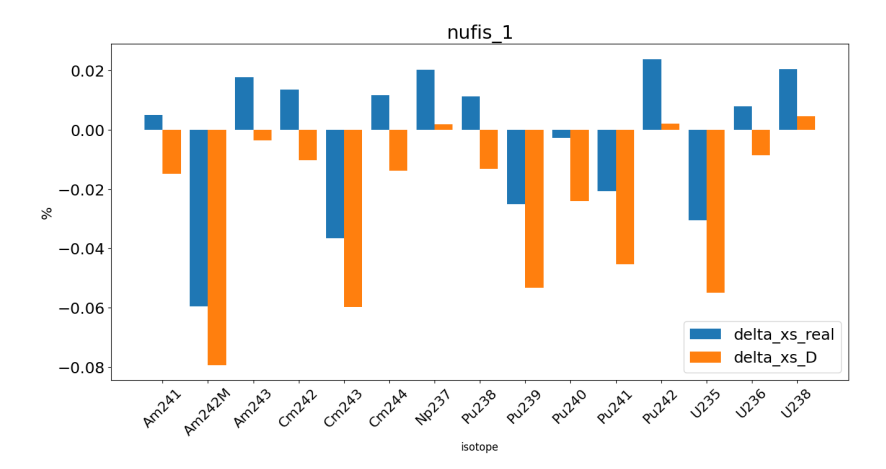


Figure 6.37: Fast group fission cross sections - relative for assembly J0913 middle of the cycle.

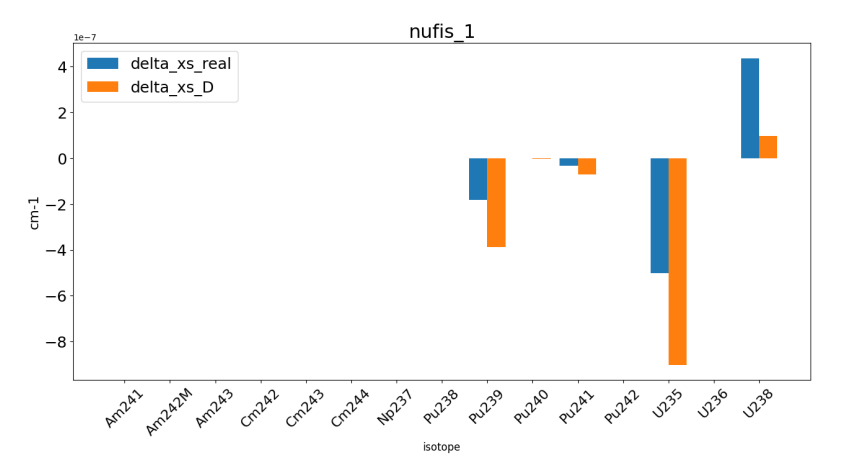


Figure 6.38: Fast group fission cross sections - absolute for assembly J0913 middle of the cycle.

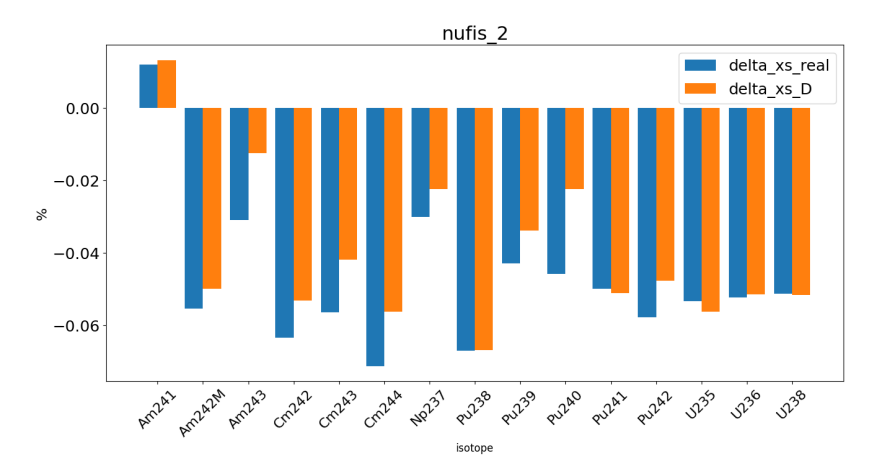


Figure 6.39: Thermal group fission cross sections - relative for assembly J0913 middle of the cycle.

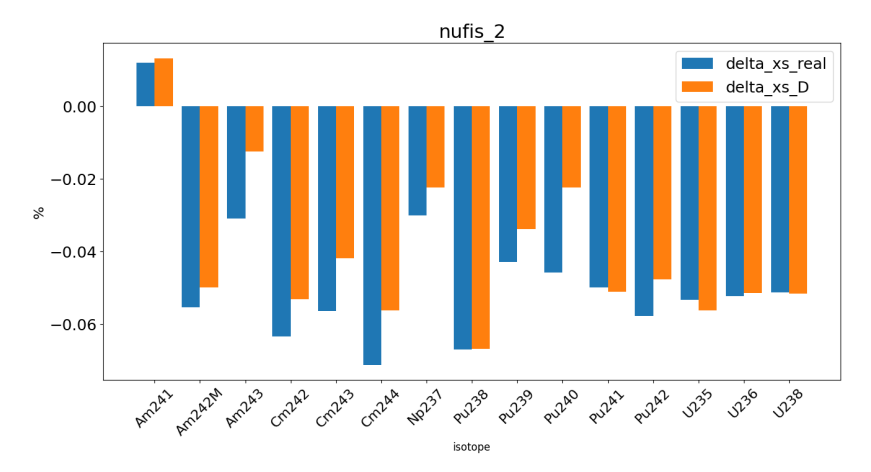


Figure 6.40: Thermal group fission cross sections - absolute for assembly J0913 middle of the cycle.

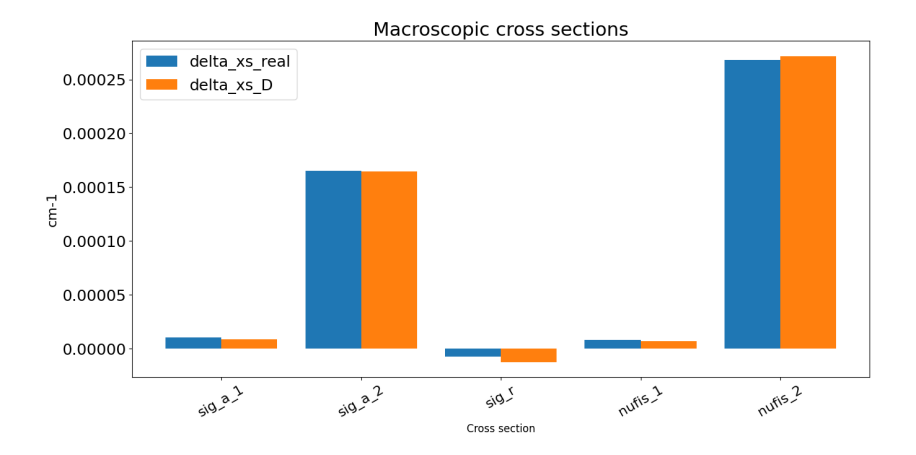


Figure 6.41: Absolute Macroscopic Cross Section for assembly J0913 middle of the cycle.

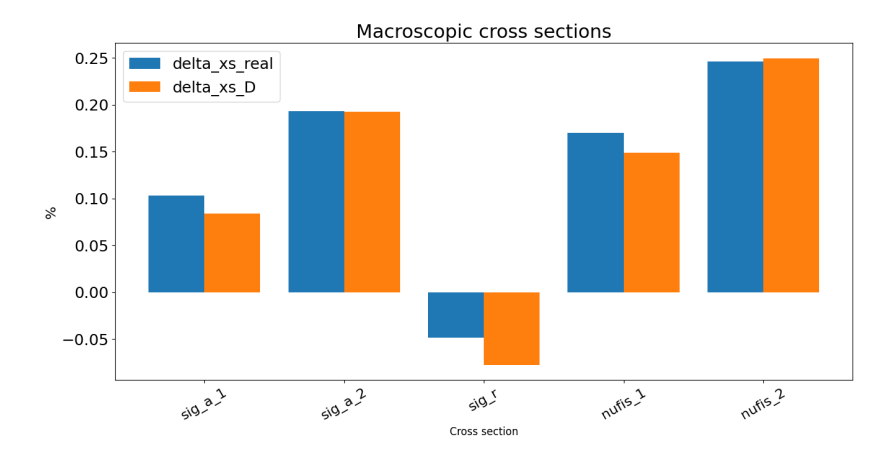


Figure 6.42: Relative Macroscopic Cross Section for assembly J0913 middle of the cycle.

Condition	$\Delta k_{\infty} [\text{pcm}]$
Without correction	-25.8
With correction	-0.6

Table 6.7: Effect of correction on Δk_{∞}

6.3.4 J0913: end of cycle

At the end of the cycle, for the same node, the model shows limited accuracy in fast energy group but a better situation for the thermal group. Significant discrepancies are observed in this range, suggesting that the model struggles to accurately capture spectral effects in fast conditions. In particular, for Pu-240, which is the most corrected one considering history effect on microscopic contribution in the fast energy group, for which the trends are opposite compared to those observed for the other isotopes. On the other hand, the thermal group results demonstrate a high level of precision, with excellent agreement between the calculated and reference values. Despite the deviations seen at the microscopic level in the fast group, the macroscopic cross sections exhibit very good accuracy. This is clearly reflected in the reactivity results: without applying the spectral correction, the deviation in the infinite multiplication factor is 1117 pcm. However, once the spectral history modelling is applied, the deviation is significantly reduced to -51 pcm. This demonstrates the effectiveness of the correction in compensating for microscopic inaccuracies and improving the overall fidelity of the results at the macroscopic scale.

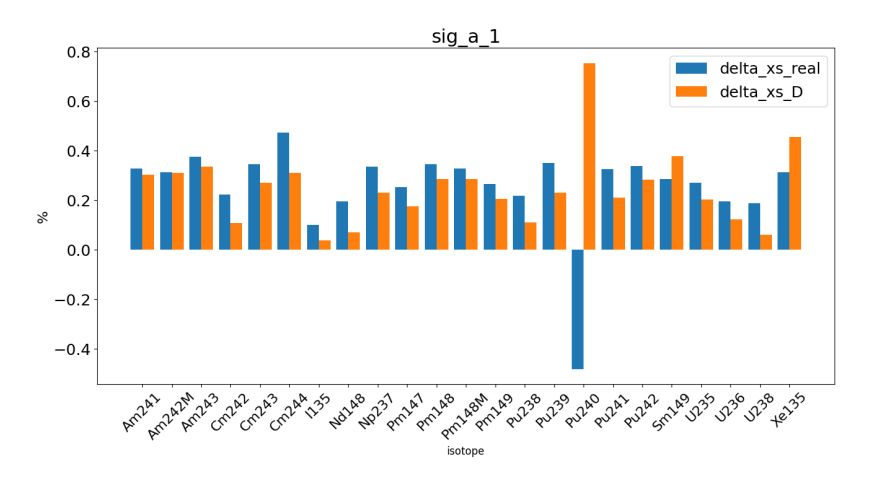


Figure 6.43: Fast group absorption cross sections - relative for assembly J0913 end of the cycle.

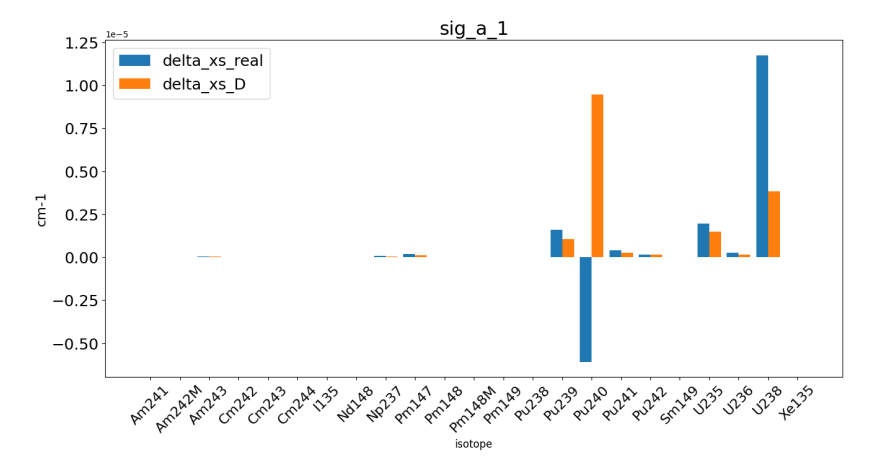


Figure 6.44: Fast group absorption cross sections - absolute for assembly J0913 end of the cycle.

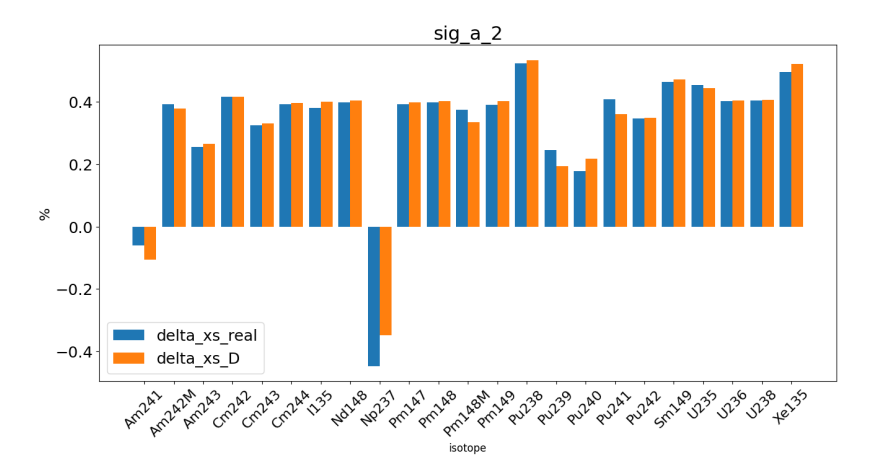


Figure 6.45: Thermal group absorption cross sections - relative for assembly J0913 end of the cycle.

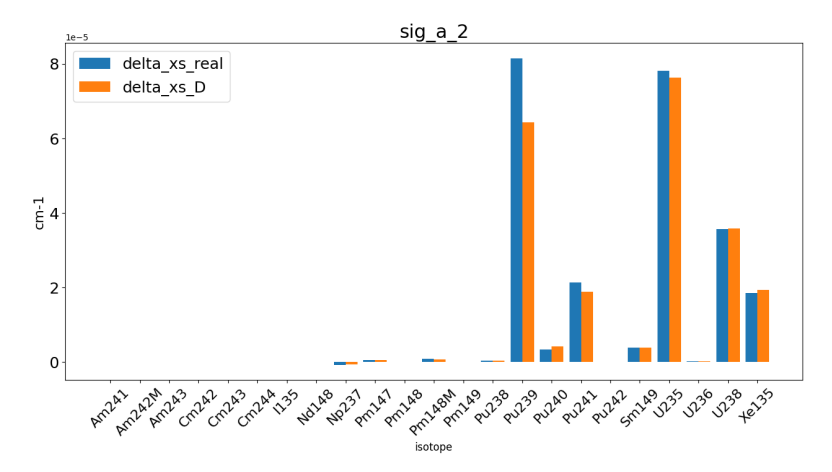


Figure 6.46: Thermal group absorption cross sections - absolute for assembly J0913 end of the cycle.

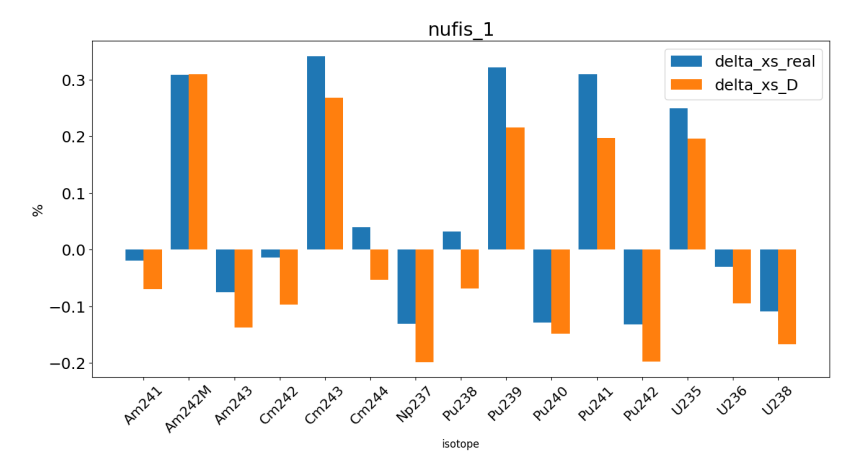


Figure 6.47: Fast group fission cross sections - relative for assembly J0913 end of the cycle.

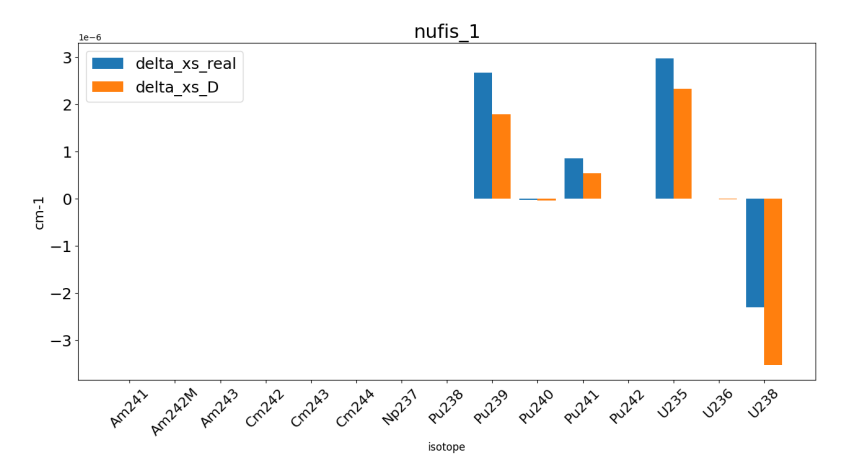


Figure 6.48: Fast group fission cross sections - absolute for assembly J0913 end of the cycle.

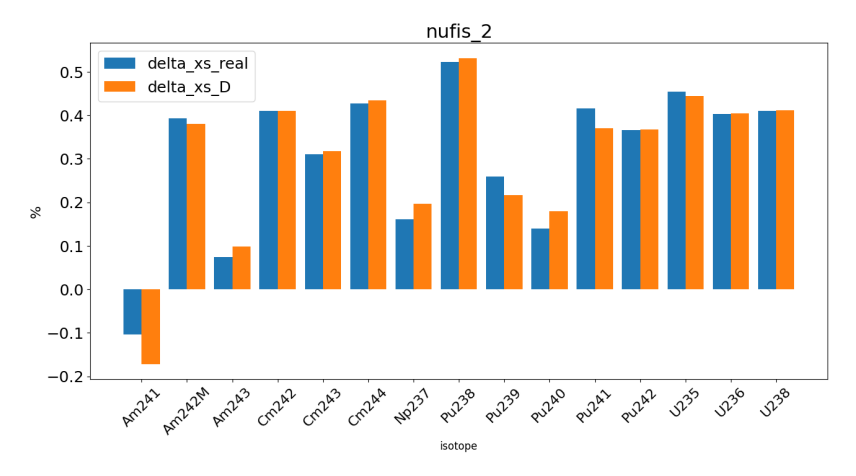


Figure 6.49: Thermal group fission cross sections - relative for assembly J0913 end of the cycle.

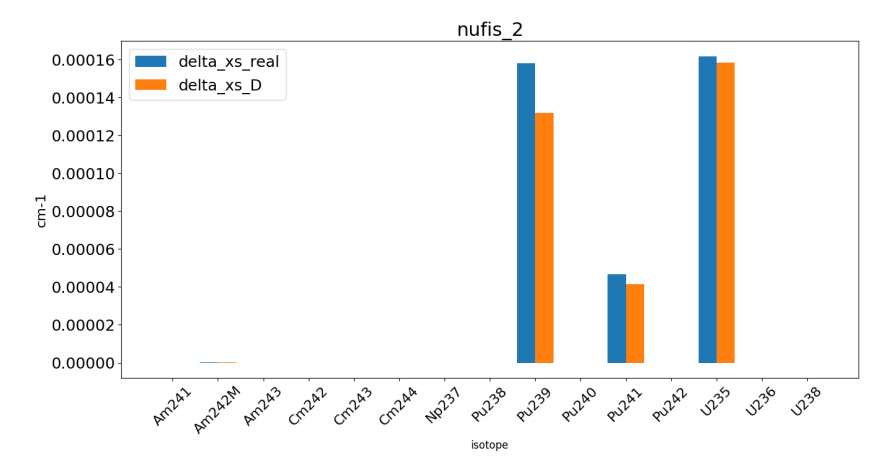


Figure 6.50: Thermal group fission cross sections - absolute for assembly J0913 end of the cycle.

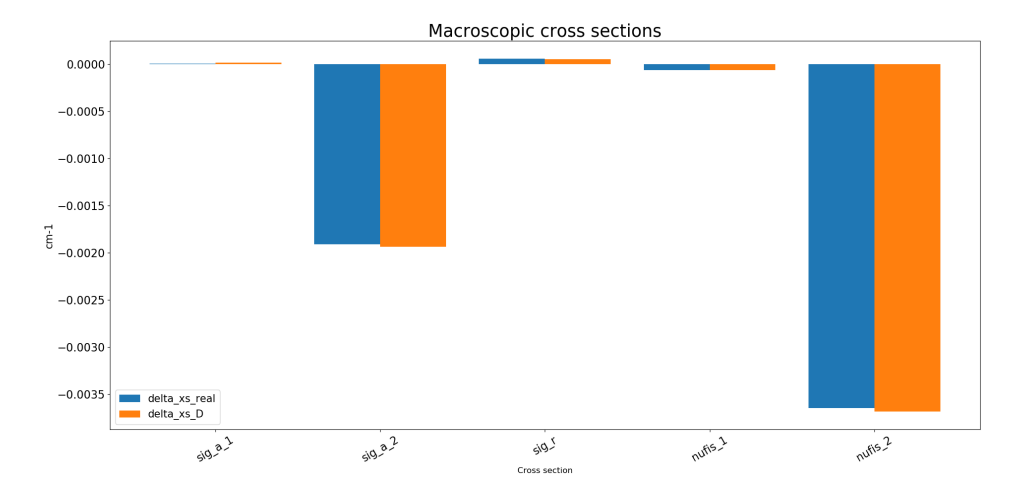


Figure 6.51: Absolute Macroscopic Cross Section for assembly J0913 end of the cycle.

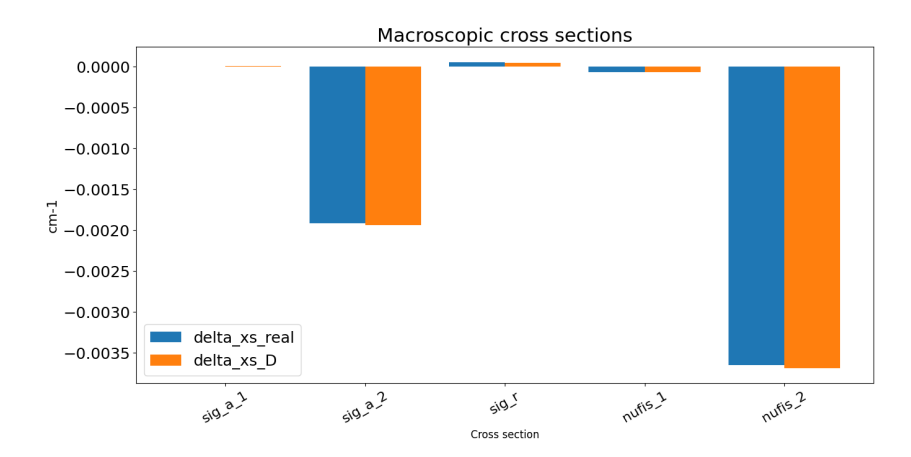


Figure 6.52: Relative Macroscopic Cross Section for assembly J0913 end of the cycle.

Condition	$\Delta k_{\infty} \; [\text{pcm}]$
Without correction	1117.8
With correction	-51.8

Table 6.8: Effect of correction on Δk_{∞}

6.4 Case study: Assembly 3

The second candidate selected for this study is the assembly containing gadolinium, which is undoubtedly an important aspect to consider. It is essential to assess whether its presence significantly affects the results. This assembly is also more enriched, making it an interesting case for further analysis. Unlike the previous assembly, additional simulations will be performed using the APOLLO3® code, which also accounts for the surrounding environment. Considering the environment reflects the actual conditions in the reactor core, where each assembly is surrounded by others with varying enrichment levels, potentially influencing its neutron spectrum. The following results will therefore include simulations in an infinite medium (as done previously) as well as with environmental effects taken into account. As before, different axial positions will be considered. The implemented cases are summarized below:

- Infinite medium: Assembly G11, axial position 5
- With environment: Assembly G11, axial position 9

The geometry implemented, Fig. 6.54 in the second case includes the interaction between assembly G11 and its neighboring assemblies located at positions G12 and F11 Fig. 5.1 both of which have a lower enrichment level. Another important parameter to consider is that in SMART, like in other core codes, all the minor isotopes are lumped in a unique macroscopic cross section and then sum up to the contribution of the other isotopes. This is the case, indeed, of the Gadolium which is treated as a contributor of the Σ_{res} .

$$\Sigma = \Sigma_{res} + \sum_{1}^{N_{isotopes}} \sigma_i * N_i$$
 (6.13)

As previously mentioned, the depletion analysis was carried out using SMART reference data, as shown in Fig. 6.55 and Fig. 6.56. For each selected axial node, the results will be evaluated at mid-cycle and end-of-cycle conditions.

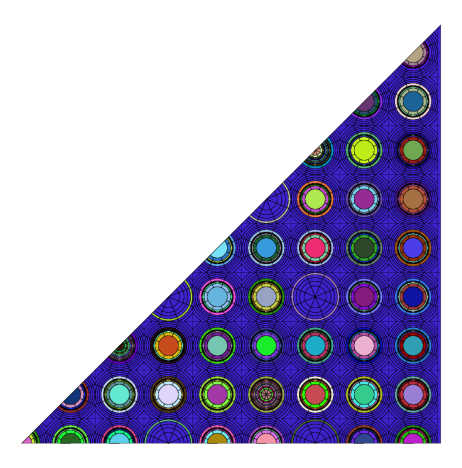


Figure 6.53: Graphical representation of the geometry implemented in APOLLO3 $^{\circledR}$ (infinite medium).

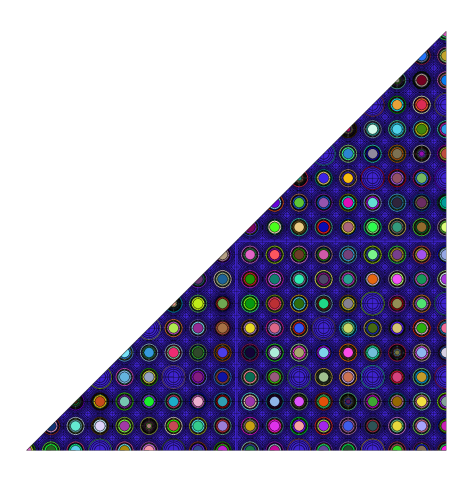


Figure 6.54: Graphical representation of the geometry including the surrounding environment implemented in APOLLO3.

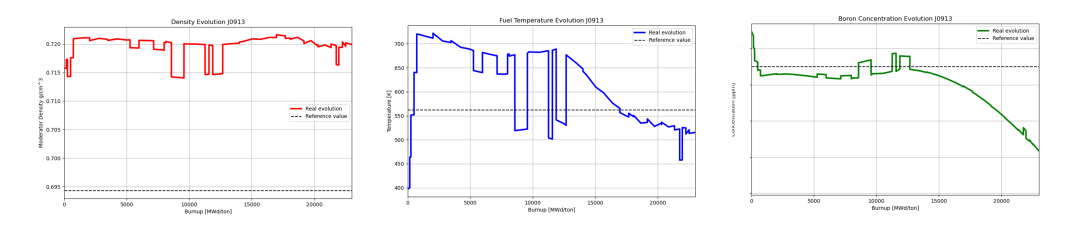


Figure 6.55: Real depletion for node G1105 (infinite medium).

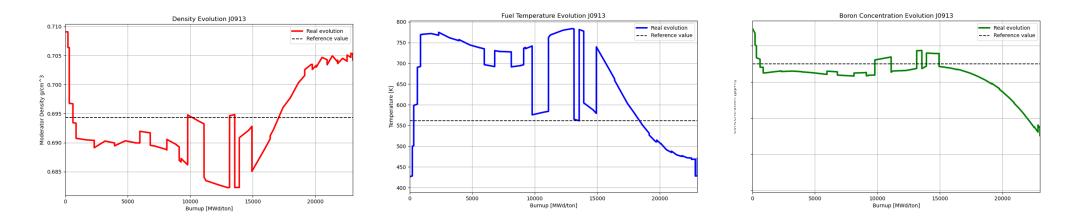


Figure 6.56: Real depletion for node G1109 (with environment).

6.4.1 G1105: middle of cycle

The axial node at position 5 exhibits a water density that remains consistently above the reference value. It is therefore necessary to assess whether this deviation has a significant impact on the simulation results. The computed results for both the fast and thermal energy ranges, in terms of absorption and fission cross sections, are satisfactory. The direction and trends of the histograms are consistent across all isotopes. Moreover, the calculated $\Delta\sigma$ values, although qualitative in nature, also reflect an acceptable level of agreement. It should be noted that in Fig. 6.65 the discrepancy observed in the absorption cross section of Gd-157 in the thermal group corresponds exactly to the discrepancy found in the total absorption cross section for the same group. The next step in the analysis focuses on the macroscopic cross sections. In this case, the individual contributions of Gd-155 and Gd-157 to the thermal absorption macroscopic cross section were explicitly included. Upon reviewing the results, a notable discrepancy appears to originate from these two isotopes especially on thermal absorption microscopic cross sections, and so on thermal absorption partial macroscopic cross section and total macroscopic cross sections. In SCIENCE V2, the term Gd-macro refers to the Gadolinium macroscopic cross sections as implemented in SMART, i.e., lumped into the partial macroscopic cross sections, while Gd-micro refers to the Gadolinium isotopes treated at the microscopic level.

In addition, the computed values of k_{∞} , suggest that the spectral history model may, in fact, worsen the prediction of k_{∞} in this specific case. This observation could indicate that the model is less effective in the presence of gadolinium. This simulation corresponds to a mid-cycle burnup condition. In order to gain further insights, an additional simulation was performed under the same conditions, but with an instantaneous change in parameters representing the end-of-cycle scenario.

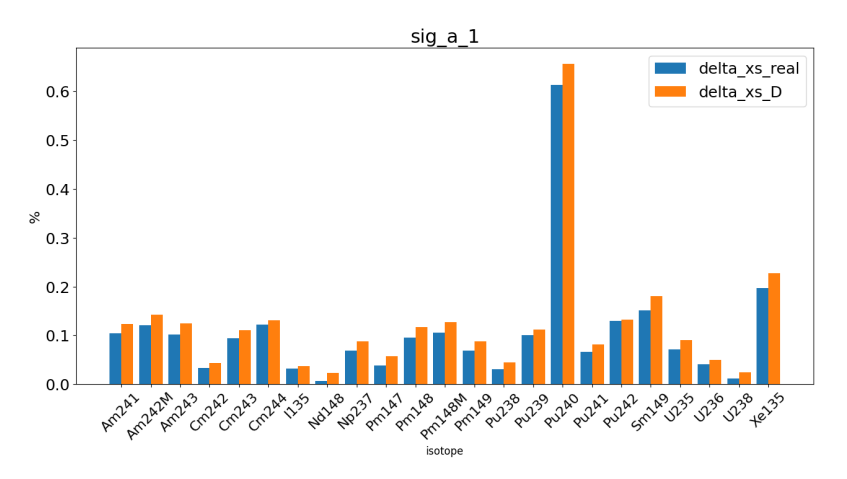


Figure 6.57: Fast group absorption cross sections - relative for assembly G1105 middle of the cycle. Gd treated as macro.

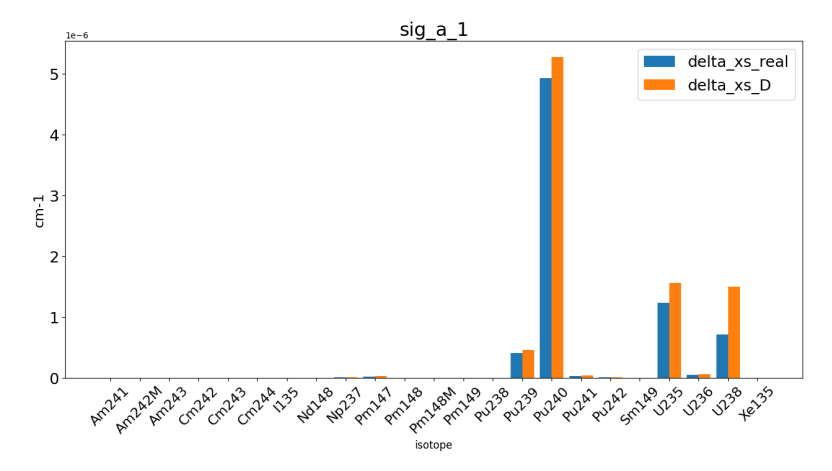


Figure 6.58: Fast group absorption cross sections - absolute for assembly G1105 middle of the cycle. Gd treated as macro.

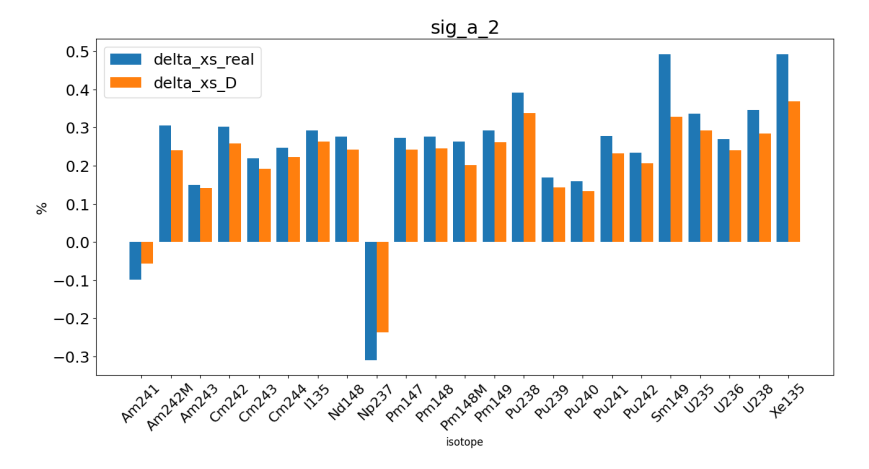


Figure 6.59: Thermal group absorrtion cross sections - relative for assembly G1105 middle of the cycle. Gd treated as macro.

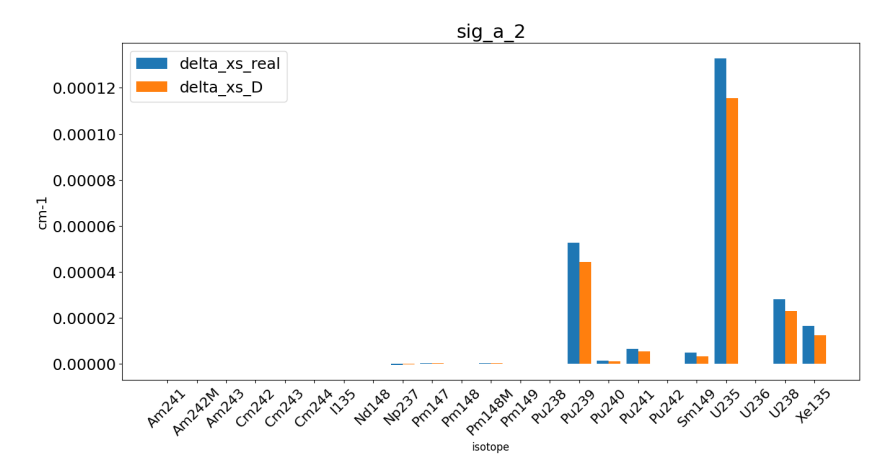


Figure 6.60: Thermal group absorption cross sections - absolute for assembly G1105 middle of the cycle. Gd treated as macro.

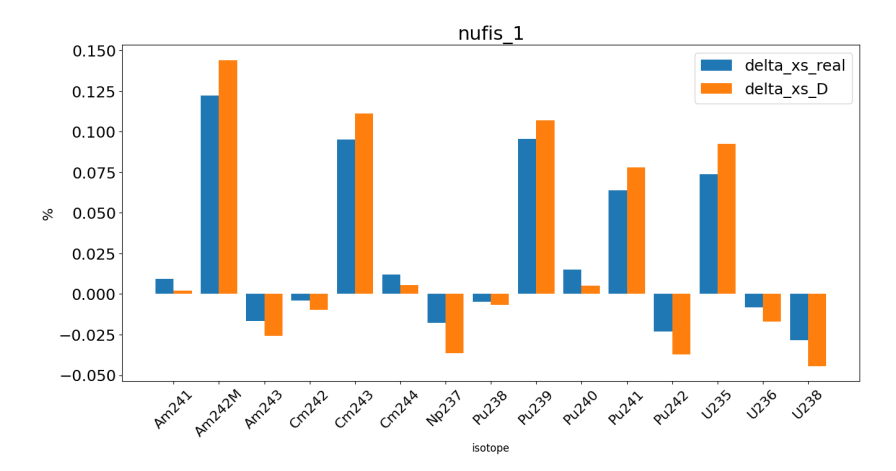


Figure 6.61: Fast group fission cross sections - relative for assembly G1105 middle of the cycle. Gd treated as macro.

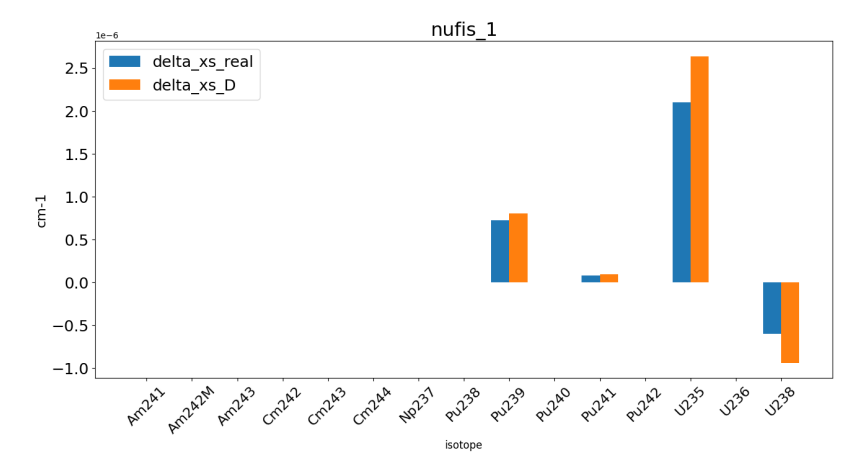


Figure 6.62: Fast group fission cross sections - absolute for assembly G1105 middle of the cycle. Gd treated as macro.

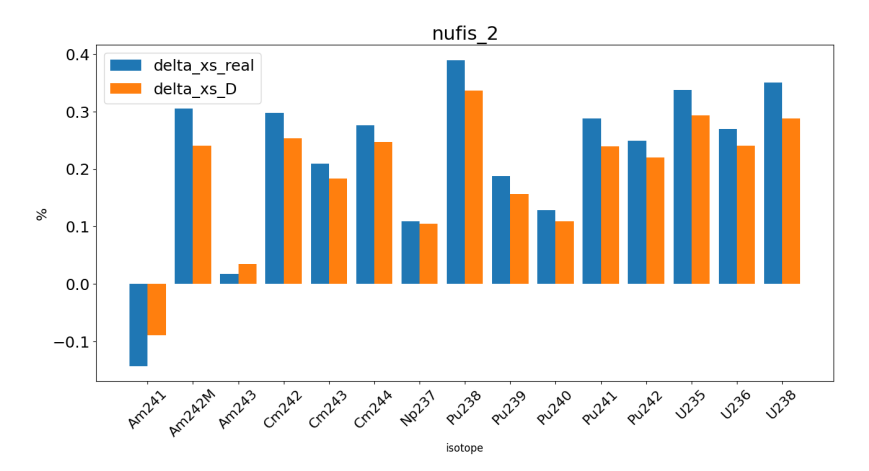


Figure 6.63: Thermal group fission cross sections - relative for assembly G1105 middle of the cycle. Gd treated as macro.

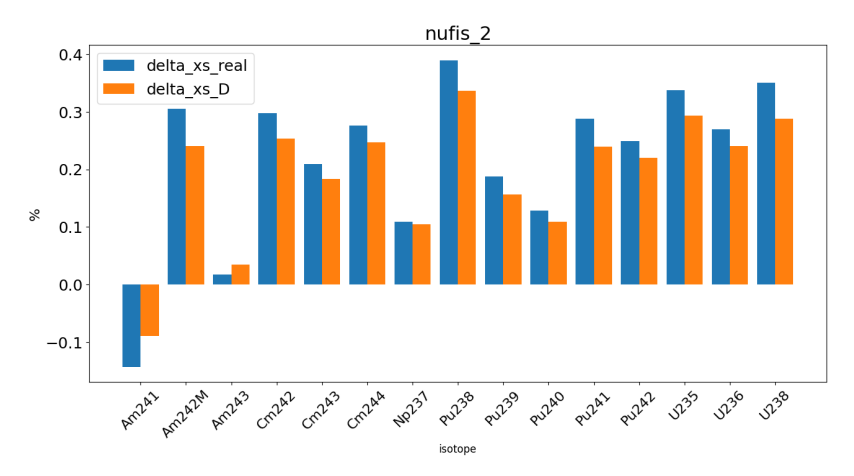


Figure 6.64: Thermal group fission cross sections - absolute for assembly G1105 middle of the cycle. Gd treated as macro.

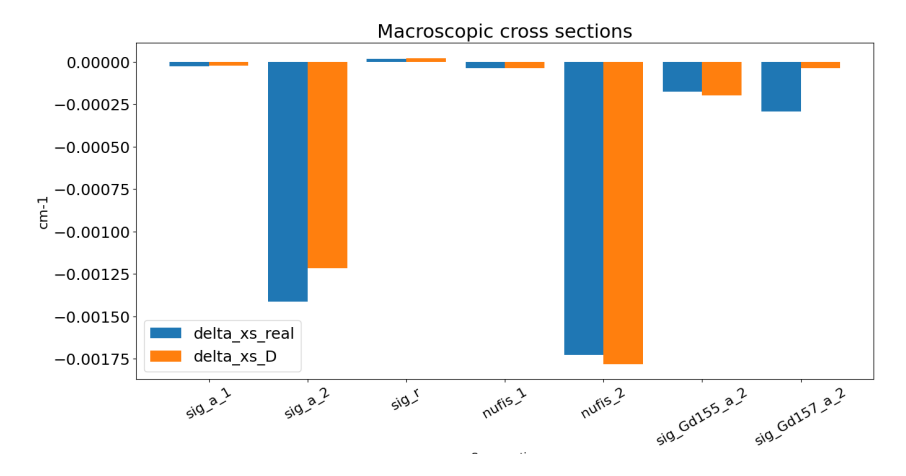


Figure 6.65: Absolute Macroscopic Cross Section for assembly G1105 middle of the cycle with Gd treated as macro.

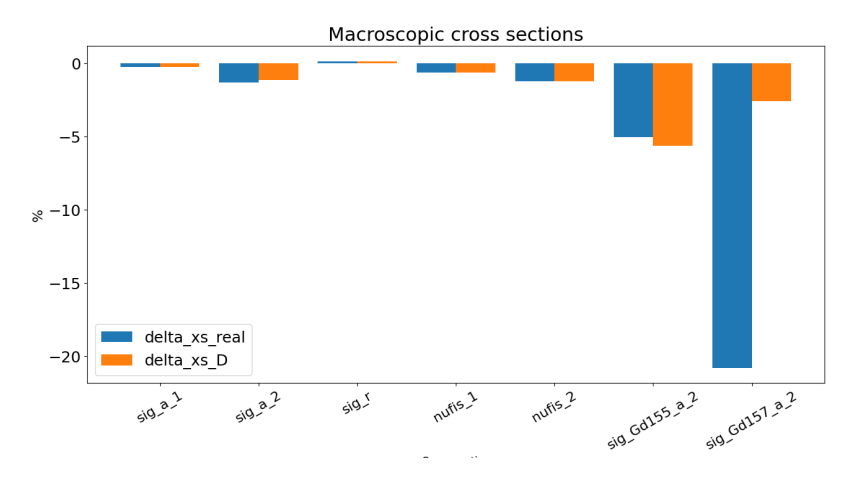


Figure 6.66: Relative Macroscopic Cross Section for assembly G1105 middle of the cycle with Gd treated as macro.

In the k_{∞} results, a third row was added, showing the correction obtained by treating gadolinium not as part of the lumped macroscopic cross sections, but instead by including its microscopic cross sections directly in the summation, weighted by its actual concentration. This alternative treatment led to a more satisfactory correction, suggesting that the default approach used by SMART, in which gadolinium is incorporated into the lumped macros may not be optimal. Handling gadolinium in this simplified way may introduce non-negligible errors, particularly due to the isotopes $^{155}{\rm Gd}$ and $^{157}{\rm Gd}$. These findings indicate that an explicit treatment of gadolinium at the microscopic level could improve the accuracy of spectral history model in SCIENCE V2

Condition	Δk_{∞} [pcm]
Without correction	-98.8
With correction $+$ Gd as macro	-192.4
With correction $+$ Gd as micro	70

Table 6.9: Effect of correction on Δk_{∞}

6.4.2 G1105: end of cycle

The results obtained at the end of the cycle (EOC) show consistent trends across the various evaluated parameters. As expected, the concentration of the main absorbing isotopes of gadolinium (in particular $^{155}\mathrm{Gd}$ and $^{157}\mathrm{Gd}$) is significantly reduced compared to the beginning of life (BOL). This reduction in thermal neutron absorption affects the local neutron spectrum and has implications for modeling accuracy. In particular, the Spectral History Model appears to be more effective at the end of the cycle, especially for assemblies without gadolinium or in which the gadolinium has been almost entirely depleted. At this stage, spectral history plays a more prominent precision in accurately determining cross sections and reactivity. The values of Δk_{∞} , Tab. [6.10] calculated without the spectral correction are approximately ~ 808 pcm, indicating a significant deviation. However, with the application of the spectral model, this error is substantially reduced—more noticeably than at mid-cycle. This behavior confirms that the use of the Spectral History Model becomes particularly important during the end of the assembly's first cycle.

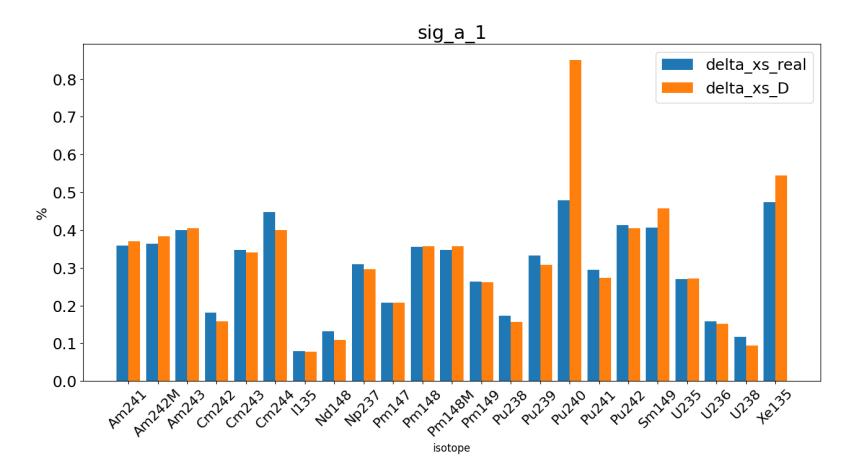


Figure 6.67: Fast group absorption cross sections - relative for assembly G1105 end of the cycle. Gd treated as macro.

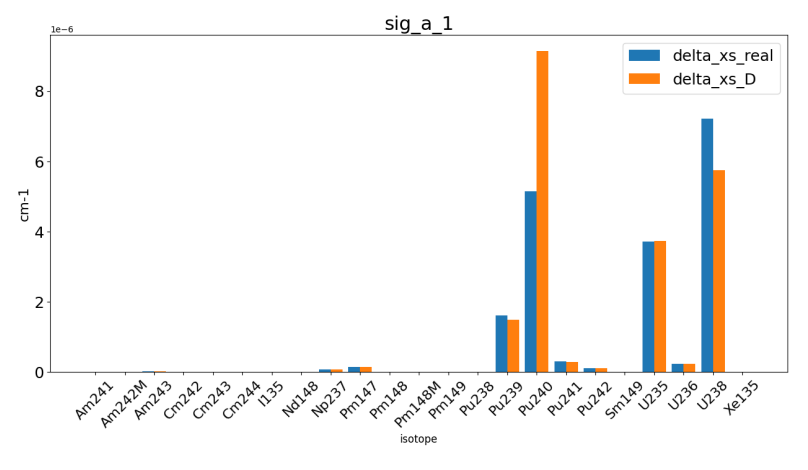


Figure 6.68: Fast group absorption cross sections - absolute for assembly G1105 end of the cycle. Gd treated as macro.

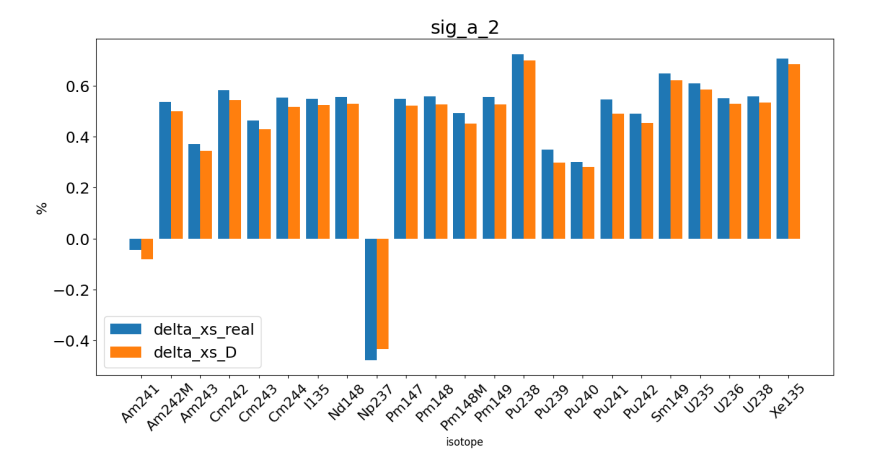


Figure 6.69: Thermal group absorption cross sections - relative for assembly G1105 end of the cycle. Gd treated as macro.

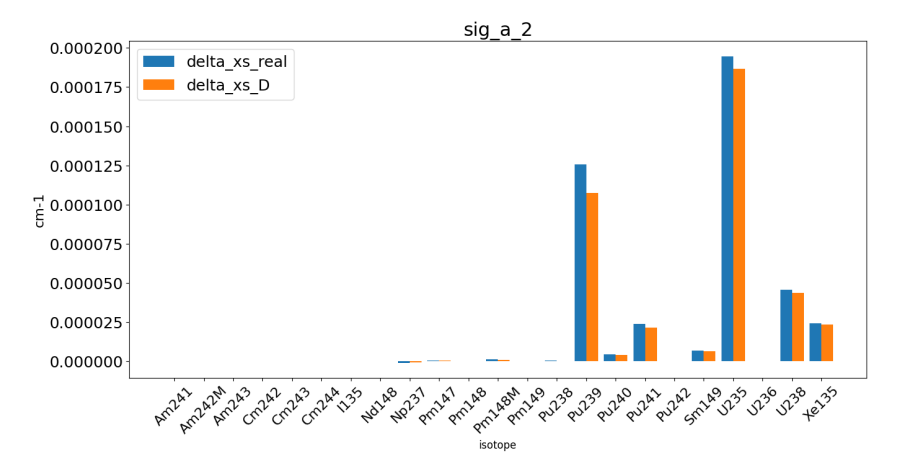


Figure 6.70: Thermal group absorption cross sections - absolute for assembly G1105 end of the cycle. Gd treated as macro.

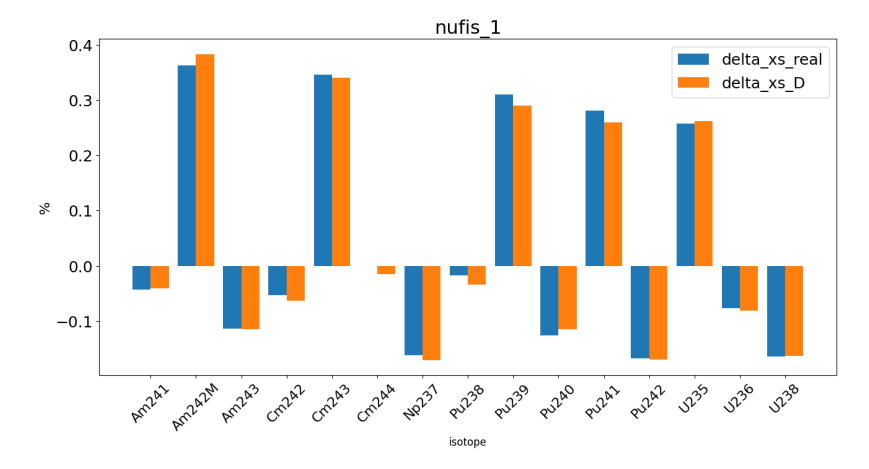


Figure 6.71: Fast group fission cross sections - relative for assembly G1105 end of the cycle. Gd treated as macro.

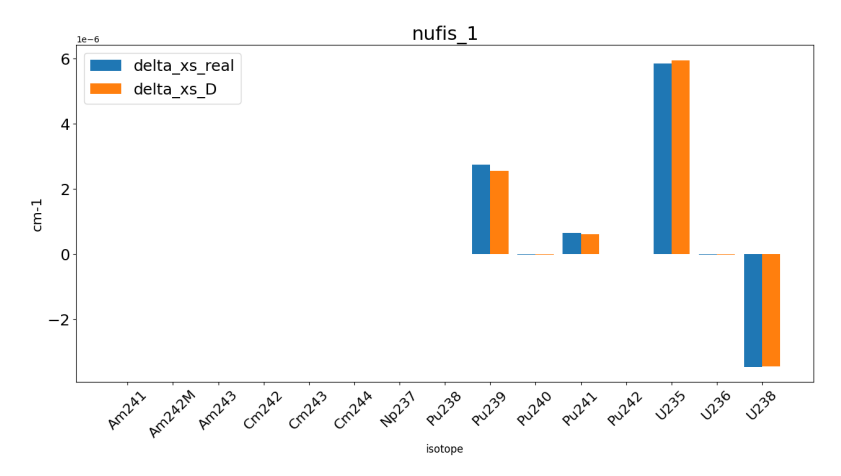


Figure 6.72: Fast group fission cross sections - absolute for assembly G1105 end of the cycle. Gd treated as macro.

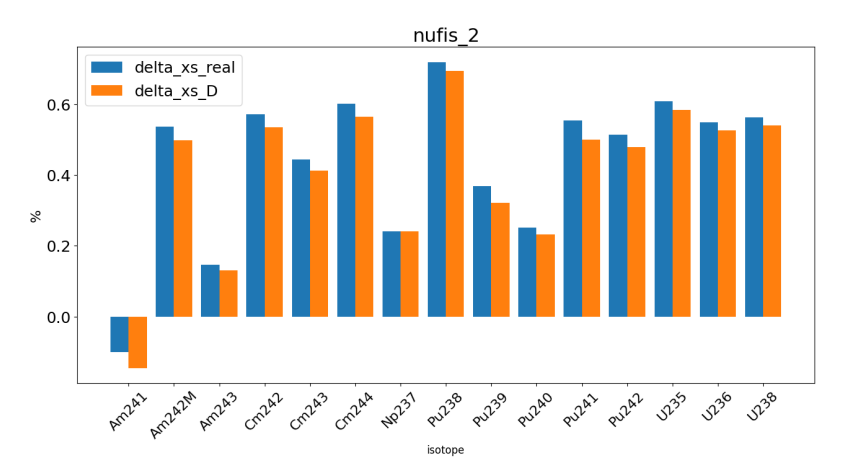


Figure 6.73: Thermal group fission cross sections - relative for assembly G1105 end of the cycle. Gd treated as macro.

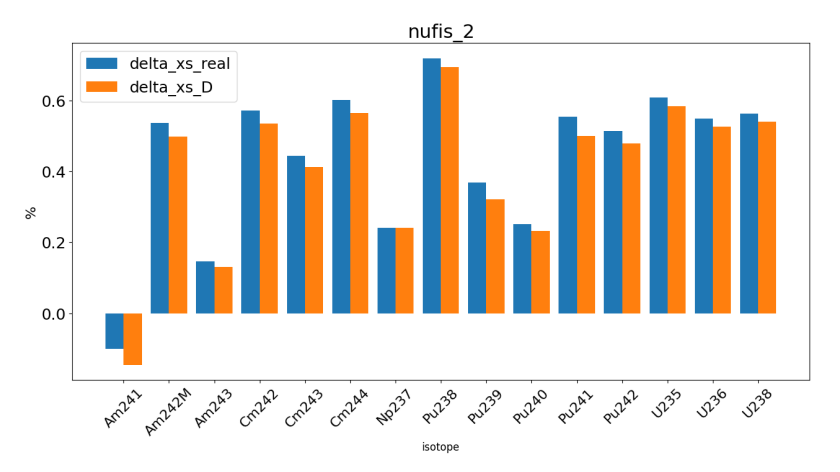


Figure 6.74: Thermal group fission cross sections - absolute for assembly G1105 end of the cycle. Gd treated as macro.

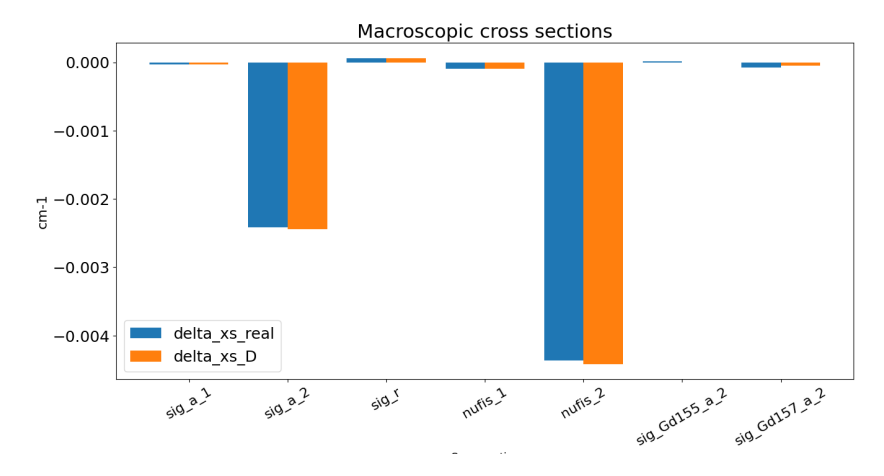


Figure 6.75: Absolute Macroscopic Cross Section for assembly G1105 end of the cycle with Gd treated as macro.

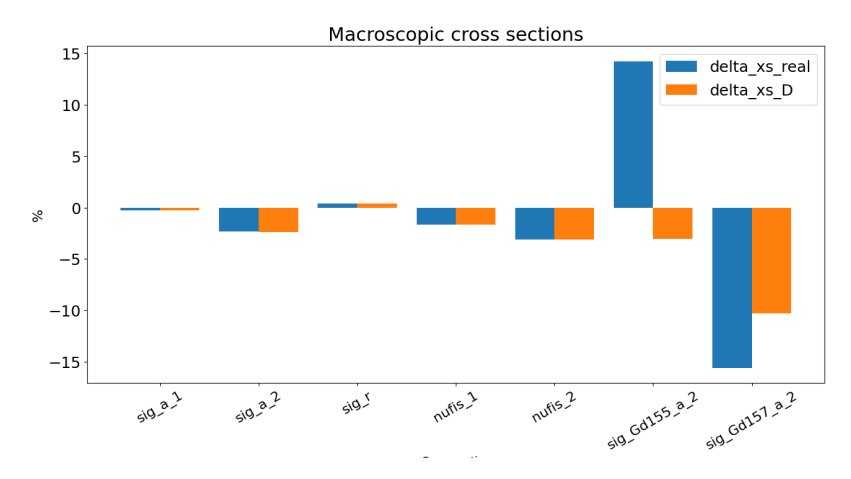


Figure 6.76: Relative Macroscopic Cross Section for assembly G1105 end of the cycle with Gd treated as macro.

Condition	Δk_{∞} [pcm]
Without correction	808
With correction	-21
With correction $+$ Gd as micro	-14

Table 6.10: Effect of correction on Δk_{∞}

6.4.3 G1109 + environment: middle of cycle

The process that led to the investigation of the efficiency of the history model began with a preliminary analysis of the reactor behavior, examining the trends of the thermophysical parameters during the cycle. At the beginning of this chapter, it is noted that a variation of the spectrum is strongly influenced by the environment, an aspect that was not initially expected to require investigation.

For this reason, it was decided to consider node 9 of assembly G, this time taking the environment into account, and the results obtained from the validation are presented below.

- The plots of the microscopic absorption cross sections show generally consistent trends for most isotopes, with the exception of ²³⁵U, where the histograms exhibit opposite behaviors. It's worth noting that the differences observed here on the micro ²³⁵U and ²³⁸U may be the origin of the discrepancy on macroscopic absorption cross section of the fast group.
- For fission microscopic cross sections, ²³⁵U again stands out as not always being correctly modeled. Nonetheless, the results for the other isotopes are generally satisfactory.
- The graphs presenting corrections to the macroscopic cross sections show overall good agreement, except for gadolinium, particularly ¹⁵⁵Gd, which displays an opposite trend compared to the reference. In particular the difference in macroscopic absorption cross section for the fast group is due to the difference in microscopic cross section of ¹⁵⁵Gd.
- The $k_{\rm inf}$ values show slight improvements when applying the spectral history model; however, the correction is not always sufficient. In the previously discussed case (G11, axial node 5, infinite medium), treating gadolinium using its microscopic cross sections led to improved accuracy when applying the spectral model. In the current case, however, treating gadolinium at the microscopic level worsened the spectral correction.

The environment surrounding the assembly, the spectrum shift due to adjacent assemblies may lead to variations in plutonium production. This, in turn, could interfere with the spectral model's correction, especially in the presence of strong absorbers like gadolinium. Therefore, explicitly accounting for environmental effects might be necessary to improve the robustness of the model. Another possibility is to consider an interpolation parameter that doesn't depend on the environment effect.

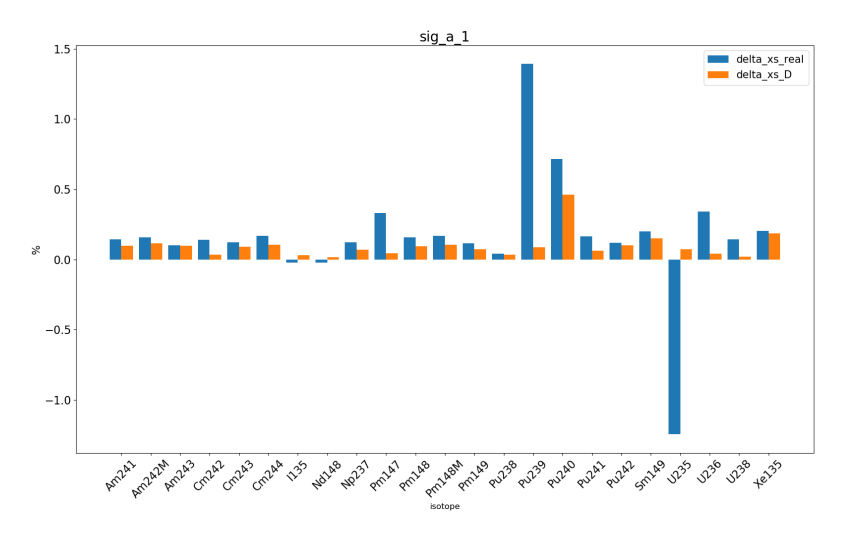


Figure 6.77: Fast group absorption cross sections - relative for assembly G1109 with environment middle of the cycle. Gd treated as macro.

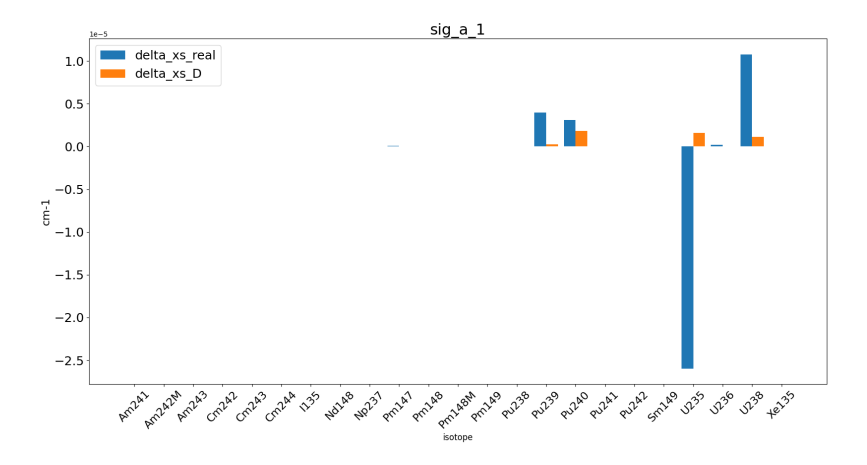


Figure 6.78: Fast group absorption cross sections - absolute for assembly G1109 with environment middle of the cycle. Gd treated as macro.

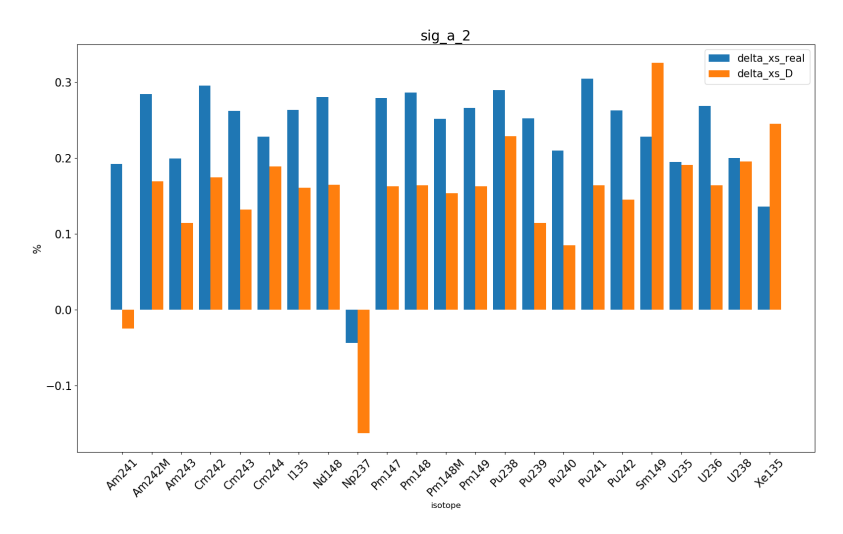


Figure 6.79: Thermal group absorption cross sections - relative for assembly G1109 with environment middle of the cycle. Gd treated as macro.

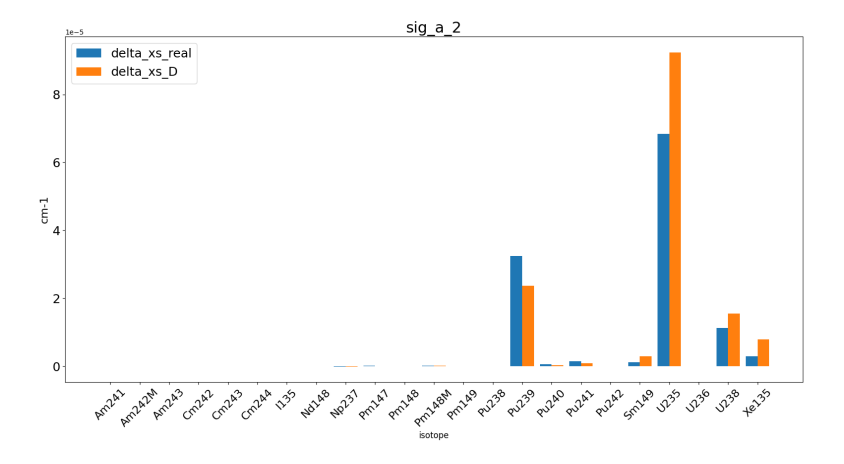


Figure 6.80: Thermal group absorption cross sections - absolute for assembly G1109 with environment middle of the cycle. Gd treated as macro.

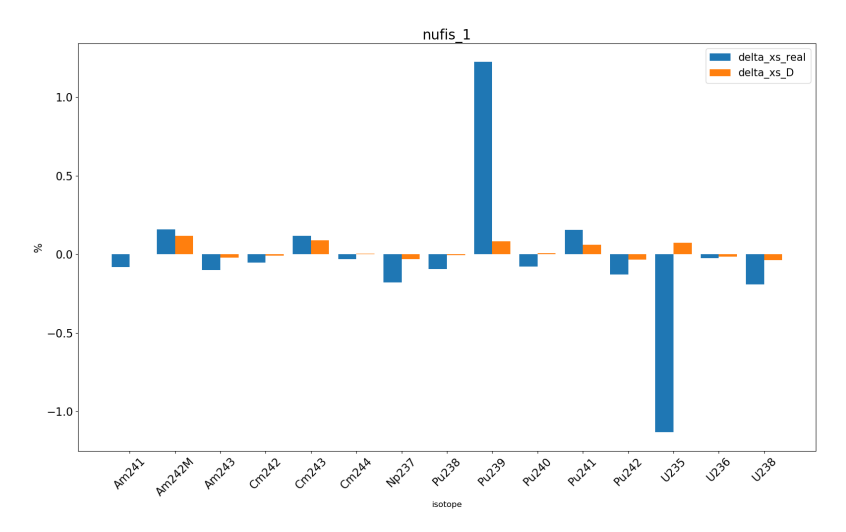


Figure 6.81: Fast group fission cross sections - relative for assembly G1109 with environment middle of the cycle. Gd treated as macro.

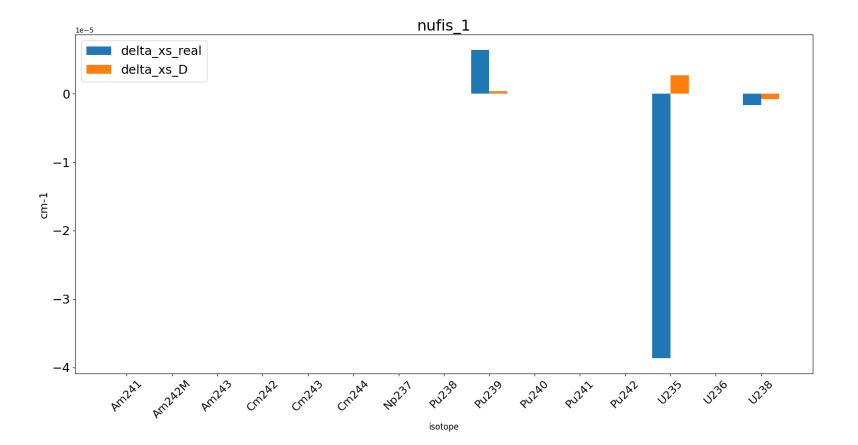


Figure 6.82: Fast group fission cross sections - absolute for assembly G1109 with environment middle of the cycle. Gd treated as macro.

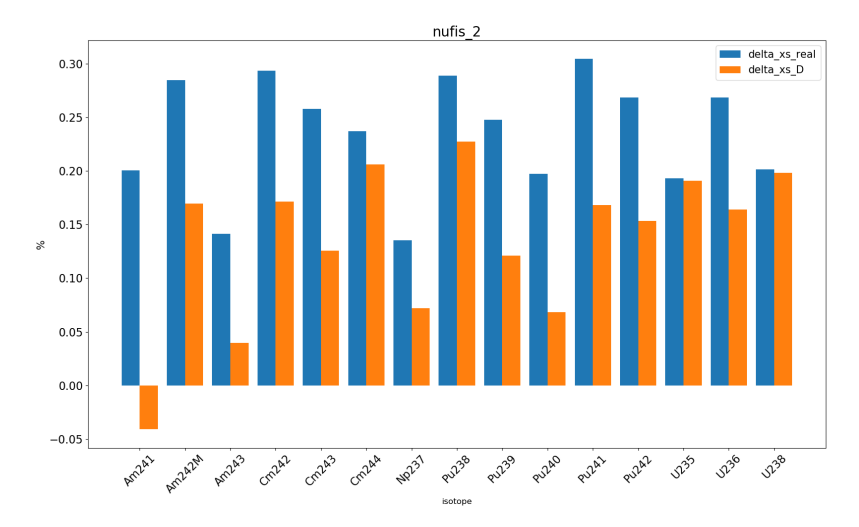


Figure 6.83: Thermal group fission cross sections - relative for assembly G1109 with environment middle of the cycle. Gd treated as macro.

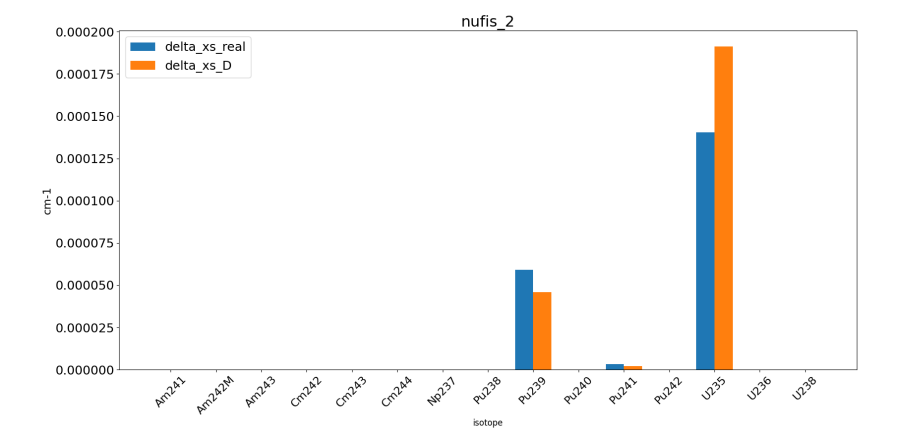


Figure 6.84: Thermal group fission cross sections - absolute for assembly G1109 with environment middle of the cycle. Gd treated as macro.

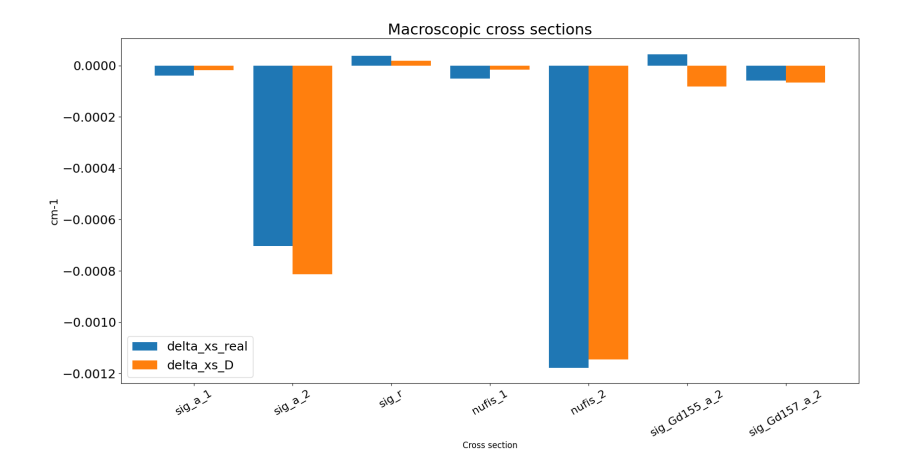


Figure 6.85: Absolute Macroscopic Cross Section for assembly G1109 with environment middle of the cycle with Gd treated as macro.

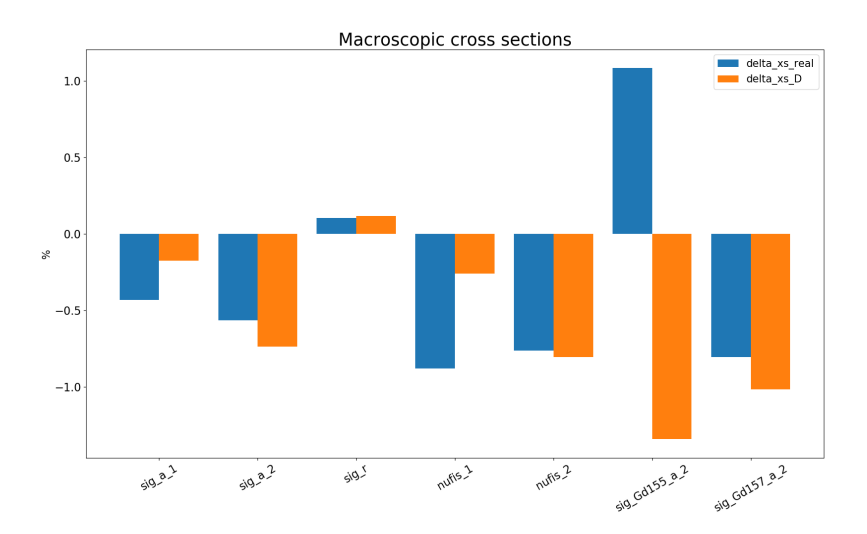


Figure 6.86: Relative Macroscopic Cross Section for assembly G1109 with environment middle of the cycle with Gd treated as macro.

Condition	Δk_{∞} [pcm]
Without correction	174
With correction $+$ Gd as macro	152
With correction $+$ Gd as micro	-232

Table 6.11: Effect of correction on Δk_{∞}

6.4.4 G1109 + environment: end of cycle

In this case, the same assembly with environmental surroundings was considered, but at a higher burnup level where the gadolinium concentration is expected to have significantly decreased. The results, as in the previous case, are generally satisfactory. However, 235 U again shows some discrepancies—particularly in the fast energy range—where its behavior in both fission and absorption occasionally follows an opposite trend compared to the reference. The macroscopic cross sections show good agreement even in this high burnup scenario. The $\Delta k_{\rm inf}$ without applying the spectral history model is approximately 808 pcm, showing a significant improvement once the model is applied. When gadolinium is treated using microscopic cross sections instead of as part of a lumped macroscopic cross section, the correction obtained is very similar to the one using the macroscopic approach. This behavior is expected, as gadolinium plays a much less dominant role at the end of the cycle due to its depletion.

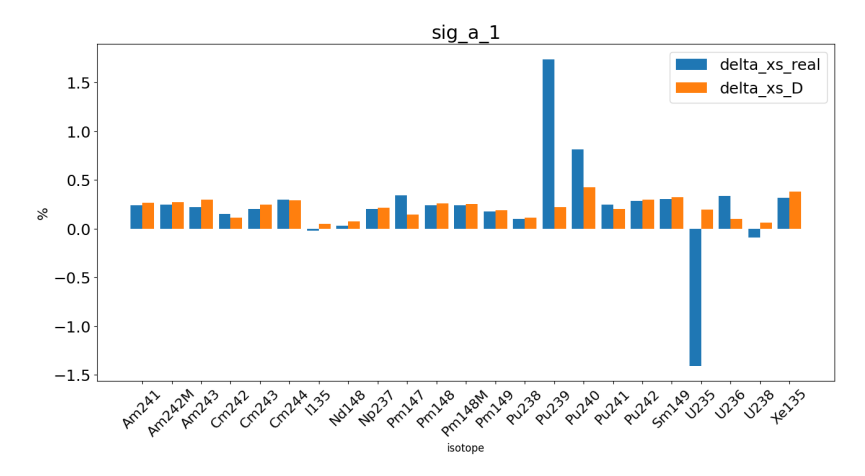


Figure 6.87: Fast group absorption cross sections - relative for assembly G1109 with environment end of the cycle. Gd treated as macro.

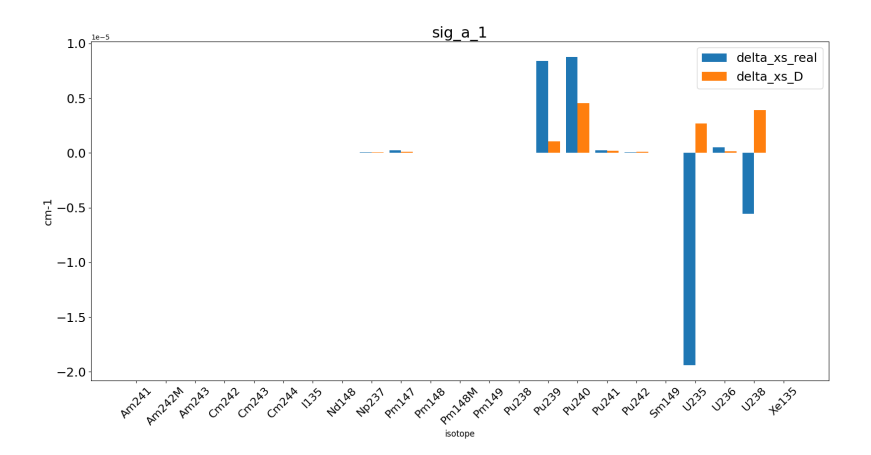


Figure 6.88: Fast group absorption cross sections - absolute for assembly G1109 with environment end of the cycle. Gd treated as macro.

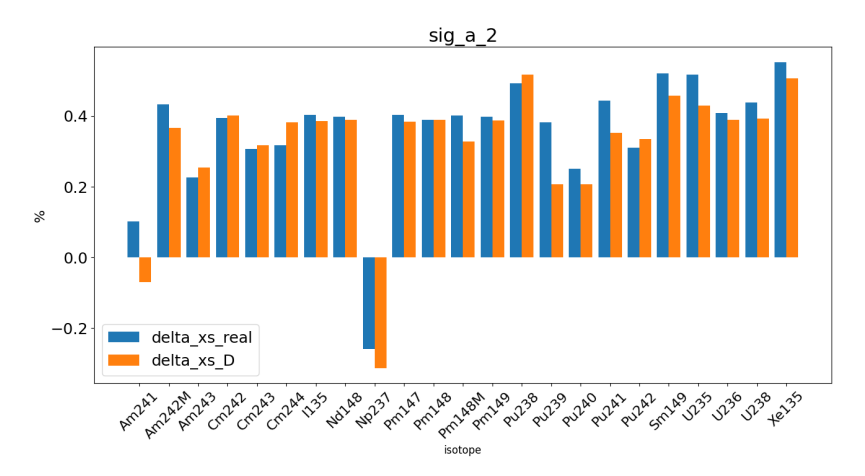


Figure 6.89: Thermal group absorption cross sections - relative for assembly G1109 with environment end of the cycle. Gd treated as macro.

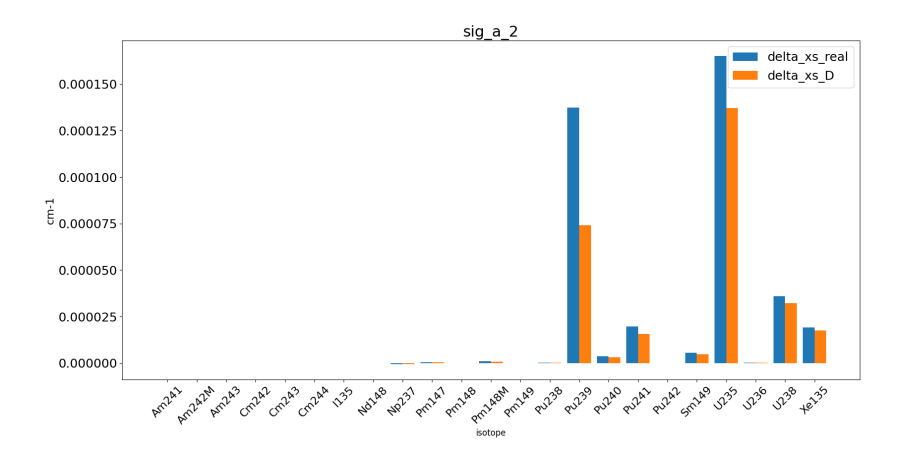


Figure 6.90: Thermal group absorption cross sections - absolute for assembly G1109 with environment end of the cycle. Gd treated as macro.

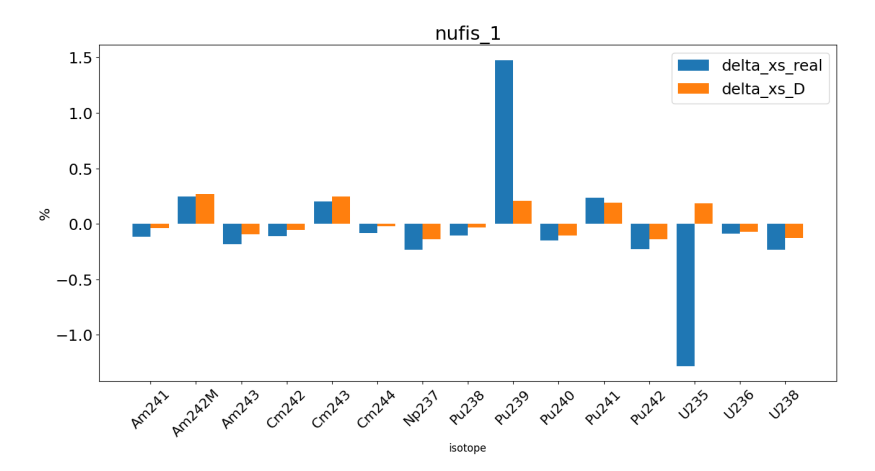


Figure 6.91: Fast group fission cross sections - relative for assembly G1109 with environment end of the cycle. Gd treated as macro.

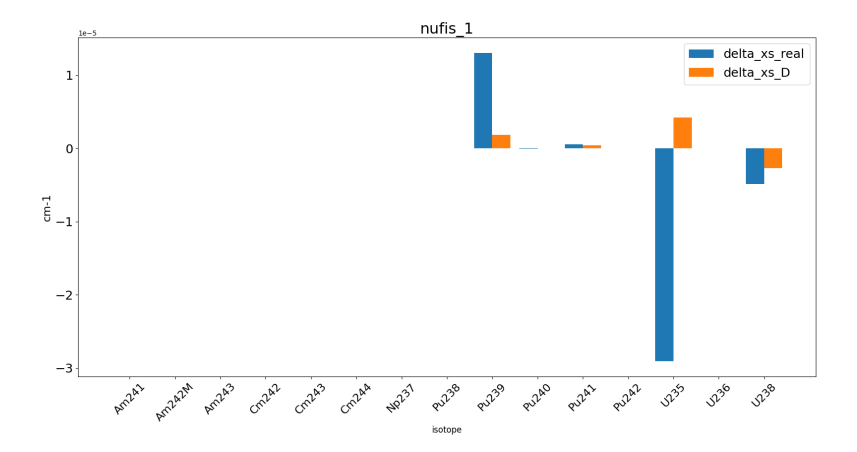


Figure 6.92: Fast group fission cross sections - absolute for assembly G1109 with environment end of the cycle. Gd treated as macro.

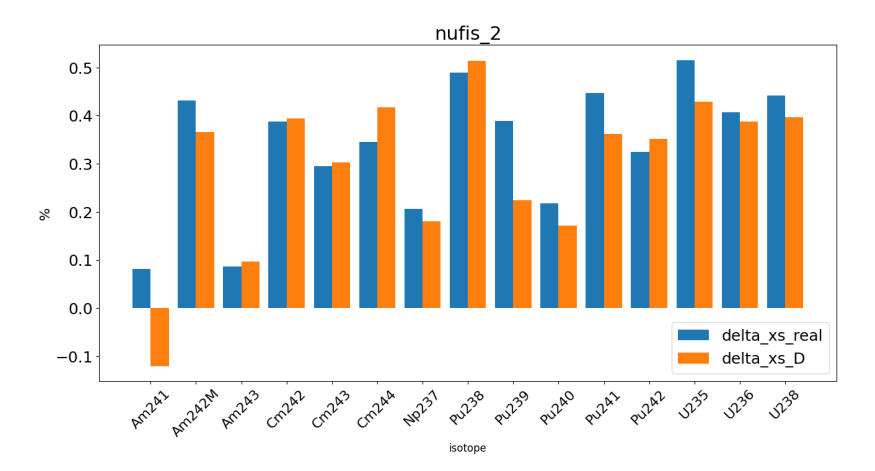


Figure 6.93: Thermal group fission cross sections - relative for assembly G1109 with environment end of the cycle. Gd treated as macro.

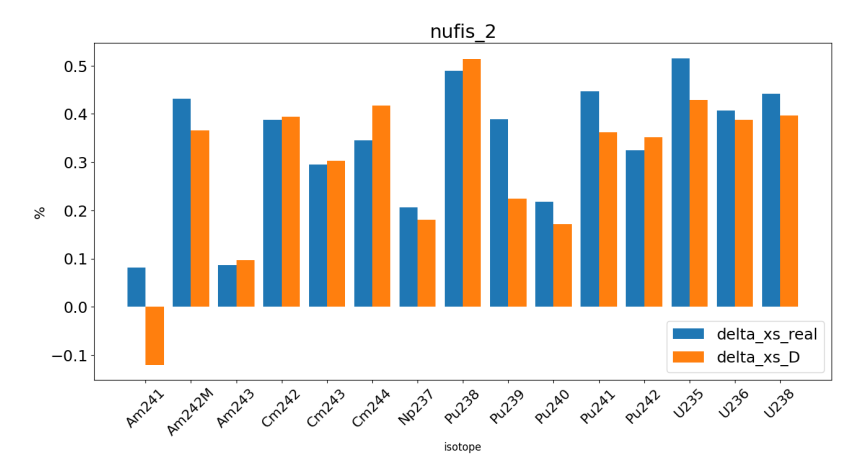


Figure 6.94: Thermal group fission cross sections - absolute for assembly G1109 with environment end of the cycle. Gd treated as macro.

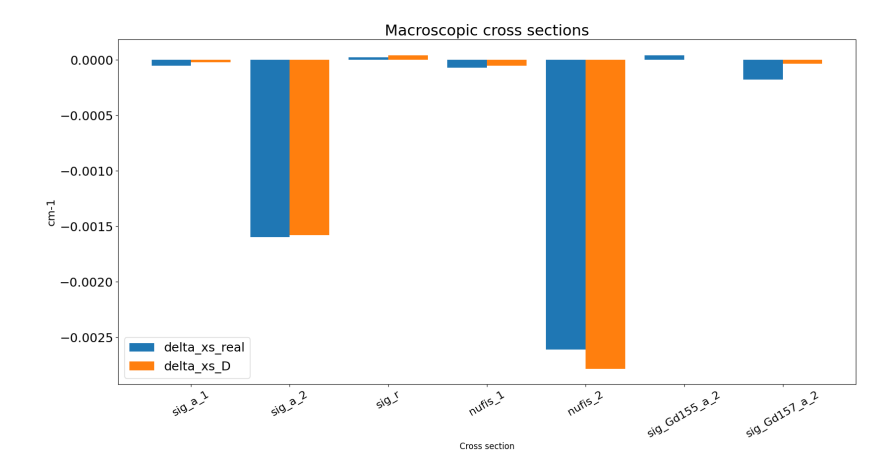


Figure 6.95: Absolute Macroscopic Cross Section for assembly G1109 with environment end of the cycle with Gd treated as macro.

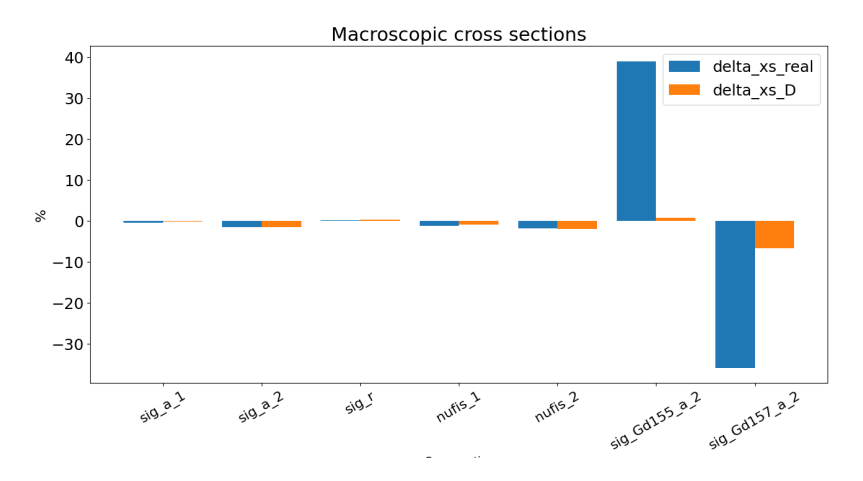


Figure 6.96: Relative Macroscopic Cross Section for assembly G1109 with environment end of the cycle with Gd treated as macro.

Condition	Δk_{∞} [pcm]
Without correction	808
With correction $+$ Gd as macro	-21
With correction $+$ Gd as micro	-14

Table 6.12: Effect of correction on Δk_{∞}

Chapter 7

Conclusion

The goal of this project is to verify whether the spectral history model implemented in SCIENCE V2 is accurate. Note that local parameters vary throughout the reactor and evolve over the cycle, which highlights the need for such a modeling approach, because the frame of the reactor core simulation follows the two-step approach, thus it faces its approximations. The core of a nuclear reactor presents many heterogeneities, starting from the fact that different families of assemblies are present within the core. In addition, control rods and the reflector, which strongly influence the spectrum in the core, are also present. By collecting data collecting data from the TSN reactor core simulation by SMART, it was decided to use deviations in order to gain a qualitative understanding of how the main parameters of the assemblies were distributed. From this initial phase, it was evident that the assembly families behave differently from one another. The most important parameters considered were moderator density, fuel temperature, boron concentration, xenon factor, the amount of plutonium produced, and the spectral index (SI). Each of these parameters was compared to so-called reference values.

The deviations from these reference values were averaged over burnup in order to capture how they changed over the course of depletion. For plutonium concentration, however, this was not necessary since it represents a pointwise value at a given burnup step, and its historical impact over depletion was not of interest. By cross-referencing this information, a clear correlation was found between higher or lower plutonium production and deviations from the reference moderator density.

In particular, by comparing the plutonium deviation with the cumulative deviation of moderator density, the following pattern was identified:

- For the nodes at the top of the assemblies, there is greater plutonium production and a moderator density lower than the reference value. Some outliers are present and are due to the presence of control rods.
- At the bottom, outliers are also present due to the reflector, which induces a change in the neutron spectrum.
- Data was analyzed family by family, and it was observed that even within the same family, some assemblies produced more or less plutonium. The first hypothesis for this behavior is that, although the assemblies are identical, they have a different environment that modifies the spectrum.
- The spectral index is the parameter that best encapsulates all the information.

In the literature, various methodologies have been proposed to better account for temporary deviations from reference values during the cycle. Among them, the use of PU as an interpolation parameter in the construction of macroscopic cross sections has shown the highest accuracy.

Indeed, the method used in SCIENCE V2 includes PU as an interpolation parameter.

The next step after observing the trends in the Taishan core simulation was to use APOLLO3® to exactly replicate the construction of macroscopic cross sections as done in SCIENCE V2. Different cases were considered, as assemblies with and without gadolinium, and either including or excluding the environment.

The results obtained are summarized below:

- For assemblies without gadolinium and without environment, the spectral history model gives excellent results.
- For assemblies with gadolinium but without environment, the results were not always satisfactory, especially when gadolinium is still present in significant quantities. Another important result is that, when gadolinium is treated as microscopic in the construction of macroscopic cross sections, the spectral models performs well.
- Assemblies with gadolinium and considering the environment yielded results that were not always satisfactory. The presence of gadolinium, especially at mid-cycle, presents a challenge that is difficult to predict accurately. The correction of the spectral model does not seem to improve the results, and in this case, treating gadolinium as microscopic further worsens the correction.

We can therefore say that the results obtained have confirmed what was initially hypothesized: assemblies exhibit different behaviors throughout the cycle. The environment was not initially hypothesized or taken into account, but it has proven to be an interesting aspect to consider. The connection with the history model is that PU is correlated with the environmental effect. To draw more definitive conclusions, additional simulations should first be considered in order to better understand the pattern between the spectral history model, plutonium production, and the environment.

For future studies, it would be interesting to simulate an assembly without gadolinium while still considering the surrounding environment. Additionally, constructing macroscopic cross sections using other interpolation parameters, such as moderator density, which is a key factor in spectral shifting, could also be relevant. Further perspectives include extending simulations to higher burnups, up to 60 GWd/t, and testing the pertinence of other spectral history parameters, as mentioned in the review.

Bibliography

- [1] CEA Saclay. Neutronics. Paris (FR). 2015. URL: https://www.cea.fr/english/Pages/resources/nuclear-energy-monographs/neutronics.aspx.
- [2] Sandra Dulla. Notes on the course Nuclear Reactor Physics and Transport Theory. 2024.
- [3] Alain Hébert. Applied Reactor Physics. Second edition. 2016.
- [4] Milan Hanus. Mathematical modeling of neutron transport, PhD thesis. University of West Bohemia. 2014.
- [5] Nuclear Power. Liquid Metals. 2025. URL: https://www.nuclear-power.com/nuclear-engineering/materials-nuclear-engineering/liquid-metals/.
- [6] Wm. J. Garland. *Reactor Physics: Multigroup Diffusion*. Department of Engineering Physics, McMaster University, Hamilton, Ontario, Canada.
- [7] Bu Search. The Neutron transport equation. 2021. URL: https://sites.bu.edu/cliveg/files/2021/09/transport-equation-derivation.pdf.
- [8] I. Bilodid and S. Mittag. Use of the local Pu-239 concentration as an indicator of burnup spectral history in DYN3D. Institute of Safety Research, Forschungszentrum Dresden-Rossendorf, Germany. 2010.
- [9] D. Price et al. «Methodology for Sensitivity Analysis of Homogenized Cross-Sections to Instantaneous and Historical Lattice Conditions with Application to AP1000[®] PWR Lattice». In: Energies 14.12 (2021), p. 3378. DOI: 10.3390/en14123378. URL: https://doi.org/10.3390/en14123378.
- [10] Antonio Galia. A Dynamic Homogenization Method for Nuclear Reactor Core Calculations. CEA. 2020.
- [11] Nuclear Power. Doppler Broadening Doppler Effect. 2023. URL: https://www.nuclear-power.com/glossary/doppler-broadening/.
- [12] OECD Nuclear Energy Agency. JANIS Java-based Nuclear Information Software, version 4.0. https://www.oecd-nea.org/janis/.
- [13] Esteban Alejandro Szames. Few group cross section modeling by machine learning for nuclear reactor. Université Paris-Saclay. 2020.
- [14] P. Guimarães and E. Müller. Parameterization of two-group nodal cross section data for POLCA-T BWR transient applications. International Conference on Mathematics, Computational Methods and Reactor Physics. 2021.
- [15] Chao Wan et al. «Research and Application of the Rehomogenization Method for PWR Core Neutron Physics Simulation». In: Nuclear Science and Engineering 197.7 (2023), pp. 1454–1466. DOI: 10.1080/00295639.2022.2158704. URL: https://doi.org/10.1080/00295639.2022.2158704.

[16] IAEA. TAISHAN-1.2023. URL: https://pris.iaea.org/pris/CountryStatistics/ReactorDetails.aspx?current=918.